WIDEBAND DIGITAL BEAMFORMING IN SONAR SYSTEMS

TOOMAS RUUBEN

TUT
PRESS

Faculty of Information Technology
Department of Radio and Communication Engineering
Chair of signal processing.
TALLINN UNIVERSITY OF TECHNOLOGY

Dissertation was accepted for the defence of the degree of Doctor of Philosophy in Telecommunication Engineering on May 11, 2009.

Supervisors: Ilmar Arro, Prof. Emeritus, D.Sc., Department of Radio and
                 Communication Engineering. Tallinn University of Technology

                 Andres Taklaja, Prof., Ph.D., Department of Radio and
                 Communication Engineering. Tallinn University of Technology

Opponents: Andres Reial, Ph.D., Senior Specialist, Multi-Antenna Terminal
                 Receivers Ericsson Research, Lund, Sweden

                 Peep Miidla, Assoc. Prof, Ph.D., University of Tartu, Faculty of
                 Mathematics

Defence of the thesis: June 18, 2009

Declaration: Hereby I declare that this thesis is my original, unaided work. It is submitted for the degree of Doctor of Philosophy in Engineering of Tallinn University of Technology, Tallinn, Estonia. It has not been submitted before for any degree of examination in any other university.

Toomas Ruuben

INFORMAATIKA JA SÜSTEEMITEHNIKA C67

SUUNADIAGRAMMIDE DIGITAALNE FORMEERIMINE LAIARIBALISTES SONARSÜSTEEMIDES

TOOMAS RUUBEN

TUT
PRESS

ABSTRACT

In multi-beam sonars, high resolution is ensured by using short-term signals and a sensor system, which together form multiple partial channels that have narrow directional diagrams. Such partial channels that exhibit narrow directional diagrams can be formed using independent sensors or sensor arrays. Unfortunately, high-power scanning signals and those of short durability are harmful to biological objects, including humans, in the vicinity of the transmitter.

Using digital signal processing technology, we can generate scanning signals of any complexity. As a rule, these signals are complex with regard to intra-pulse modulation (i.e. wide band in the frequency band) and guarantee adaptive-optimum reception of these spread-spectrum signals with acoustic power that is hundreds and thousands of times lower. At the same time, the technical and tactical characteristics of the sonar (or radar) do not deteriorate, rather, vice versa. Reducing the acoustic power of the transmitters below the 10-watt level allows us to eliminate the danger zone in the vicinity of the transmitter. Power consumption and dimensions of the system are reduced, and the distance at which it is detected with reconnaissance technology is also reduced. This feature is especially important for military systems. But there are some problems with beamforming when spread-spectrum signals are used as scanning signals.

This thesis will analyse the dynamics of spread-spectrum signals in sensor arrays. The scanning signal and sensor array are connected analytically and the influence of the sensor array in a dynamic regime will be studied. Derived from the characteristics of this type of signal, the sensor array is not able to use classical phase compensation for the purpose of beam steering. Time lag compensations of the signals should be used to achieve a high resolution in all partial directions. We can compensate the time lags directly by using a Matrix algorithm, but it will only work in the most correct way within a frequency domain that uses the characteristics of Fourier transform. One advantage of this method is that it also enables us to immediately perform an optimal reception to evaluate the actual round-trip time delay. However, disadvantage is the large demand for resources and the power and memory capacity of the processor. Another proposal developed by the author of this work is to use a method where phase compensation is used in blocks with time lag compensation. This method enables us to reduce the required computing power and therefore, the cost of the hardware. The work describes all three methods and compares their quality indicators. Computer modelled time and space diagrams are displayed for each of the methods.

KOKKUVÕTE

Kiirtelehviksonarites tagatakse kõrge lahutusvõime lühikese kestvusega signaalide kasutamisel või suure baasiga signaalide puhul signaali lühikese ekvivalentse kestvusega ning sensorsüsteemiga, mis formeerib hulgaliselt kitsa suunadiagrammiga partsiaalkanaleid. Kitsa suunadiagrammiga partsiaalkanalid võivad olla moodustatud nii iseseisvate sensorite kui ka sensorivõre abil. Kahjuks on lühikese kestvusega kuid suure võimsusega sondeerivad signaalid keskkonnale ohtlikud, kaasaarvatud inimestele, kes viibivad saatja sensorvõre vahetus läheduses.

Kasutades digitaalset signaalitöötlust on võimalik genereerida suvalise keerukusastmega sondeerivaid signaale. Sellised signaalid on reeglina impulsisiseselt keeruliselt moduleeritud ja omavad laia spektrit. Neid tuntakse kui hajaspektersignaale ning nende kasutamise korral on võimalik sooritada optimaalne vastuvõtt sadades kuni tuhandetes kordades väiksema akustilise võimsusega. Samal ajal sonari või ka radari tehnilised ning taktikalised näitajad ei halvene ning võivad hoopis paremaks minna. Süsteemi akustilise võimsuse vähendamine alla *10 W* võimaldab elimineerida ohutsooni saatja vahetus läheduses. Väheneb ka süsteemi üldine võimsustarve, mõõtmed ning ka vahemaa, kus militaarsed vastuluuresüsteemid võiksid süsteemi avastada. Samas eksisteerivad mõningad probleemid suunadiagrammide formeerimisel kui sondeerivate signaalidena on kasutusel hajaspektersignaalid.

Käesolev doktoritöö analüüsib hajaspektersignaalide dünaamikat sensorvõredes. Sondeerivad signaalid ja sensorvõre seostatakse analüütiliselt ning tuuakse välja nende vastastikune mõju dünaamilises režiimis. Tulenevalt hajaspektersignaalide omadustest, ei ole võimalik sensorvõre suunadiagrammi juhtimiseks kasutada klassikalist faasilist kompensatsiooni. Et saavutada kõrget lahutusvõimet kõikides partsiaalsuundades, on vaja kasutada signaalide ajaliste viidete kompenseerimist. Me võime kompenseerida ajalised viited otseselt kasutades nn Maatriks algoritmi kuid kõige korrektsemalt töötab viidete kompenseerimine sagedusruumis mis kasutab selleks Fourier' teisenduse omadusi. Meetodi eeliseks on veel see, et ta võimaldab samaaegselt sooritada ka optimaalse vastuvõtu signaalide viiteaegade hindamiseks. Puuduseks on jällegi suhteliselt suur arvutuste maht, mis nõuab suurt mälumahtu ja kiiret signaaliprotsessorit. Ühe lahendusena pakutakse välja käesoleva töö autori poolt välja töötatud viidete kompenseerimise meetod, kus kasutatakse klassikalist faasilist kompensatsiooni plokkide kaupa. Selle meetodi kasutamisel on võimalik vähendada vajaminevat arvutusvõimsust ja seega ka riistvara maksumust. Kõik meetodid on arvutil modelleeritud ning esitatud on ka vastavad ajalised ja ruumilised diagrammid.

ACKNOWLEDGEMENTS

TÄNUSÕNAD

CONTENTS

1 INTRODUCTION

Mapping the seabed and navigation have historically been the main fields of application for sonar systems. Nowadays, the localisation of technical installations such as oil platforms, undersea gas pipelines and so on has also been included in this field. In the military, defence against mines, as well as investigating catastrophes have played an essential role. So the essential parameters are the precise measurement of distance and radial resolution [1][31].

In the beginning of the history of sonars (or radars) signals with simple structure (so-called monopulse type of signals) were used. It is known that precision can be improved by cutting the temporal duration of the scanning signal used to activate the environment. At the same time, the acoustic power should be increased in order to ensure a sufficient operating radius and noise stability. Ordinary sonars can have acoustic power that reaches several kWs to activate the environment. Such signals are harmful to the environment, including humans who happen to be in the vicinity of such sonar systems. It was discovered later (since 1958) that signals with complex structures (based on Barker's codes, M-sequences) are good to be used for the purpose of diminishing radiated power. At the same time it was not possible to realize these new ideas due to the technology level of these days. The progress of digital technology enabled implementing signals with spread spectrum but in reality it was possible to use them only in the case of mechanical scanning.

The radial resolution of a sonar system is determined by the width of the beam pattern – the narrower it is the better. In the case of a electrical scanning (classical phased array), the width of the beam pattern is determined by the spatial length of the sensor array, and the beam pattern of the sensor array is typically calculated using harmonic vibrations of infinite duration at a constant magnitude. It is known that via electrical steering, the beam pattern becomes wider when the arrival angle of the signal on the array becomes larger (against the normal sensor array).

The main objective of the present thesis is to enhance the precision of the measurement of the distance, while the power of the impulse of the sonar system is reduced and the radial resolution increased in the case of large angles. Consequently of the objects of this work is to analyze the behaviour of complex signals in sensor array and beamforming with this type of signals. Complex signals are normally considered as wideband signals and signal processing in sensor arrays is reduced to the bandwidth of the sensor array (Ultra Wideband Array). Also, dividing of the sensor array into sub-arrays is normally observed on the purpose of increasing of the bandwidth of the sensor array or on the purpose of suppressing of grating lobes (so-called sub-arrays with arbitrary structure). Another approach where dynamics of the signals in sensor array in time domain is observed in the current work. Such approach enables thorough analysis of the processes taking place in sensor array.

The thesis consists of a theoretical part and a practical part. The theoretical part is, to a large extent, a review that at first deals with the propagation of acoustic waves in the environment. Then the theory of complex aperture theory, array theory, classical methods of signal processing and problems connected with optimal reception are dealt with. As known, sensor arrays may be one-dimensional, planar or three-dimensional. The present paper observes the one-dimensional equidistant sensor array where isotropic sensors are used. It is also presumed that a propagation environment of acoustic waves and sensors has a linear function in addition to the planar wave front (Chapter 4.1). The main focus is on the generation and processing of the electrical signals, which are applied to the sensors and created by them. A simple type of sensor array is selected in order that the behaviour (dynamics) of the signals work well in the sensor array. As can be seen in the theoretical parts of the present thesis, the transition to planar or even more complicated array types is only a technical matter and actually means adding one or several measures to the mathematical apparatus. In order to describe the processes occurring in the sensor array, parts of the scanning signals (chips) are also used. Adaptive arrays are also a fast developing topic, but since they are excluded from the main problems of the present work, only a short summary of the methods applied is presented here.

The practical side of the paper begins with studies of the qualities of the scanning signals (the functions of infiniteness), first and foremost, because the power of the impulse and the preciseness of estimating the time lag are related to the scanning signal itself. The main emphasis is on the section dealing with the ambiguity function $\psi(\tau, 0)$. The aim of the present thesis is not to estimate the Doppler frequency shift (or the speed of objects), since this is not needed when mapping the seabed. At the same time, in the later stages it is possible to involve the part dealing with this problem. When analysing the scanning signals, the problems related to the energy of the signal are also dealt with. It is found that while using spread-spectrum signals, it is possible to reduce the power of the impulse of the system and at the same time enhance the precision of estimating the time lag. Special attention is paid to using scanning signals based on novel nested codes. The codes based on nested codes remarkably enable to increase operating range of the sonar or radar.

In the next part of the thesis, we observe how the scanning signals behave, based on spread-spectrum signals, in the sensor arrays. If a signal of this type falls on the sensor array from the normal direction, the sensor array behaves adequately. This means that, for a physically movable sonar [1] (or radar [20]) , there is no need to use additional methods of signal processing, except for optimal reception where the structure of the scanning signal must be considered. However, optimal reception of this type of signals with matched filters is highly resource-intensive. Also the complexity of the algorithm of the separation of quadrature components is well-known. A new solution of optimal reception directly on intermediate frequency is

proposed in this work. This method enabled to abandon algorithm of the separation of quadrature components.

Next, the behaviour of spread-spectrum signals is observed in the sensor array while the scanning signal is falling on the sensor array along a normal angle. First the classical phase array is used as a model, and it is explained that the classical phase array is not applicable for steering beam patterns using spread-spectrum signals. Respective detailed analysis has been implemented in the current work. Then three different signal-processing algorithms for steering the beam pattern of the sensor array are presented such as Block-phase method developed by the author of this work, MATRIX and Advanced FFT algorithm. Also, the indicators of quality and technical viability are estimated for them.

The MATRIX algorithm is technically simpler but requires a high sampling frequency (approximately 16 samples in each signal period). Advanced FFT algorithm gives good results but unfortunately requires high computing power. It is also notable that the algorithm mentioned above is an alternative to adaptive methods of beamforming. The Block-phase method gives approximately the same results as Advanced FFT algorithm but with decreased computing power. The novelty of this algorithm lies in the use of dynamically variable sub-arrays new principle. This enables scanning the beam electronically within the span of 180 degrees in the case of low power spread spectrum signals described above.

The present thesis is a theoretical research paper. At the same time, the innovative principles presented here have been introduced in the new sonar and radar systems being established.

2 REVIEW

2.1 TYPES OF SONAR SYSTEMS

Sonars use different methods to form beam patterns dependent upon the tasks demanded of them. They are divided into two large classes: side-scan sonars and multi-beam sonars. Side-scan sonars are able to map a very wide sector of the seabed. The cost is relatively low and it is economical to use, but at the same time its precision for determining the location of objects is lower than that of multi-beam sonars. This is particularly noticeable on uneven seabeds and is caused by the small number of sonars. Multi-beam sonars have a lower spatial resolution than side-scan sonars (due to the width of the beam pattern) and cover a smaller part of the seabed at a time, but the precision with which it can position is higher. Multi-beam sonars are only recommended for use in cases where the seabed is very uneven. It should be noted that while side-scan sonar measurement results are damaged by simultaneous multiple reflections, the measurement results of the multi-beam sonars are only damaged in situations when the objects reflecting signals are located too close to each other. Thus, one of the essential problems with multi-beam sonars is enhancing the resolution. Different methods for enhancing the resolution have been worked out on the basis of spectral analysis [5][36], for instance: Minimum Variance, Eigen- vector, MUSIC and Minimum Norm. As a rule these methods produce a better result than the classical formation of beam patterns based on the Fourier transform. From among the parametric methods Root-Music and the ESPRIT method can also be mentioned. Multi-channel active sonars, which are fixed on a rigid traverse, are the simplest sonar systems. Here all the channels operate independently and at one frequency. A problem arises in the appearance of overlapping beam patterns at greater depths and also in the formation of areas of ambiguity at greater depths. To solve such problems, the commutation of channels is used, or also semi-active systems, where a crescent of a circle is used in place of a straight traverse. In such cases, all the channels are spatially separated due to the selectivity of the spatially separated sensors [6].

2.2 THE MAIN TECHNICAL DATA OF SONAR SYSTEMS

While designing sonar systems, the following technical data are considered:

1. the permitted speed of the carrier to ensure precise measurement results
2. measurement area or range of action
3. the measurement precision of the distance either in general or by regions
4. the range of working frequencies
5. implemented scanning signals
6. sounding frequency

7. the transmitter's output power
8. the viewing angle grasped simultaneously
9. the width of the sensor's beam pattern
10. the power required
11. the requirements of the main computer
12. the usable interfaces
13. the number of channels

2.3   AUTHOR'S CONTRIBUTION

1. Ordinary sonars can have acoustic power that reaches several kWs in order to ensure a sufficient operating radius and noise stability.

   Problems:

   a. High power signals are harmful to the environment, including humans who happen to be in the vicinity of sonar or radar system.
   b. System is easily detected with reconnaissance technology (important for military systems).

   Solutions:

   a. It is possible to use digital signal processing technology and spread spectrum scanning signals to reduce acoustic or radiation power below 10-watt level.
   b. Detailed analysis for the scanning signals and the functions of their ambiguity is done (Chapter 5.1). Models are created in MathCad environment. The signals based on novel nested codes are highlighted which remarkably enable to increase operating range of the sonar or radar with reduced power.
   c. Behaviour of complex spread spectrum signals in conventional phased array and beamforming with this type of signals is analyzed by the author. For this purpose, several mathematical models are created in MathCad environment (Chapter 5.2).

2. Majority of present sonar or radar systems use phased array for beam steering (electrical scanning).

   Problems:

   a. In the case of an electrical scanning, the beam pattern of the sensor array is typically calculated using harmonic vibrations of infinite duration at a constant magnitude. It is known, that via electrical

steering, the beam pattern becomes wider when the angle of the signal on the array becomes larger (Chapters 4.2, 4.3 and 5.2). Additionally, in our case, we do not use harmonic vibrations with long duration.

b. On the assumption of modelling results above and derived from the characteristics of signals based on nested codes, sensor array is not able to use classical phase compensation for the purpose of beam steering (Chapter 5.2).

Solutions:

a. Proper mathematical apparatus and modelling environment for sensor arrays is created.

b. Proper research about dynamics of spread-spectrum signals in sensor array in time domain is performed for the purpose to develop new algorithms (Chapter 5.2).

c. Three different signal-processing algorithms for steering the beam pattern of sensor array in the case of spread spectrum scanning signals are developed and proposed (Chapters 5.3, 5.4 and 5.5). Based on the algorithms, modelling environment is developed and used.

3. Results and realization opportunities.

a. First (MATRIX) algorithm gives good results but requires high sampling frequency (Chapters 5.3 and 5.8).

b. Advanced FFT algorithm (Chapter 5.4) gives good results but requires high computing power.

c. Developed novel Block-phase algorithm based on dynamically variable sub arrays gives approximately the same results as advanced FFT algorithm but with decreased computing power (Chapter 5.5).

d. A new solution of optimal reception directly on intermediate frequency [15] [16] is introduced in this work. This method enabled to abandon algorithm of the separation of quadrature components.

The most significant result of this work is the set of signal processing algorithm(s) whereby we can efficiently enhance the precision of the measurements of the distance, while the power of the impulse of the sonar system is reduced and the radial resolution is increased in the case of large signal falling angles.

3   STATEMENT OF THE TASK

3.1   THE REDUCTION OF THE POWER OF THE IMPULSE IN SONAR SYSTEMS

When estimating the distance between objects, the temporal/spatial duration of a signal plays an essential role. The shorter the signal the more precise the results. At the same time, if we want a wider working radius for the sonar, we must use high-energy signals. Noise in the surroundings must also be considered. The higher the energy of the scanning signals, the higher the probability of discovering the object against the background of noise. On the other hand, increasing the power of the signals causes negative phenomena. First, a sonar working at high impulse power would be harmful to the environment. From the military aspect, it would become easily detectable for the enemy. Thus, there is a problem and scanning signals should be used to cut the power of the impulse of the sonar system while other tactical parameters remain at least at the same level. The given problem is dealt with in depth in Chapter 5.1 of the present paper.

3.2   ACHIEVING RESOLUTION USING LARGE ANGLES

Classically, the formation of beam patterns is viewed at narrow scanning signals. It is known that in the case of phase compensation, the width of the beam pattern gets wider in direct proportion to the way the falling angle of the signal gets larger on the array against the sensor array norm [2][3]. This topic is dealt with in more depth in Chapter 4.3 of the present thesis. According to the requirement of reducing the power of the sonar impulse we must abandon the use of narrow beam scanning signals and introduce spread-spectrum signals (see Chapter 5.1). Thus, the signal processing in the sensor array transfers to a completely other basis and we have to investigate how the spread-spectrum signals behave and how to process them in order to achieve satisfactory or even better results. First and foremost we are interested in those situations where spread-spectrum signals fall on the array at different angles against the norm. What could the resolution of the system be? Mathematical models of the scanning signals and the sensor array should be created to solve this problem and they should be transformed analytically. By investigating the dynamics of the sensor array using different scanning signals it is possible to work out different algorithms for the formation of the beam patterns. In the present work, three different algorithms and indicators of the quality of them are analysed. The problem mentioned above is the main task of the present thesis and is, to a large extent, dealt with in Chapters 5.2-5.8.

3.3 ANALYSIS OF THE METHODS OF OPTIMAL RECEPTION

Estimating the distance and location of objects is the most essential activity in mapping the seabed. To estimate the distance of objects, the system has to realise the section of the ambiguity function $\psi(\tau,0)$, which, as a rule, falls back to optimal reception. Optimal reception is a resource consuming procedure. The algorithm for separating quadrature components is also technically quite complicated. Hence, two tasks follow: Is it possible to effectively integrate the formation of the beam pattern and the optimal reception (Chapters 5.4 and 5.6) and is it possible to abandon the search for the quadrature components by using the modified optimal receiver (Chapter 5.6).

3.4 ESTIMATING THE RESULTS BY MEANS OF MODELLING

Nowadays, several types of mathematical packages MATLAB [22] [23], Mathematica, Maple and MathCad are widely used around the world. One of the primary tasks is to make a choice between the MATLAB and MathCad, which is not dealt with in a separate chapter of the present work, but according to the preliminary estimates, the "MathCad" package appeared to be more suitable (version 13.1) first and foremost, because realising the complicated mathematical expressions is somewhat simpler in MathCad. All the results and graphs presented in this paper have been worked out by means of modelling. This is also valid for the theoretical parts at the beginning of the paper. The printouts of "MathCad" technical files are not integrated into the present work, but are available separately if needed.

3.5 ANALYSIS AND ESTIMATES OF THE REALISATION OPPORTUNITIES

Although the present work is a research paper, a rough estimate of the requirements must be given for realising solutions. This topic is dealt with in Chapter 6. First, this concerns the computer and memory capacity required. Since computer technology has developed quickly, this has enabled us to use such algorithms that were impossible to realise a couple of years ago. Here we admit in advance that the principles applied in the present work will be introduced in sonar and radar systems currently being developed in Estonia.

4 THEORETICAL FOUNDATION OF THE STATEMENT OF THE TASK

4.1 ACOUSTIC WAVES PROPAGATION IN FLUIDS, WAVE EQUATION

This chapter concentrates on fundamental topics in the areas of acoustic wave propagation [2] and will help the reader understand the remaining chapters. Later on linear wave equation derived here will be use at complex aperture theory (chapter 4.2).

Sound waves in environments, such as air and water, are longitudinal waves, that is, the fluid molecules (mass) move back and forth in the direction of wave propagation, producing adjacent regions of compression and rarefaction (expansion).Fluids have the two major characteristics known as elasticity and mass density that are responsible for acoustic (sound) wave propagation. The elasticity, or bulk modulus, of a fluid, which is equal to the reciprocal of its compressibility, causes the fluid to resist being compressed or expanded. It enables the fluid to restore itself to the original (equilibrium) state that it was in before the application of any forces, and determines the potential energy of an infinitesimal volume element of fluid. The mass density of fluid provides inertia and determines the kinetic energy of an infinitesimal volume element of fluid.

In the absence of any applied forces, an infinitesimal volume element of fluid has an equilibrium or ambient density of ρ_0 kilograms per cubic meter, is under an ambient pressure of p_0 pascals (Newton's per square meter), and is at an ambient temperature of T_0. degrees Celsius. The presence of an acoustic (sound) wave produces changes in pressure, velocity, density, and temperature in the fluid, each change being proportional to the amplitude of the wave. The change in pressure from the equilibrium or ambient value p_0 that is due to the presence of an acoustic wave is called the acoustic pressure p. If the amplitude of the acoustic wave is large, perhaps $p \gg p_0$, then nonlinear effects become important. As a result, a nonlinear wave equation must be used to describe the propagation of large amplitude acoustic waves. However, if the amplitude of the acoustic wave is small, so that $p/p_0 \ll 1$, then nonlinear effects become negligible. In further, we shall be concerned with the derivation of the linear wave equation.

Let us assume that fluid particle $dV = dxdydz$ with mass dm is in motion with velocity vector $\mathbf{U}$ (in space and time):

$$\mathbf{U} = U_X\,\hat{x} + U_Y\,\hat{y} + U_Z\,\hat{z} \quad \text{ja} \quad \mathbf{U} = \mathbf{U}(t,\mathbf{r}) = \mathbf{U}(t,x,y,z). \qquad (4.1.1)$$

Total acceleration of an infinitesimal volume element of fluid dV can be expressed as

$$\frac{d}{dt}\mathbf{U} = \frac{\partial}{\partial t}\mathbf{U} + (\mathbf{U} \bullet \nabla)\mathbf{U}, \qquad (4.1.2)$$

where

$$\nabla = \frac{\partial}{\partial x}\hat{x} + \frac{\partial}{\partial y}\hat{y} + \frac{\partial}{\partial z}\hat{z} \qquad (4.1.3)$$

The first term on the right-hand side of Eq. (4.1.2) represents a local acceleration and the second term on the right-hand side represents a convective acceleration. U_X, U_Y ja U_Z are the speeds of the fluid particle dV in the X, Y and Z directions and are given by

$$U_X = \frac{dx}{dt}, U_Y = \frac{dy}{dt}, U_Z = \frac{dz}{dt}. \qquad (4.1.4)$$

Newton's second law of motion states that the force vector $\mathbf{dF}$ is expressed as

$$\mathbf{dF} = dm\frac{d}{dt}\mathbf{U}. \qquad (4.1.5)$$

Newton's second law of motion given by Eq. (4.1.5) and Eq. (4.1.2) can be expressed in scalar form as follows

$$dF_X = dm\frac{d}{dt}U_X, \qquad (4.1.6)$$

$$dF_Y = dm\frac{d}{dt}U_Y, \qquad (4.1.7)$$

$$dF_Z = dm\frac{d}{dt}U_Z. \qquad (4.1.8)$$

and then we take equations of gravitational body forces acting to the fluid particle dV in the X, Y and Z directions. At that, equation (4.1.2) can also be written in scalar form as follows:

$$\frac{d}{dt}U_X = \frac{\partial}{\partial t}U_X + \mathbf{U} \bullet \nabla U_X, \qquad (4.1.9)$$

20

$$\frac{d}{dt}U_Y = \frac{\partial}{\partial t}U_Y + \mathbf{U} \bullet \nabla U_Y, \qquad (4.1.10)$$

$$\frac{d}{dt}U_Z = \frac{\partial}{\partial t}U_Z + \mathbf{U} \bullet \nabla U_Z. \qquad (4.1.11)$$

Taking into account equation of stress tensor (in other words, the ij-th component of stress at a point and dS_j is a corresponding surface area)

$$\sigma_{ij} = \frac{dF_i}{dS_j}, \qquad i,j = 1,2,3....., \qquad (4.1.12)$$

and equations

$$dF_X = (\frac{\partial}{\partial x}\sigma_{XX} + \frac{\partial}{\partial y}\sigma_{XY} + \frac{\partial}{\partial z}\sigma_{XZ} + \rho g_X)dV, \qquad (4.1.13)$$

$$dF_Y = (\frac{\partial}{\partial x}\sigma_{YX} + \frac{\partial}{\partial y}\sigma_{YY} + \frac{\partial}{\partial z}\sigma_{YZ} + \rho g_Y)dV, \qquad (4.1.14)$$

$$dF_Z = (\frac{\partial}{\partial x}\sigma_{ZX} + \frac{\partial}{\partial y}\sigma_{ZY} + \frac{\partial}{\partial z}\sigma_{ZZ} + \rho g_Z)dV, \qquad (4.1.15)$$

$$dm = \rho dV, \qquad (4.1.16)$$

yields the differential equations of motion for a fluid particle dV in the X, Y and Z directions according to:

$$\rho\frac{d}{dt}U_X = \frac{\partial}{\partial x}\sigma_{XX} + \frac{\partial}{\partial y}\sigma_{XY} + \frac{\partial}{\partial z}\sigma_{XZ} + \rho g_X, \qquad (4.1.17)$$

$$\rho\frac{d}{dt}U_Y = \frac{\partial}{\partial x}\sigma_{YX} + \frac{\partial}{\partial y}\sigma_{YY} + \frac{\partial}{\partial z}\sigma_{YZ} + \rho g_Y, \qquad (4.1.18)$$

$$\rho\frac{d}{dt}U_Z = \frac{\partial}{\partial x}\sigma_{ZX} + \frac{\partial}{\partial y}\sigma_{ZY} + \frac{\partial}{\partial z}\sigma_{ZZ} + \rho g_Z. \qquad (4.1.19)$$

g_X, g_Y ja g_Z are the components of the gravitational acceleration vector in the X, Y ja Z directions.

Expressing the nine components of stress σ_{ij} in terms of the nine components of the rate-of-strain tensors as

$$\sigma_{ij} = \left[-P + (\mu_v - \frac{2}{3}\mu)\Delta \right]\delta_{ij} + 2\mu\varepsilon_{ij}, \quad i,j = 1,2,3. \qquad (4.1.20)$$

where

$$P \triangleq -\frac{1}{3}(\sigma_{11} + \sigma_{22} + \sigma_{33}) \qquad \text{-is the normal stress in an ideal fluid at}$$

rest,

$$\mu_v \qquad \text{-volume (bulk) viscosity of the fluid,}$$
$$\mu \qquad \text{-shear viscosity of the fluid,}$$
$$\Delta = \nabla \bullet \mathbf{U} \qquad \text{-local rate of expansion of a fluid particle as it moves,}$$
$$\delta_{ij} \qquad \text{-Kronecker delta,}$$
$$\varepsilon_{ij} \triangleq \frac{1}{2}\left(\frac{\partial}{\partial x_j}U_i + \frac{\partial}{\partial x_i}U_j \right) \qquad \text{-rate-of-strain tensor}$$

and taking into account, that the coefficients μ_v and μ are constants, we obtain the following single vector Navier-Stokes equation of motion (see also [2] Chapter.1.1):

$$\rho\frac{d}{dt}\mathbf{U} = -\nabla P + \rho\mathbf{g} + (\mu_v + \frac{4}{3}\mu)\nabla(\nabla \bullet \mathbf{U}) - \mu\nabla \times (\nabla \times \mathbf{U}). \qquad (4.1.21)$$

Since the velocity vector $\mathbf{U}$ can always be separated into a longitudinal and transversal parts

$$\mathbf{U} = \mathbf{U}_L + \mathbf{U}_T, \qquad (4.1.22)$$

then also the Navier-Stokes equation of motion given by Eq. (4.1.21) can be decomposed into two separate equations as:

$$\rho\frac{d}{dt}\mathbf{U}_L = -\nabla P + (\mu_v + \frac{4}{3}\mu)\nabla^2\mathbf{U}_L - \rho\mathbf{g}_L, \qquad (4.1.23)$$

$$\rho\frac{d}{dt}\mathbf{U}_T = \rho\mathbf{g}_T - \mu\nabla \times (\nabla \times \mathbf{U}_T). \qquad (4.1.24)$$

Fluid motion due to acoustic (sound) waves is longitudinal and compressible. Therefore, the equation of motion given by Eq. (4.1.23) is to be used in the derivation of the linear wave equation.

When an electro-acoustic transducer vibrates, fluid mass will flow due to the compression and expansion of the fluid medium. If fluid mass is being added inside of volume element, then we obtain equation of continuity (conservation of mass)

$$\frac{\partial}{\partial t}\rho + \nabla \bullet (\rho \mathbf{U}) = \rho Q .$$
(4.1.25)

Here Q is the volume flow rate per unit volume of fluid due to the sound source (i.e. Q has units of inverse seconds).

The pressure P, which is the instantaneous or total pressure in pascals (Pa), can be decomposed as follows

$$P = p_0 + p$$
(4.1.26)

where p_0 is the equilibrium or ambient pressure and p is called the acoustic pressure. The acoustic pressure represents the change in pressure in the fluid medium from the ambient value due to the presence of an acoustic (sound) wave. The same be valid about the fluid density ρ and the relative change in the density of the fluid s expressed as

$$s = \frac{\rho - \rho_0}{\rho_0} .$$
(4.1.27)

Here ρ_0 is the equilibrium or ambient density of the fluid. The compression of a fluid due to the passage of an acoustic (sound) wave is best described as being adiabatic. Therefore, the adiabatic equation of state will be used in the derivation of the linear wave equation

$$p \approx s / K_E \ \text{ or } \ p \approx B_E s .$$
(4.1.28)

Measure $B_E = 1 / K_E$ is the adiabatic bulk modulus (Pa) and measure K_E is the adiabatic compressibility of the fluid with units of inverse pascals

$$K_E = \frac{1}{\gamma p_0} .$$
(4.1.29)

Here γ is the ratio of the specific heat at constant pressure to the specific heat at constant volume of the gas and defined as the heat necessary to raise the temperature of a unit mass of fluid one degree when the fluid is kept at a constant pressure and at a constant volume. Adiabatic speed of sound in liquids is given by

$$c = \sqrt{\frac{1}{K_E \rho_0}} = \sqrt{\frac{B_E}{\rho_0}} . \tag{4.1.30}$$

The fluid-particle velocity vector $\mathbf{U}_L$ Eg. (4.1.23) can be decomposed into two separate vectors (the equilibrium or ambient fluid velocity vector $\mathbf{u}_0$ and the acoustic fluid velocity vector $\mathbf{u}$) as follows:

$$\mathbf{U}_L = \mathbf{u}_0 + \mathbf{u} . \tag{4.1.31}$$

Let assume that the fluid medium is at rest in the absence of an acoustic wave, that is $\mathbf{u}_0 = 0$

$$\mathbf{U}_L = \mathbf{u} . \tag{4.1.32}$$

On the assumption of Eq. (4.1.23) and using Eqs. (4.1.32),(4.1.2),(4.1.27), it is possible to derive a linearized version of the Navier-Stokes equation of motion Eg. (4.1.23), which is valid for small-amplitude acoustic signals respectively

$$\rho_0 \frac{\partial}{\partial t} \mathbf{u} \approx -\nabla p + \mu' \nabla (\nabla \bullet \mathbf{u}) + \rho_0 s \mathbf{g}_L , \tag{4.1.33}$$

$$\mu' = \mu_v + \frac{4}{3} \mu . \tag{4.1.34}$$

If we refer back to Eg. (4.1.31) and assume that the equilibrium density ρ_0 is not a function of time, then

$$\frac{\partial}{\partial t} \rho = \rho_0 \frac{\partial}{\partial t} s , \tag{4.1.35}$$

and we can derive a simplified version of the equation of continuity (4.1.25)

$$\frac{\partial}{\partial t} s + \frac{\nabla \rho_0}{\rho_0} \bullet \mathbf{u} + \nabla \bullet \mathbf{u} \approx Q , \tag{4.1.36}$$

Now we will use Eqs. (4.1.33) and (4.1.36) as basis for the derivation of the linear

wave equation and the adiabatic equation of state (on the assumption of Eqs, (4.1.28) and (4.1.30))

$$p \approx \rho_0 s c^2 . \qquad (4.1.37)$$

We must begin by eliminating the acoustic pressure p from the linearized Navier-Stokes equation of motion given by Eq. (4.1.33) Taking the gradient of both sides of the equation of state given by Eq. (4.1.37) yields

$$\nabla p \approx 2\rho_0 s c \nabla c + c^2 \nabla(\rho_0 s) . \qquad (4.1.38)$$

Substituting Eq. (4.1.38) into Eq. (4.1.33), taking the partial derivate with respect to time t and it is assumed that μ', ρ_0, c ja $\mathbf{g}_L$ are not functions of time and dividing both sides of the resulting equation by $\rho_0 c^2$, we obtain

$$\frac{1}{c^2}\frac{\partial^2}{\partial t^2}\mathbf{u} \approx \left[-2\frac{\nabla c}{c} - \frac{\nabla \rho_0}{\rho_0} + \frac{\mathbf{g}_L}{c^2} \right]\frac{\partial s}{\partial t} - \nabla \frac{\partial s}{\partial t} + \frac{\mu'}{\rho_0 c^2}\frac{\partial}{\partial t}\nabla(\nabla \bullet \mathbf{u}) . \qquad (4.1.39)$$

Since the entire first term on the right-hand side of Eq. (4.1.39) involving the square brackets is negible compared to the second term (in case of $c = 1500\ m/s$, $f = 1 - 1000\ Hz$) Eq. (4.1.39) reduces to

$$\frac{1}{c^2}\frac{\partial^2}{\partial t^2}\mathbf{u} \approx -\nabla \frac{\partial s}{\partial t} + \frac{\mu'}{\rho_0 c^2}\frac{\partial}{\partial t}\nabla(\nabla \bullet \mathbf{u}) , \qquad (4.1.40)$$

and upon substituting Eqs. (4.1.36) into Eq. (4.1.40) and replacing $\mathbf{u} = \nabla \varphi$ (φ-is the scalar velocity potential), we obtain

$$\nabla(\nabla^2 \varphi) + \nabla\left(\frac{\nabla \rho_0}{\rho_0} \bullet \nabla \varphi \right) + \frac{\mu'}{\rho_0 c^2}\nabla\frac{\partial}{\partial t}\nabla^2 \varphi - \frac{1}{c^2}\nabla\frac{\partial^2}{\partial t^2}\varphi \approx \nabla Q . \qquad (4.1.41)$$

Estimating the magnitudes of the elements of the velocity potential φ on Eq. (4.1.4) (in case of $c = 1500\ m/s$, $f = 1 - 1000\ Hz$. See also [2], pages 30-33.), we can write

$$\frac{\mu'}{\rho_0 c^2}\nabla\frac{\partial}{\partial t}\nabla^2 \varphi \approx \nabla\left(\frac{\mu'}{\rho_0 c^2}\frac{\partial}{\partial t}\nabla^2 \varphi \right) \qquad (4.1.42)$$

and

$$\frac{1}{c^2}\nabla\frac{\partial^2}{\partial t^2}\varphi \approx \nabla\left(\frac{1}{c^2}\frac{\partial^2}{\partial t^2}\varphi\right). \qquad (4.1.43)$$

Substituting Eqs. (4.1.42) and (4.1.43) into Eq. (4.1.41), we obtain

$$\nabla\left[\nabla^2\varphi + \frac{\nabla\rho_0}{\rho_0}\bullet\nabla\varphi + \frac{\mu'}{\rho_0 c^2}\frac{\partial}{\partial t}\nabla^2\varphi - \frac{1}{c^2}\nabla\frac{\partial^2}{\partial t^2}\varphi\right] \approx \nabla Q. \qquad (4.1.44)$$

Since in the case of a homogeneous fluid medium the speed of sound and equilibrium density are constants and gradients of c and ρ_0 are zero vectors, we obtain from Eq. (4.1.44) the linear wave equation for small-amplitude acoustic signals in terms of the scalar velocity potential $\varphi(t,\mathbf{r})$ with units of square meters per second (m^2/s).

$$\left[1 + \frac{\mu'}{\rho_0(\mathbf{r})c^2(\mathbf{r})}\frac{\partial}{\partial t}\right]\nabla^2\varphi(t,\mathbf{r}) - \frac{1}{c^2(\mathbf{r})}\frac{\partial^2}{\partial t^2}\varphi(t,\mathbf{r}) \approx x_M(t,\mathbf{r}). \qquad (4.1.45)$$

In the case of an ideal fluid where there is no viscosity Eq.(4.1.45) reduces to

$$\nabla^2\varphi(t,\mathbf{r}) - \frac{1}{c^2(\mathbf{r})}\frac{\partial^2}{\partial t^2}\varphi(t,\mathbf{r}) \approx x_M(t,\mathbf{r}). \qquad (4.1.46)$$

Here

$$x_M(t,\mathbf{r}) = Q(t,\mathbf{r}) \qquad (4.1.47)$$

is the input acoustic signal to the fluid medium in inverse seconds, and represents the volume flow rate per unit volume of fluid at time t and position $\mathbf{r} = (x, y, z)$. Beforehand we can say that the given equation will associate the acoustic output signal of the transmitting aperture $x_M(t,\mathbf{r})$ with the input signal of the receiving aperture.

Relationship between the acoustic pressure and the scalar velocity potential is expressed by formula

$$\left[1 + \frac{\mu'}{\rho_0(\mathbf{r})c^2(\mathbf{r})}\frac{\partial}{\partial t}\right]p(t,\mathbf{r}) \approx -\rho_0(\mathbf{r})\frac{\partial}{\partial t}\varphi(t,\mathbf{r}) + \mu' x_M(t,\mathbf{r}). \qquad (4.1.48)$$

In case of an ideal fluid Eq. (4.1.48) reduce to

26

$$p(t,\mathbf{r}) \approx -\rho_0(\mathbf{r})\frac{\partial}{\partial t}\varphi(t,\mathbf{r}). \tag{4.1.49}$$

When the source distribution $x_M(t,\mathbf{r})$ in location $\mathbf{r} = (x,y,z)$ has a time-harmonic dependence, that is,

$$x_M(t,\mathbf{r}) = x_{f,M}(\mathbf{r})\exp(+j2\pi ft) \tag{4.1.50}$$

where $x_{f,M}(\mathbf{r})$ is the spatial-dependent part of the source distribution and f is the frequency in hertz, then the resulting velocity potential also has a time-harmonic dependence, that is,

$$\varphi(t,\mathbf{r}) = \varphi_f(\mathbf{r})\exp(+j2\pi ft). \tag{4.1.51}$$

Here $\varphi_f(\mathbf{r})$ is the spatial-dependent part of the velocity potential. Therefore, upon substituting Eqs. (4.1.50) and (4.1.51) into the time-dependent wave equation given by Eq. (4.1.45), we obtain the following time-independent lossy Helmholtz equation

$$\nabla^2\varphi_f(\mathbf{r}) + K^2(\mathbf{r})\varphi_f(\mathbf{r}) \approx \frac{x_{f,M}(\mathbf{r})}{1+j\omega\tau(\mathbf{r})}. \tag{4.1.52}$$

Here

$$K(\mathbf{r}) = \frac{\omega}{c(\mathbf{r})}\frac{1}{\sqrt{1+j\omega\tau(\mathbf{r})}} \tag{4.1.53}$$

is the complex wave number in radians per meter and

$$\tau(\mathbf{r}) = \frac{\mu'}{\rho_0(\mathbf{r})c^2(\mathbf{r})}. \tag{4.1.54}$$

In the case of sea water, on frequencies below 50 *kHz,* it can be seen that $\omega\tau(\mathbf{r}) \ll 1$ and Hemholtz equation reduce to

$$\nabla^2\varphi_f(\mathbf{r}) + K^2(\mathbf{r})\varphi_f(\mathbf{r}) \approx x_{f,M}(\mathbf{r}). \tag{4.1.55}$$

Substituting the solution $\varphi_f(\mathbf{r})$ and Eq. (4.1.55) into Eq. (4.1.51) will yield a time-harmonic solution of the wave equation given by Eq. (4.1.45). Time harmonic solutions are very important, because solutions of the wave equation for source

distributions with arbitrary time dependence can be obtained from time-harmonic solutions by using Fourier transform techniques. Complex wave number can be decomposed into real and imaginary part

$$K(\mathbf{r}) = k(\mathbf{r}) - j\alpha(\mathbf{r}), \qquad (4.1.56)$$

Whrere $k(\mathbf{r})$ and $\alpha(\mathbf{r})$ are the real wave number and real attenuation coefficient respectively. The phase speed (*m/s*) is given by

$$c_p(\mathbf{r}) = c(\mathbf{r})\sqrt{2}\left[\frac{1+\left[\omega\tau(\mathbf{r})\right]^2}{\sqrt{1+\left[\omega\tau(\mathbf{r})\right]^2}+1}\right]^{1/2}. \qquad (4.1.57)$$

Therefore, the real wave number can be expressed as

$$k(\mathbf{r}) = \frac{\omega}{c_p(\mathbf{r})}. \qquad (4.1.58)$$

Real attenuation coefficient in neper per meter is given by

$$\alpha(\mathbf{r}) = \frac{\omega}{c(\mathbf{r})}\frac{1}{\sqrt{2}}\left[\frac{\sqrt{1+\left[\omega\tau(\mathbf{r})\right]^2}-1}{1+\left[\omega\tau(\mathbf{r})\right]^2}\right]^{1/2}. \qquad (4.1.59)$$

The real attenuation coefficient $\alpha(\mathbf{r})$ is responsible for the attenuation of sound waves in viscous fluids. In the case of an ideal fluid where there is no viscosity $\alpha(\mathbf{r}) = 0$. In the case of real, viscous fluids, the phase speed $c_p(\mathbf{r})$ is not equal to the speed of sound $c(\mathbf{r})$. However, in the case of sea water $c_p(\mathbf{r}) \approx c(\mathbf{r})$ since $\omega\tau(\mathbf{r}) \ll 1$ for the typical range of frequecies used in underwater acoustics.

4.2   COMPLEX APERTURE THEORY

This chapter discusses the complex aperture theory and will help the reader understand the remaining chapters because the array theory (chapter 4.3) is based on the complex aperture theory [2].

We consider that the fluid medium is as linear filter and free-space spatial impulse response (Green function) is the solution of the linear wave equation Eq. (4.1.46). We will look the different types of apertures, aperture functions and near- and

farfield directivity functions.

In the field of optics, a rectangular or circular hole in an opaque screen is referred to as a rectangular or circular aperture. In electromagnetic, the meaning of the word „aperture" has been extended to refer either a single electromagnetic antenna or array of electromagnetic antennas. Similarly, in acoustic, the word „aperture" is used to refer to either a single electroacoustic transducer or an array of electroacoustic transducers. Aperture can be active as a transmitter (Fig. 4.2.1) or passive as a receiver (Fig. 4.2.2).
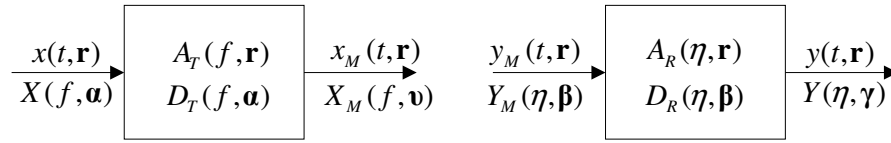
$$\xrightarrow[X(f,\boldsymbol{\alpha})]{x(t,\mathbf{r})} \boxed{\begin{array}{c} A_T(f,\mathbf{r}) \\ D_T(f,\boldsymbol{\alpha}) \end{array}} \xrightarrow[X_M(f,\boldsymbol{\upsilon})]{x_M(t,\mathbf{r})} \qquad \xrightarrow[Y_M(\eta,\boldsymbol{\beta})]{y_M(t,\mathbf{r})} \boxed{\begin{array}{c} A_R(\eta,\mathbf{r}) \\ D_R(\eta,\boldsymbol{\beta}) \end{array}} \xrightarrow[Y(\eta,\boldsymbol{\gamma})]{y(t,\mathbf{r})}$$

Fig. 4.2.1. Transmit aperture   Fig. 4.2.2. Receive aperture

In case of the transmit aperture

$x(t,\mathbf{r})$ -Input electrical signal at time t, in spatial location $\mathbf{r} = (x, y, z)$.

$$X(f,\boldsymbol{\alpha}) = F_t F_{\mathbf{r}} \left\{ x(t,\mathbf{r}) \right\} = \int\limits_{-\infty}^{\infty} \int\limits_{-\infty}^{\infty} x(t,\mathbf{r}) \exp(-j2\pi ft) \exp(+j2\pi \boldsymbol{\alpha} \bullet \mathbf{r}) dt d\mathbf{r} \,.$$

$A_T(f,\mathbf{r})$ - Complex frequency response at spatial location $\mathbf{r}$ of the transmit aperture (complex transmit aperture function). If we treat the aperture as a linear filter with impulse response $\alpha_T(t,\mathbf{r})$, then complex frequency response can be expressed as

$$A_T(f,\mathbf{r}) = F_t \left\{ \alpha_T(t,\mathbf{r}) \right\} = \int\limits_{-\infty}^{\infty} \alpha_T(t,\mathbf{r}) \exp(-j2\pi ft) dt \,. \qquad (4.2.1)$$

$D_T(f,\boldsymbol{\alpha})$ - Far-field directivity function of the complex transmit aperture function. Is given by

$$D_T(f,\boldsymbol{\alpha}) = F_{\mathbf{r}} \left\{ A_T(f,\mathbf{r}) \right\} = \int\limits_{-\infty}^{\infty} A_T(f,\mathbf{r}) \exp(+j2\pi \boldsymbol{\alpha} \bullet \mathbf{r}) d\mathbf{r} \,. \qquad (4.2.2)$$

$x_M(t,\mathbf{r})$ - The output acoustic signal from the transmit aperture, which is also the input acoustic signal to the fluid medium, can be expressed as follows

$$x_M(t,\mathbf{r}) = \int\limits_{-\infty}^{\infty} X(f,\mathbf{r})A_T(f,\mathbf{r})\exp(+j2\pi ft)df , \qquad (4.2.3)$$

where

$$X(f,\mathbf{r}) = F_t\{x(t,\mathbf{r})\} = \int\limits_{-\infty}^{\infty} x(t,\mathbf{r})\exp(-j2\pi ft)dt .$$

$X_M(f,\mathbf{v})$-The complex frequency and angular spectrum of the input acoustic signal to the fluid medium can be expressed as

$$X_M(f,\mathbf{v}) = \int\limits_{-\infty}^{\infty} X(f,\boldsymbol{\alpha})D_T(f,\mathbf{v}-\boldsymbol{\alpha})d\boldsymbol{\alpha} . \qquad (4.2.4)$$

In the given expressions, values $\boldsymbol{\alpha}=(f_x,f_y,f_z)$, $\mathbf{v}=(\upsilon_x,\upsilon_y,\upsilon_z)$, $\boldsymbol{\beta}=(\beta_x,\beta_y,\beta_z)$ and $\boldsymbol{\gamma}=(\gamma_x,\gamma_y,\gamma_z)$ are the three dimensional vectors of the spatial frequencies in the X, Y and Z directions. Thus we can write

$$f_x = \frac{u}{\lambda} \quad u = \sin\theta\cos\psi , \qquad (4.2.5)$$

$$f_x = \frac{\upsilon}{\lambda} \quad \upsilon = \sin\theta\sin\psi , \qquad (4.2.6)$$

$$f_x = \frac{w}{\lambda} \qquad\qquad w = \cos\theta . \qquad (4.2.7)$$

In case of the receive aperture the situation is analogous. Therefore $y_M(t,\mathbf{r})$ is input acoustic signal to the receive aperture at time t and spatial location $\mathbf{r}$.

The output acoustic signal from the transmit aperture $x_M(t,\mathbf{r})$ and the input acoustic signal to the receive aperture $y_M(t,\mathbf{r})$ are associated with the linear wave equation

$$\nabla^2 y_M(t,\mathbf{r}) - \frac{1}{c^2(\mathbf{r})}\frac{\partial^2}{\partial t^2}y_M(t,\mathbf{r}) = x_M(t,\mathbf{r}) . \qquad (4.2.8)$$

Hence $y_M(t,\mathbf{r})$ is the solution of that equation

$$y_M(t,\mathbf{r}) = \int\limits_{-\infty}^{\infty}\int\limits_{-\infty}^{\infty} x_M(t_0,\mathbf{r}_0)h_M(t,\mathbf{r};t_0,\mathbf{r}_0)dt_0 d\mathbf{r}_0 , \qquad (4.2.9)$$

where $h_M(t,\mathbf{r};t_0,\mathbf{r}_0)$ is free-space spatial impulse response of the fluid medium „**Green's function**".

$Y_M(\eta,\boldsymbol{\beta})$ is the complex frequency (η) and angular spectrum of the output acoustic signal from the fluid medium expressed as

$$Y_M(\eta,\boldsymbol{\beta}) = F_t F_{\mathbf{r}}\{y_M(t,\mathbf{r})\} = \int\limits_{-\infty}^{\infty}\int\limits_{-\infty}^{\infty} y_M(t,\mathbf{r})\exp(-j2\pi\eta t)\cdot$$
$$\cdot\exp(+j2\pi\boldsymbol{\beta}\bullet\mathbf{r})dtd\mathbf{r} \qquad (4.2.10)$$

When transfer function of the fluid medium $H_M(t,\mathbf{r};f,\mathbf{v})$ and its space-time Fourier transmission $B(\phi,\mathbf{k};f,\mathbf{v}) \equiv F_t F_{\mathbf{r}}\{H(t,\mathbf{r};f,\mathbf{v})\}$ is used, we can find associations between spectrums of the input and output acoustic signals ($Y_M(\eta,\boldsymbol{\beta})$, $X_M(f,\mathbf{v})$). Here ϕ is the speed of changes of the transfer function in time in hertz and $\mathbf{k} = (k_x,k_y,k_z)$ is the speed of the changes of the corresponding spatial frequencies in time. See also [2] chapters 9.2.and 9.3. Similarly to the transmit aperture we can write formulas for the receive aperture as follows:

$$A_R(\eta,\mathbf{r}) = F_t\{\alpha_R(t,\mathbf{r})\} = \int\limits_{-\infty}^{\infty}\alpha_R(t,\mathbf{r})\exp(-j2\pi\eta t)dt, \qquad (4.2.11)$$

$$D_R(\eta,\boldsymbol{\beta}) = F_{\mathbf{r}}\{A_R(\eta,\mathbf{r})\} = \int\limits_{-\infty}^{\infty} A_R(\eta,\mathbf{r})\exp(+j2\pi\boldsymbol{\beta}\bullet\mathbf{r})d\mathbf{r}. \qquad (4.2.12)$$

Output electrical signal from the receive aperture is given by

$$y(t,\mathbf{r}) = \int\limits_{-\infty}^{\infty} Y_M(\eta,\mathbf{r})A_R(\eta,\mathbf{r})\exp(+j2\pi\eta t)d\eta, \qquad (4.2.13)$$

where

$$Y_M(\eta,\mathbf{r}) = F_t\{y_M(t,\mathbf{r})\} = \int\limits_{-\infty}^{\infty} y_M(t,\mathbf{r})\exp(-j2\pi\eta t)dt. \qquad (4.2.14)$$

The complex frequency and angular spectrum of the output electrical signal from the receive aperture is given by

$$Y(\eta,\boldsymbol{\gamma}) = \int\limits_{-\infty}^{\infty} Y_M(\eta,\boldsymbol{\beta})D_R(\eta,\boldsymbol{\gamma}-\boldsymbol{\beta})d\boldsymbol{\beta}, \qquad (4.2.15)$$

or

$$Y(\eta,\gamma) = F_t F_{\mathbf{r}}\{y(t,\mathbf{r})\} = \int\limits_{-\infty}^{\infty}\int\limits_{-\infty}^{\infty} y(t,\mathbf{r})\exp(-j2\pi\eta t)\cdot$$
$$\cdot\exp(+j2\pi\gamma\bullet\mathbf{r})dtd\mathbf{r} \tag{4.2.16}$$

By approximating the time-independent free-space Green's function

$$g_f(\mathbf{r}\,|\,\mathbf{r}_0) \triangleq -\frac{\exp(-jk|\mathbf{r}-\mathbf{r}_0|)}{4\pi|\mathbf{r}-\mathbf{r}_0|} \tag{4.2.17}$$

via Fresnel expansion

$$g_f(\mathbf{r}\,|\,\mathbf{r}_0) \triangleq -\frac{\exp(-jkr)}{4\pi r}\exp(+jk\,\hat{r}\bullet\mathbf{r}_0)\exp(-jk\frac{r_0^2}{2r}) \tag{4.2.18}$$

and Fraunhofer expansion

$$g_f(\mathbf{r}\,|\,\mathbf{r}_0) \triangleq -\frac{\exp(-jkr)}{4\pi r}\exp(+jk\,\hat{r}\bullet\mathbf{r}_0), \tag{4.2.19}$$

both the near-field and far-field directivity functions or beam patterns can be derived for complex apertures. By using the Fresnel expansion, we shall derive a criterion that establishes the boundary between the near-field and far-field regions of an aperture as

$$1.356R < r < \pi R^2/\lambda, \tag{4.2.20}$$

$$r > \pi R^2/\lambda > 1.356R. \tag{4.2.21}$$

Here R is the maximum value of the radial distance to a source point. (for example circle radius in case of circular piston). Value $1.356R$ is very important because it denote the minimal distance from aperture from where Fresnel expansion be valid. The near-field directivity function of complex transmit aperture (based on the Fresnel approximation) is given by

$$D_T(f,r,\mathbf{\alpha}) = F_{\mathbf{r}_0}\left\{A_T(f,\mathbf{r}_0)\exp\left(-jk\frac{r_0^2}{2r}\right)\right\}$$
$$= \int\limits_{-\infty}^{\infty} A_T(f,\mathbf{r}_0)\exp\left(-jk\frac{r_0^2}{2r}\right)\exp(+j2\pi\mathbf{\alpha}\bullet\mathbf{r}_0)d\mathbf{r}_0 \tag{4.2.22}$$

Here:

$k = 2\pi / \lambda$ -wave number in radians per meter,

$\exp\left(-jk\dfrac{r_0^2}{2r}\right)$ -quadratic phase factor,

r - magnitude of the position vector to a field point,

r_0 - magnitude of the position vector to a source point.

The far-field directivity function of the complex transmit and receive apertures are given by:

$$D_T(f,\boldsymbol{\alpha}) = F_{\mathbf{r}_0}\left\{A_T(f,\mathbf{r}_0)\right\} = \int_{-\infty}^{\infty} A_T(f,\mathbf{r}_0)\exp(+j2\pi\boldsymbol{\alpha}\bullet\mathbf{r}_0)d\mathbf{r}, \quad (4.2.23)$$

$$D_R(\eta,\boldsymbol{\beta}) = F_{\mathbf{r}_R}\left\{A_R(\eta,\mathbf{r}_R)\right\} = \int_{-\infty}^{\infty} A_R(\eta,\mathbf{r}_R)\exp(+j2\pi\boldsymbol{\beta}\bullet\mathbf{r}_R)d\mathbf{r}. \quad (4.2.24)$$

We can see, that the far-field directivity function can be obtained from the near-field directivity function (Eq. 4.2.22) by neglecting the quadratic phase factor. Thus, we can use the near-field directivity function to calculate the far-field directivity function but the opposite case is not possible. The complex transmit aperture function is given by

$$A_T(f,\mathbf{r}_0) = F_{\boldsymbol{\alpha}}^{-1}\left\{D_T(f,\boldsymbol{\alpha})\right\} = \int_{-\infty}^{\infty} D_T(f,\boldsymbol{\alpha})\exp(-j2\pi\boldsymbol{\alpha}\bullet\mathbf{r}_0)d\boldsymbol{\alpha}. \quad (4.2.25)$$

Now we shall drop subscript notation T and R which has been used to distinguish between transmit and receive apertures, respectively, since we shall now be concerned with apertures in general. The complex aperture function can be expressed as

$$A(f,\mathbf{r}_a) = a(f,\mathbf{r}_a)\exp\left[+j\theta(f,\mathbf{r}_a)\right], \quad (4.2.26)$$

where $a(f,\mathbf{r}_a)$ is the amplitude and $\theta(f,\mathbf{r}_a)$ is the phase of the complex frequency response at spatial location $\mathbf{r}_a$. Both are real functions.

Consider the case of a linear aperture of length L lying along the X axis. The far-field directivity function is given by

$$D(f,f_x) = F_{x_a}\left\{A(f,x_a)\right\} = \int_{-L/2}^{L/2} A(f,x_a)\exp(+j2f_x x_a)dx_a, \quad (4.2.27)$$

where x_a is a positions on the aperture and aperture function can be rewritten as

$$A(f,x_a) = a(f,x_a)\exp\left[+j\theta(f,x_a)\right].\tag{4.2.28}$$

The normalized far-field beam patterns at different amplitude windows in case of the complex frequency response of the transducer is equal to the amplitude response, perhaps $\theta(f,x_a)=0$, $A(f,x_a)=a(f,x_a)$ be expressed in general $D_N(f,f_x) = F_{x_a}\{a(f,x_a)\}/D_{\max}$.

In case of the rectangular amplitude window

$$D_N(f,f_x) = \mathrm{sinc}(f_x L),\tag{4.2.29}$$

$$D_N(f,u) = \mathrm{sinc}\left(\frac{L}{\lambda}u\right),\tag{4.2.30}$$

$$D_N(f,\theta,\psi) = \mathrm{sinc}\left(\frac{L}{\lambda}\sin\theta\cos\psi\right).\tag{4.2.31}$$

The width of the main lobe of the normalized (and unnormalized) far-field beam pattern depends on the ratio L/λ. Therefore, the beamwidth is directly proportional to the wavelength λ and inversely proportional to the length L of the aperture (transducer). As a result, the beamwidth can be decreased by keeping the length L of the aperture constant while increasing the frequency f, or by keeping the frequency constant while increasing the length L of the aperture.

Fig. 4.2.3 shows the polar plot of the magnitude of the normalized horizontal far-field beam pattern of the rectangular amplitude window. The main lobe is quite tight but amount of the sidelobes and their level is a bit high. In case of the triangular amplitude window the amplitude of the complex frequency response of the transducer is triangular in shape along the length L of the transducer. The main lobe of the beam pattern of the triangular window is wider than that of the rectangular amplitude window, but the sidelobe levels are lower. The width of the main lobe of the Hamming beam pattern (see Fig. 4.2.4) is again wider than that of the rectangular window but the sidelobe levels are very low. Also cosine, Hanning, and Blackman amplitude windows can be used to obtain the far-field directivity functions. All diagrams are modelled by using package MathCad.
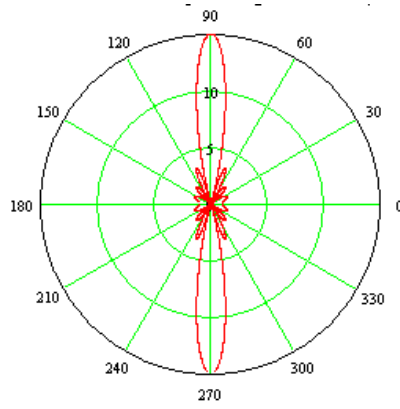
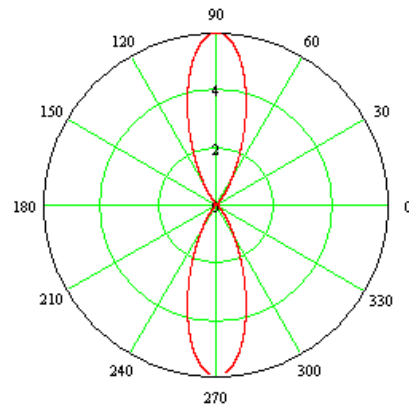Fig. 4.2.3 Beam pattern of the rectangular window   Fig. 4.2.4 Beam pattern of the Hamming window

In general, if an amplitude window is an even function of a spatial coordinate, then the corresponding far-field beam pattern will be a real and even function of the appropriate direction cosine. Similary, if an amplitude window is an odd functionof a spatial coordinate, then the corresponding far-field beam pattern will be an imaginary and odd function of the appropriate direction cosine. The most common measure of horizontal beamwidth

$$\Delta\theta = 2\sin^{-1}\left(\frac{\Delta u}{2}\right), \frac{\Delta u}{2} \leq 1 \qquad (4.2.32)$$

and vertical beamwidth

$$\Delta\Psi = 2\sin^{-1}\left(\frac{\Delta u}{2}\right), \frac{\Delta u}{2} \leq 1, \qquad (4.2.33)$$

is the 3-dB beamwidth. The 3-dB beamwidth $\Delta u = u_+ - u_-$ (see [2] Fig. 6.3.15).

Phase response of a linear aperture is responsible for beam steering or beam tilting. Thus, the normalized far-field beam pattern is given by

$$D'_N(f, f_x) = F_{x_a}\left\{a(f, x_a)\exp\left[+j\theta(f, x_a)\right]\right\}/D_{\max}. \qquad (4.2.34)$$

Now, assume that the phase response across the aperture is a linear function of x_a, that is $\theta(f, x_a) = \theta_1(f)x_a$, where $\theta_1(f) = -2\pi f_x$ and $f_x = u/c$, we can write

35

$$F_{x_a}\left\{a(f,x_a)\exp\left[+j\theta 2\pi f_x' x_a\right]\right\}/D_{\max}=D_N(f,f_x-f_x'),\qquad(4.2.35)$$

$$D_N'(f,u)=D(f,u-u').\qquad(4.2.36)$$

Therefore, a linear phase response across the length of the aperture will cause the beam to be steered in the direction $u=u'$ in direction-cosine space, which is equivalent to steering or tilting beam pattern to $\theta=\theta'$ in polar coordinates. When the beam pattern is steered, its shape and beamwidth remain unchanged when plotted as a function of direction cosine (see [2] Fig. 6.3-19). However, they do change when the beam pattern is plotted as a function of the spherical angles. When a far-field beam pattern is steered or tilted, its beamwidth will increase from a minimum value at broadside to a maximum value at end fire. Achieving resolution using large angles is one of the statements of the task of the present work. On Figs. 4.2.5 and 4.2.6 are presented the far field beam patterns in case of different angles (modelled with package MathCad).
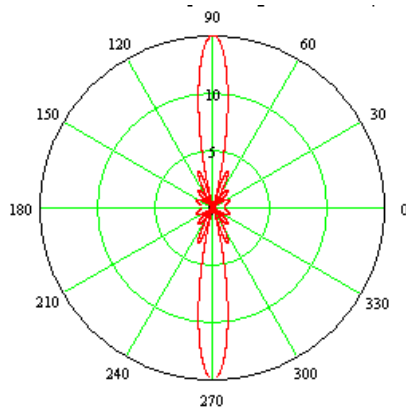
Fig. 4.2.5 Beam pattern at 0^0 Fig. 4.2.6 Beam pattern at 60^0
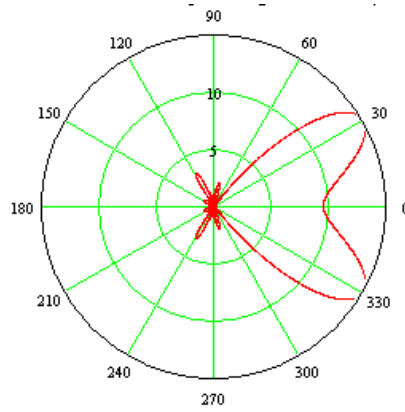
When the phase response across the length of the aperture is a quadratic function of x_a, that is $\theta(f,x_a)=\theta_2(f)x_a^2$, then a far-field beam pattern can be focused to the near-field. In principle, the quadratic phase variation compensates for wavefront curvature at near-field distances from the aperture.

In case of a planar aperture of arbitrary shape lying in the *XY* plane, we obtain the following two-dimensional spatial Fourier transform expression for the far-field directivity function

$$D(f, f_x, f_y) = F_{x_a} F_{y_a} \left\{ A(f, x_a, y_a) \right\} =$$

$$= \int\limits_{-\infty}^{\infty} \int\limits_{-\infty}^{\infty} A(f, x_a, y_a) \exp(+j2\pi(f_x x_a + f_y y_a) dx_a dy_a \quad , \qquad (4.2.37)$$

where x_a is a position at x axis direction and y_a is a position at y axis direction and aperture function is given by

$$A(f, x_a, y_a) = a(f, x_a, y_a) \exp\left[+j\theta(f, x_a, y_a) \right]. \qquad (4.2.38)$$

Now normalized far-field beam pattern can be expressed as ([2] Fig. 6.5.3).

$$F_{x_a} F_{y_a} \left\{ a(f, x_a, y_a) \exp\left[+j2\pi(f_x' x_a + f_y' y_a) \right] \right\} / D_{max} = \qquad (4.2.39)$$

$$= D_N(f, f_x - f_x', f_y - f_y')$$

$$D_N'(f, u, v) = D(f, u - u', v - v') / D_{max} \qquad (4.2.40)$$

If the complex aperture function is separable in the rectangular coordinates, then the corresponding far-field beam pattern is equal to the product of the individual beam patterns:

$$D(f, f_x, f_y) = D_X(f, f_x) D_Y(f, f_y). \qquad (4.2.41)$$

One of the most common examples of a planar aperture lying in the *XY* plane is a single electroacoustic transducer, rectangular in shape (rectangular piston). Analogous to the rectangular piston, another very common example of a planar aperture lying in the *XY* plane is a single electroacoustic transducer, circular in shape with radius *a* (circular piston). By comparing a circular piston with rectangular piston, it can be seen that a circular piston will have a slightly larger beamwidth. However, the levels of the first sidelobes of the normalized far-field directivity functions of a circular piston are less than at rectangular piston.

Directivity is basically a measure of the beamwidth and sidelobe levels of a far-field beam pattern. For example, in transmit mode, it is a measure of its ability to concentrate the available acoustic power into a preferred direction. The general expression for the directivity is given by

$$D = 4\pi / \int\limits_{0}^{2\pi} \int\limits_{0}^{2\pi} \left| D_N(f, \theta, \psi) \right|^2 \sin\theta d\theta d\psi. \qquad (4.2.42)$$

The decibel equivalent of the directivity is directivity index

$$\mathbf{DI} \equiv 10\log_{10} D\, dB. \qquad\qquad (4.2.43)$$

For an omnidirectional source D=1 ja $\mathbf{DI}$=0. In general, the directivity of an aperture increases with increasing frequency or physical size, since the beamwidth of the corresponding far-field beam pattern decreases with increasing frequency or size.

4.3   ARRAY THEORY

This chapter gives the basic theory about the sensor arrays which are constructed from different apertures. I will explain how the amount of sensors and their complex weight are affected to the beamforming in the near- and far-field [2] [3].

An array can be thought as a sampled aperture, that is, an aperture that is excited only at points or in localized areas. Consider a linear array lying along the X axis. Amount of elements N can be even or odd. In the case of even number of elements the complex frequency response (complex aperture function) of this array can be expressed as

$$A(f, x_a) = \sum_{n=1}^{N/2} \left[c_{-n}(f)e_{-n}(f, x_a - x_{-n}) + c_n(f)e_n(f, x_a - x_n) \right]. \qquad (4.3.1)$$

Here $c_n(f)$ is the frequency-dependent complex weight associated with element n and $e_n(f, x_a)$ is the complex frequency response (complex aperture function) of element n. The complex frequency response of the whole array is equal to the linear superposition of the complex-weighted frequency responses of all the individual elements in the array. The complex weights are used to control the complex frequency response of the array and, thus, the array's far-field directivity function via amplitude and phase. In general far-field beam battern can be expressed as

$$D(f, f_x) = E(f, f_x)S(f, f_x). \qquad\qquad (4.3.2)$$

Here $E(f, f_x) = F_{x_a}\{e(f, x_a)\}$ is the far-field beam pattern of one of the identical elements in the array. In general $x_{-n} \neq x_n$ and

$$S(f, f_x) = \sum_{n=1}^{N/2} \left[c_{-n}(f)\exp(+j2\pi f_x x_{-n}) + c_n(f)\exp(+j2\pi f_x x_n) \right] \qquad (4.3.3)$$

is the far-field directivity function of an equivalent linear array of identical, complex-weighted, omnidirectional point elements. Taking the inverse spatial Fourier transform of Eq. (4.2.41) we obtain the complex frequency response (complex aperture function) of a linear array of N (even) identical, complex-weighted, omnidirectional point elements

$$s(f,x_a) = F_{f_x}^{-1}\{S(f,f_x)\} = \sum_{n=1}^{N/2}\left[c_{-n}(f)\delta(x_a - x_{-n}) + c_n(f)\delta(x_a - x_n)\right].(4.3.4)$$

It is interesting to note that a linear array of N (even) identical, complex-weighted elements can be thought as a spatial FIR filter and this expression can be thought of as the spatial impulse response of the array. In the case of linear array composed of an odd number of elements $N'=(N-1)/2$ and

$$A(f,x_a) = \sum_{n=-N'}^{N'}\left[c_n(f)e_n(f,x_a - x_n)\right], \tag{4.3.5}$$

$$D(f,f_x) = \sum_{n=-N'}^{N'}\left[c_n(f)E_n(f,f_x)\exp(+j2\pi f_x x_n)\right], \tag{4.3.6}$$

$$D(f,f_x) = E(f,f_x)S(f,f_x), \tag{4.3.7}$$

$$S(f,f_x) = \sum_{n=-N'}^{N'}\left[c_n(f)\exp(+j2\pi f_x x_n)\right], \tag{4.3.8}$$

$$s(f,x_a) = F_{f_x}^{-1}\{S(f,f_x)\} = \sum_{n=-N'}^{N'}\left[c_n(f)\delta(x_a - x_n)\right]. \tag{4.3.9}$$

In the case of arbitrary amont of elements N complex aperture function can be expressed as

$$A(f,x_a) = e(f,x_a) *_{x_a} s(f,x_a). \tag{4.3.10}$$

If the length L of the individual elements is small compared to a wavelength, then the far-field beam pattern of the array is, in effect, dependent on $S(f,f_x)$ alone because elements are omnidirectional for all practical purposes and

$$D(f,f_x) = S(f,f_x). \tag{4.3.11}$$

In general complex weight can be expressed as

$$c_n(f) = a_n(f)\exp\left[+j\theta_n(f)\right], \tag{4.3.12}$$

where $a_n(f)$ is real, frequency-dependent amplitude weight and is an even function of the index n. $\theta_n(f)$ is frequency-dependent phase weight and is an odd function of the index n regarding to $n = 0$ and so

$$a_{-n}(f) = a_n(f) \text{ ja } \theta_{-n}(f) = -\theta_n(f). \tag{4.3.13}$$

The equations for the far-field beam pattern can be simplified if the elements are equally spaced ($x_n = x_{-n}$). In the case of an even number of elements

$$S(f, f_x) = 2\sum_{n=1}^{N/2} a_n(f)\cos\left[2\pi f_x(n-0.5)d + \theta_n(f)\right]. \tag{4.3.14}$$

In the case of an odd number of elements

$$S(f, f_x) = a_0(f) + 2\sum_{n=1}^{N'} a_n(f)\cos\left[2\pi f_x nd + \theta_n(f)\right]. \tag{4.3.15}$$

The most common set of amplitude weights are simply sampled values of the continuous amplitude windows already discussed in the previous chapter of this paper. Amplitude weighting can be implemented by connecting each element in the array in series with an electronic amplifier. However, the use of electronic amplifiers is really not necessary, since amplitude weights, as well as phase weights, can be implemented by using digital signal processing (digital beamforming). For example in the case of rectangular amplitude weight $a_n(f) = 1$ we yield the far-field directivity function of a linear array of N odd identical elements

$$S(f, f_x) = \frac{\sin(\pi f_x Nd)}{\sin(\pi f_x d)} \tag{4.3.16}$$

and when switching to polar coordinates

$$S(f, \theta, \psi) = \frac{\sin(\pi N \dfrac{d}{\lambda}\sin\theta\cos\psi)}{\sin(\pi \dfrac{d}{\lambda}\sin\theta\cos\psi)}. \tag{4.3.17}$$

We know, that different amplitude windows yield far-field beam patterns with different sidelobe levels and beamwidths, and as sidelobe levels decrease,

beamwidth generally increases. However, the Dolph-Chebyshev method of amplitude weighting makes it possible to optimize the far-field beam patterns of arrays so that for any specified sidelobe level relative to the level of the main lobe, the narrowest possible main-lobe beamwith is achieved, or for any specified main-lobe beamwidth, the lowest possible sidelobe level is achieved. One disadvantage of the Dolph-Chebyshev method is that all of the sidelobes are at the same level, they do not fall off in value (See also [2] example 7.1-5)

Far-field beam pattern of the array when it is complex weighted is given by

$$D'(f, f_x) = \sum_{n=-N'}^{N'} a_n(f) \exp\{+j[2\pi f_x nd + \theta_n(f)]\}. \qquad (4.3.18)$$

If the phase weights are function of frequency and is a linear phase variation applied across the length of the array, perhaps $\theta_n(f) = -2\pi f_x'nd$, $n = -N',...,0,...,N'$, and $f_x' = u'/\lambda$, we can write

$$D'(f, f_x) = \sum_{n=-N'}^{N'} a_n(f) \exp[+j2\pi(f_x - f_x')nd], \qquad (4.3.19)$$

$$D'(f, f_x) = D(f, f_x - f_x'), \qquad (4.3.20)$$

$$D'(f, u) = D(f, u - u'). \qquad (4.3.21)$$

We know, that a phase shift $\theta_n(f)$ in radians is equivalent to a time delay τ_n in seconds, that is

$$\theta_n(f) = 2\pi f \tau_n, \ \tau_n = \frac{\theta_n(f)}{2\pi f}, \qquad (4.3.22)$$

$$\tau_n = -u'nd/c, \ n = -N',...,0,...,N'. \qquad (4.3.23)$$

In the case of long duration signals, the use of time-delay circuits to do beam steering is really not necessary, since beam steering can be accomplished via phase weighting, which can be implemented by using digital signal processing (digital beamforming). It is possible to perfom delay compensation and formation of the beam pattern in the frequency domain. In principle we must compute the complex frequency spectrum from the signal in each channel of the array, then multyplay all given spectrum values in each channel with the expression $\exp[-j\theta_n(f)]$. From

41

results we must take the inverse Fourier transform and then we obtain delayed signal as a final result.

Next we will consider the far-field beam patterns and the discrete Fourier transform. The far-field directivity function of a linear array of N (odd) identical, equally spaced, complex-weighted, omnidirectional point elements lying along the X axis is given by

$$D(f,f_x) = \sum_{n=-N'}^{N'} c_n(f)\exp\left[+j2\pi f_x nd\right]. \qquad (4.3.24)$$

A more efficient way to compute directivity function is to evaluate it at the following set of discrete values of f_x

$$f_x = m\Delta f_x, \ m=-N',...,0,...,N', \qquad (4.3.25)$$

where

$$\Delta f_x = \frac{1}{Nd} \qquad (4.3.26)$$

is the maximum allowable spatial-frequency spacing. Upon substituting Egs. (4.3.2) and (4.3.26) into Eq. (4.3.19), we obtain

$$D(f,m) = \sum_{n=-N'}^{N'} c_n(f)W_N^{mn}, m=-N',...,0,...N', \qquad (4.3.27)$$

Where

$$W_N = \exp(+j2\pi/N). \qquad (4.3.28)$$

Therefore, evaluating the beam pattern at bin number m corresponds to evaluating the beam pattern at spatial frequency $f_x = m\Delta f_x$. The summation on the right-hand side of Eq. (4.3.27) is the discrete Fourier transform (DFT) of the set of complex weights $C_n(f)$, $n=-N',...,0,...,N'$. One can then use a fast Fourier transform (FFT) computer algorithm to compute the (DFT), and hence the far-field beam pattern.The far-field beam pattern given by Eq.(4.3.27) is periodic with period N, that is

$$D(f,m+N) = D(f,m). \qquad (4.3.29)$$

Most commonly available FFT algorithms assume that the total number of data points to be processed is equal to an integer power of two ($N=2^b$). If N does not

satisfy this condition, then simply add enough zeros to the original data sequence until the total number of data points is equal to an integer power of two.

In order to guarantee only one main lobe within the visible region, according to general sampling theory, the interelement spacing d must be chosen properly. In the opposite case, unwanted main lobes may appear within the visible region. (Fig. 4.3.2). The grating lobes will be avoided when the following condition is satisfied:

$$d < \lambda_{\min} / 2 \qquad (4.3.30)$$

Fig. 4.3.3 show that as the interelement spacing decreases, the main-lobe beamwidth will increase when the frequency is held constant and the length of the aperture is decreased. Fig. 4.3.1 shows the beam pattern example where the amount of the elements of the array $N = 15$, interelement spacing $d = 0,0015\,m$ and minimal wavelength $\lambda_{\min} = 0,003\,m$. Fig. 4.3.2 shows the beam pattern in case the interelement spacing is bigger than half of wavelength and Fig. 4.3.3 shows the beam pattern in case the interelement spacing is decreased but other parameters are she same as in example brought on Fig. 4.3.2.
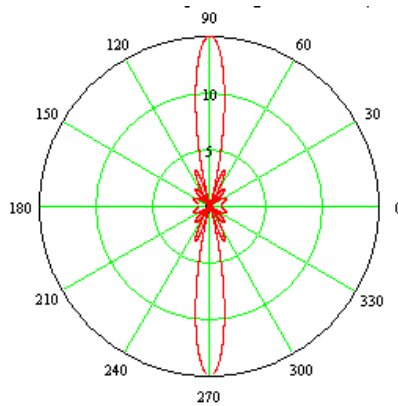
Fig. 4.3.1 $N = 15$, $d = 0,0015m$, $\lambda_{\min} = 0,003m$

In example on Fig. 4.3.2 we reduced amount of elemets on purpose to compare results with the results on Fig. 4.3.1. All beam patterns shown here are calculated by using package MathCad on the basis of Eqs. (4.3.12) and (4.3.24).

The near-field directivity function is given by

$$D(f,r,f_x) = \sum_{n=-N'}^{N'} C_n(f)\exp\left[-jk\frac{(nd)^2}{2r}\right]\exp(+j2\pi f_x nd). \qquad (4.3.31)$$

43

The phase weights are given by

$$\theta_n(f) = -2\pi f_x' nd + \frac{k}{2r'}(nd)^2, \ n = -N',...,0,...,N'.$$ (4.3.32)

The first term on the right-hand side is responsible for beam steering, whereas the second term is responsible for focusing.
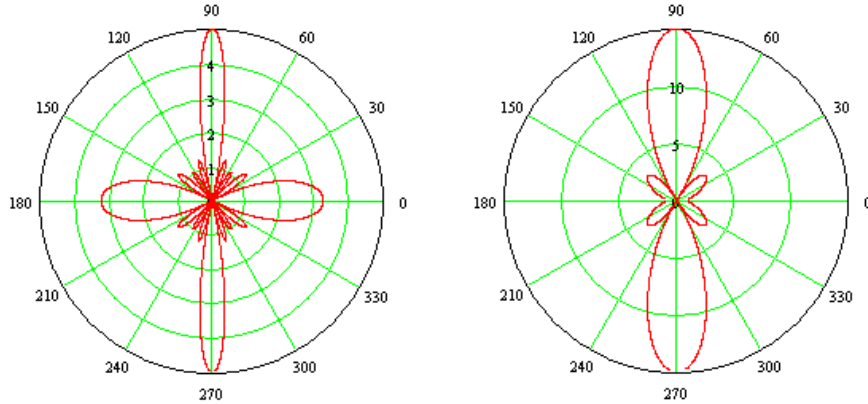
Fig. 4.3.2 $N = 5$, $d = 0,0054 \ m$, $\lambda_{min} = 0,003 \ m$. Fig. 4.3.3 $N = 15$, $d = 0,00075 \ m$

One of the potential advantage of using an array of elements is related with the signal-to-noise ratio (SNR).
The array gain (AG) is defined as follows (array of N (odd) identical elements)

$$AG \equiv 10\log_{10}(SNR_A / SNR) \ db.$$ (4.3.33)

Here SNR_A is the output signal-to noise power ratio of the array and is given by

$$SNR_A \equiv \frac{E\left\{|s_T(t)|^2\right\}}{E\left\{|n_T(t)|^2\right\}}$$ (4.3.34)

and SNR is the output signal-to-noise power ratio at the center element in the array

$$SNR \equiv \frac{E\left\{|s_0(t)|^2\right\}}{E\left\{|n_0(t)|^2\right\}}.$$ (4.3.35)

44

$E\left\{\left|s_T(t)\right|^2\right\}$ is the total output signal power, $E\left\{\left|s_0(t)\right|^2\right\}$ is the output signal power at the center element in the array, $E\left\{\left|n_T(t)\right|^2\right\}$ is the total output noise power, $E\left\{\left|n_0(t)\right|^2\right\}$ is the output noise power at the center element in the array.

It can be shown ([2] examples 7.3.1 and 7.3.2) that there is no advantage (AG=0) with regard to the signal-to-noise ratio in using an array of elements rather than a single element. However, if we assume that the far-field beam pattern of the array has been steered in the direction of the incident plane wave radiated by the sound source, we obtain

$$AG \equiv 10\log_{10} N \ db \qquad (4.3.36)$$

Therefore, if the number of elements is doubled, then the AG is increased by 3 dB.

In the case of planar array composed of an odd number $M \times N$ of elements lying in the XY plane $M' = (M-1)/2$, $N' = (N-1)/2$ and

$$A(f,x_a,y_a) = \sum_{m=-M'}^{M'} \sum_{n=-N'}^{N'} \left[c_{mn}(f) e_{mn}(f,x_a - x_m, y_a - y_n) \right], \qquad (4.3.37)$$

$$D(f,f_x,f_y) = \sum_{m=-M'}^{M'} \sum_{n=-N'}^{N'} \left[c_{mn}(f) E_{mn}(f,f_x,f_y) \exp(+j2\pi(f_x x_m + f_y y_n)) \right],$$
$$(4.3.38)$$

$$D(f,f_x,f_y) = E(f,f_x,f_y) S(f,f_x,f_y), \qquad (4.3.39)$$

$$S(f,f_x,f_y) = \sum_{m=-M'}^{M'} \sum_{n=-N'}^{N'} \left[c_{mn}(f) \exp(+j2\pi(f_x x_m + f_y y_n)) \right], \qquad (4.3.40)$$

$$s(f,x_a,y_a) = F_{f_x}^{-1} F_{f_y}^{-1} \left\{ S(f,f_x,f_y) \right\} =$$
$$= \sum_{m=-M'}^{M'} \sum_{n=-N'}^{N'} \left[c_{mn}(f) \delta(x_a - x_m) \delta(y_a - y_n) \right] \qquad (4.3.41)$$

Taking the inverse spatial Fourier transform of the product theorem given by Eq. (4.3.39) yields

$$A(f,x_a,y_a) = e(f,x_a,y_a) *_{x_a} *_{y_a} s(f,x_a,y_a). \qquad (4.3.42)$$

We know, that the far-field beam pattern of an omnidirectional point element is equal to a constant Therefore we obtain the following expression for the far-field directivity function as

$$D(f, f_x, f_y) = S(f, f_x, f_y).$$ (4.3.43)

Complex weights can be expressed as

$$c_{mn}(f) = a_{mn}(f) \exp\left[+j\theta_{mn}(f)\right].$$ (4.3.44)

Like complex apertures, planar arrays can be rectangular, or circular. Also, complex weights can be separable (analogous to separable functions in complex aperture theory) and we obtain the following form for the product theorem for planar arrays

$$D(f, f_x, f_y) = E(f, f_x, f_y) S_X(f, f_x) S_Y(f, f_Y).$$ (4.3.45)

In the case of concentric circular arrays ([2] Fig. 7.4-4), the far-field beam pattern is given by

$$D(f, \theta, \psi) = \sum_{m=1}^{M} \sum_{n=1}^{N} c_{mn}(f) \exp\left[+j\frac{2\pi r_m}{\lambda}\sin\theta\cos(\psi - \phi_n)\right].$$ (4.3.46)

If the phase weights are given by

$$\theta_{mn}(f) = -2\pi f_x' m d_x - 2\pi f_y' n d_y,$$
$$m = -M',...,0,...,M',$$ (4.3.47)
$$n = -N',...,0,...,N',$$

a linear phase variation applied across the array will cause the beam pattern to be steered in the direction $u = u'$ and $v = v'$ in direction-cosine space and its shape and beamwidth remain unchanged when plotted as function of direction cosines. However, they do change when the beam pattern is plotted as a function of the spherical angles. Shifted far-field directivity function is given by

$$D(f, f_x, f_y) = D(f, f_x - f_x', f_y - f_y'),$$ (4.3.48)

$$D(f, u, v) = D(f, u - u', v - v').$$ (4.3.49)

Phase shift in radians is equivalent to a time delay in seconds, that is

$$\theta_{mn}(f) = 2\pi f \tau_{mn}, \qquad (4.3.50)$$

$$\tau_{mn} = -\frac{u'md_x}{c} - \frac{v'nd_y}{c}. \qquad (4.3.51)$$

Half of the time delays will be positive and half will be negative Eq. (4.3.47).

The near-field directivity function (based on the Fresnel approximation) of a planar array of $M \times N$ (odd) identical, equally spaced, complex-weighted, omnidirectional point elements lying in the *XY* plane is given by

$$D(f,r,f_x,f_y) = \sum_{m=-M'}^{M'} \sum_{n=-N'}^{N'} c_{mn}(f) \exp\left\{ -jk \frac{\left[(md_x)^2 + (nd_y)^2 \right]}{2r} \right\} \qquad (4.3.52)$$

$$\times \exp\left[+j2\pi(f_x md_x + f_y nd_y) \right].$$

The phase weights are given by

$$\theta_{mn}(f) = 2\pi f_x' md_x - 2\pi f_y' nd_y + k\frac{\left[(md_x)^2 + (nd_y)^2 \right]}{2r'}. \qquad (4.3.53)$$

The first two terms on the right-hand side of Eq. (4.3.53) are responsible for beam steering, whereas the third term is responsible for focusing.

Arrays can be also three-dimensional, cylindrical or spherical. From mathematical aspect, this means addition of third (*Z*) axis. Corresponding equations are given in literature [2] (chapter 7.6).

5 SOLUTIONS

5.1 SCANNING SIGNAL AND THE REDUCTION OF THE POWER OF THE IMPULSE

Because the main issue described in the work is the fact, that there are problems steering the beam pattern of the sensor array using spread-spectrum signals, it is important to analyse spread-spectrum signals first and create proper mathematical model for them.

Sonars that use scanning signals without intra-pulse modulation can discover objects located at different distances. Their measurement precision depends on the duration of the pulse and the wave's dispersion speed. On reception scattered signals from objects, the higher the registered signal energy, the higher the detection probability of the object. Based on the principle of uncertainty, in the case of optimal scanning signals, the precision of objects is determined by its effective working range within the frequency band. Accordingly, on reception scattered signals from an object we can create energetically equivalent situations in two different ways [6][12]:

1. Scanning signal is short, without intra-pulse modulation and uses high power

$$E_{S1} = P_1 \cdot T_1.$$ (5.1.1)

2. Scanning signal has high duration, is complex with regard to intra-pulse modulation (i.e. wide in the frequency band), but with reduced power

$$E_{S2} = P_2 \cdot T_2.$$ (5.1.2)

Here E_S is the energy of the scanning signal, P is signal power and T is the duration. Both signals are energetically equivalent when the following conditions are fulfilled

$$B = \frac{T_2}{T_1}, \ T_2 > T_1,$$ (5.1.3)

$$B = \frac{P_1}{P_2}, \ P_1 > P_2,$$ (5.1.4)

$$E_{S1} = E_{S2},$$ (5.1.5)

As a rule, a complex scanning signal (signals are complex with regard to intra-pulse modulation) can be expressed by

$$s(l) = \sum_{p=0}^{KV-1} \sum_{k=0}^{KH-1} A(l - \tau, k + (p \cdot KH)) \cdot W(l, p, k). \qquad (5.1.6)$$

Here, values of the phase manipulated complex scanning signal k component (chip) at discrete time l are:

$$A(l, k) = a(l - k \cdot LDi), \qquad (5.1.7)$$

where

$$a(l) = \begin{cases} 1 \rightarrow 0 \le l \le (LDi - l) \\ 0 \rightarrow otherwise \end{cases} \qquad (5.1.8)$$

and

$$W(l, p, k) = \cos\left[\omega_0 \cdot \left(\frac{l}{fs} \right) + \left| \phi_p - \phi_k \right| \right] \qquad (5.1.9)$$

l	-discrete time, $l = \overline{0, (L-1)}$,
L	-duration of the signal in samples,
LDi	-duration of the signal element in samples,
KH	-amount of (nested code) internal components,
KV	-amount of (nested code) external components,
τ	-signal delay,
ω_0	-support (centre) frequency,
fs	-sampling frequency,
ϕ_p	-phase of p-th external component $\phi_p \in \{0^0, 180^0\}$,
ϕ_k	-phase of k-th internal component $\phi_k \in \{0^0, 180^0\}$.

When switching to complex amplitude then equation (5.1.6) can be expressed as

$$s(l) = \sum_{p=0}^{KV-1} \sum_{k=0}^{KH-1} A(l - \tau, k + (p \cdot KH)) \cdot \exp(\phi_p - \phi_k). \qquad (5.1.10)$$

By manipulating the signal phases ϕ_p and ϕ_k using a Barker's code of 5 elements as

49

$$\begin{cases} +1,+1,+1,-1,+1; \\ +1,+1,+1,-1,+1; \\ +1,+1,+1,-1,+1; \\ -1,-1,-1,+1,-1; \\ +1,+1,+1,-1,+1; \end{cases} \qquad (5.1.11)$$

we can obtain a very good signal for distance measuring in sonar systems. Changes to the phases are made according to the values of the Barker's codes. Every external element of the code includes an internal code.

The graph for this signal (in continuous time) is depicted in Fig. 5.1.1.
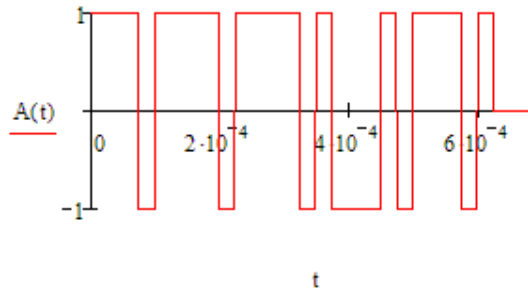
Fig. 5.1.1. Scanning signal

In theory the Barker's codes are short unique codes that exhibit very good correlation properties. Concerning the limited number and the length of Barker's codes, the nested Barker's codes shown above allow us to further increase the system resolution at the same power level. These short elementary- and either nested codes are in principle Direct Sequence Spread Spectrum (DSSS) signals. The term "*spread spectrum*" simply means that the energy radiated by the transmitter is spread out over a wider amount of RF spectrum than would otherwise be used. In case of DSSS, the transmitter actually spreads the energy out over a wider portion of the RF spectrum and do not jump from frequency to frequency as Frequency Hopped Spread Spectrum (FHSS) systems.

As we can see from Figs. 5.1.2 to 5.1.10, the spreading process would cause the transmitted spectrum to increase in with by a factor of $(KH \cdot KV):1$ [47]. Here τ_e is the length of the Barker's code element (chip).

50
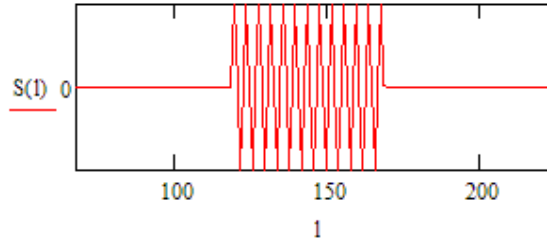
Fig. 5.1.2. Scanning signal without intra-pulse modulation $f_0 = 250\ kHz,\ T = 50\ \mu s$
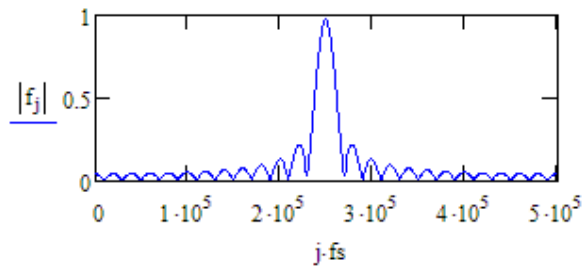
Fig. 5.1.3. Frequency spectrum of the signal without intra-pulse modulation
$f_0 = 250\ kHz,\ T = 50\ \mu s$
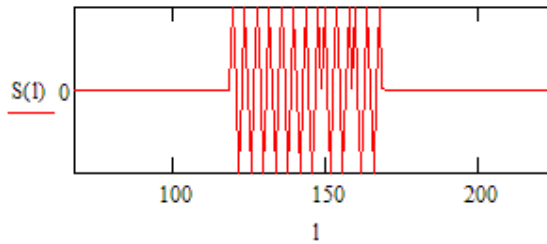
Fig. 5.1.4. Scanning signal manipulated with 5 element Barker's code
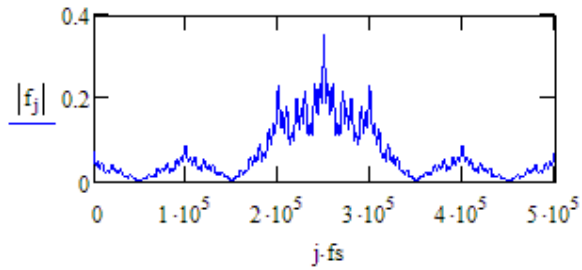$f_0 = 250\ kHz,\ T = 50\ \mu s,\ \tau_e = 10\ \mu s$
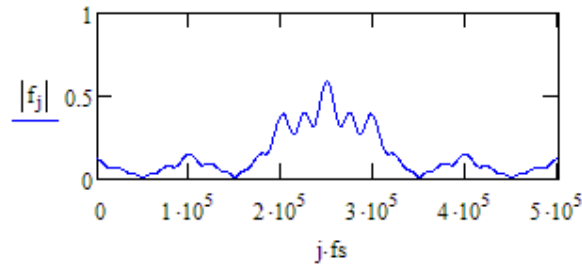
Fig. 5.1.5. Frequency spectrum of the signal manipulated with 5 el. Barker's code
$f_0 = 250\ kHz,\ T = 50\ \mu s,\ \tau_e = 10\ \mu s,\ KH \cdot KV = 5$

51
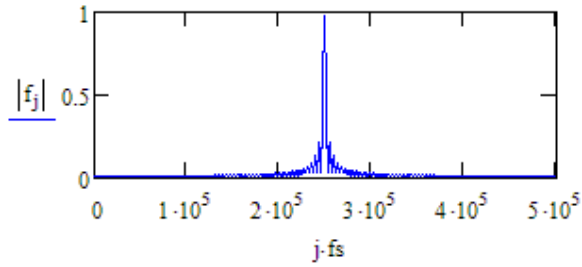
Fig. 5.1.6. Frequency spectrum of the signal without intra-pulse modulation
$$f_0 = 250 \ kHz, \ T = 110 \ \mu s$$
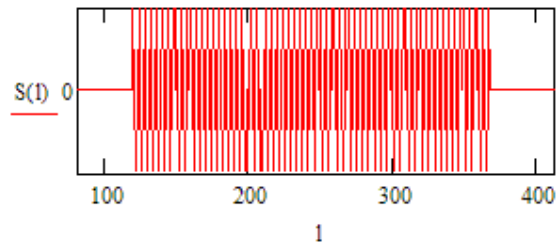
Fig. 5.1.7. Scanning signal manipulated with 11 element Barker's code
$$f_0 = 250 \ kHz, \ T = 110 \ \mu s, \ \tau_e = 10 \ \mu s$$

Fig. 5.1.8. Frequency spectrum of the signal manipulated with 11 el. Barker's code
$$f_0 = 250 \ kHz, \ T = 110 \ \mu s, \ \tau_e = 10 \ \mu s, \ KH \cdot KV = 11$$
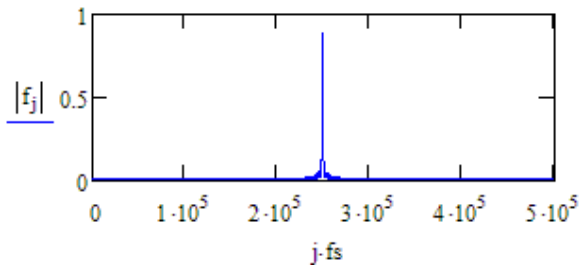
Fig. 5.1.9. Frequency spectrum of the signal without intra-pulse modulation
$$f_0 = 250 \ kHz, \ T = 1,21 \ ms$$

52
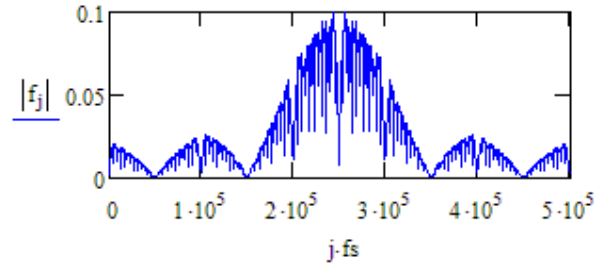
Fig. 5.1.10. Frequency spectrum of the signal manipulated with 121 el. nested code
$f_0 = 250 \ kHz, \ T = 1,21 \ ms, \ \tau_e = 10 \ \mu s, \ KH \cdot KV = 121$

The measured characteristics of a scanning signal are determined by the function of ambiguity [29][32].

$$\psi_0(\tau, \Delta\omega) = \frac{1}{2E_s}\left|\int\limits_{-\infty}^{\infty} \overset{0}{A}(t)\overset{0}{A^*}(t-\tau)e^{-j\Delta\omega t}dt\right| = $$

$$\frac{1}{2E_s}\left|\int\limits_{-\infty}^{\infty} \overset{0}{A^*}(t)\overset{0}{A}(t-\tau)e^{-j\Delta\omega t}dt\right| \tag{5.1.12}$$

Here t is continuous time and $\Delta\omega$ is frequency shift (Doppler frequency). As our purpose is to differentiate between objects as precisely as possible and to estimate distance in mapping the seafloor, we are primarily interested in the pattern of the function of uncertainty $\psi_0(\tau,0)$ which is depicted in Fig. 5.1.11.
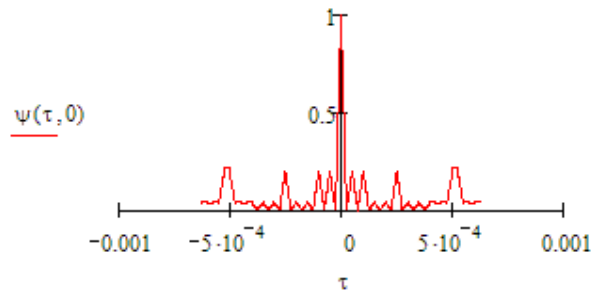
Fig. 5.1.11. The pattern of the function of uncertainty $\psi_0(\tau,0)$ in case of $KH = 5, \cdot KV = 5$

Signal equivalent durability T_e is determined by the main lobe width of the function of ambiguity and is many times less than the durability of the scanning signal T. The equivalent durability T_e is determined by the effective bandwidth of the scanning signal, if calculated using:

53

$$T_e = \frac{1}{F_e}, \tag{5.1.13}$$

where

$$F_e = \sqrt{\frac{\int\limits_{-\infty}^{\infty} f^2 S^2(f) df}{\int\limits_{-\infty}^{\infty} S^2(f) df}} \tag{5.1.14}$$

and where $S^2(f)$ is its power spectrum. Let us note that in the case of a scanning signal without intra-pulse modulation,

$$T_e = T, \quad F_e = \frac{1}{T}, \quad B = T \cdot F_e = 1. \tag{5.1.15}$$

The adaptive optimum filter stores all the energy of the received signal at a single moment in time by narrowing the bandwidth to $1/T$ for a simultaneous noise signal. Thus, we can synthesize different systems using low pulse power. Differences between the units can be determined by their purpose. Let us discuss some of them.

We assume that the purpose is to increase the system's recognition ability, and at the same time, decreasing the power level from the constant power resources. When $B=1$, then in the filter output, the maximum value of the signal with a right-angle winding line is

$$OF_1(t_0) = E_{S1} = \frac{A^2 T_1}{2}, \tag{5.1.16}$$

where A is the amplitude.

Let us look now at a signal with the same durability $T_2 = T_1$, the equivalent duration of which is B times smaller than $T_e = T_1 / B$. Accordingly, the effective bandwidth is B times larger or $F_{e2} = B * F_{e1}$. Therefore,

$$OF_2(t_0) = E_{S2} = \frac{B^2 A^2 T_e}{2}. \tag{5.1.17}$$

Having found the ratio:

$$H = \frac{E_{S2}}{E_{S1}} = \frac{B^2 A^2 T_e}{A^2 T_1} = \frac{B^2 A^2 T_1}{A^2 T_1 B} = B \,, \tag{5.1.18}$$

we can see that in addition to an increase in the system's resolving ability, we can reduce the power of the transmitter B times without causing a deterioration in the system's characteristics. If a greater ability to recognise an object is not needed, then:

$$T_2 = B \cdot T_1, \quad T_e = T_1, \quad F_{e2} = F_{e1} \tag{5.1.19}$$

and

$$\mathrm{OF}_2(t_0) = E_{S2} = \frac{B^2 A^2 T_1}{2} \tag{5.1.20}$$

And

$$H = \frac{E_{S2}}{E_{S1}} = \frac{B^2 A^2 T_e}{A^2 T_1} = \frac{B^2 A^2 T_1}{A^2 T_1} = B^2 \,. \tag{5.1.21}$$

Theoretically, it is possible to synthesize signals using a basis B of any size; consequently, scanning can be performed at any pulse power level no matter how small.

In practice, if there is a shifting object or shifting sonar or both, we must consider the constraints resulting from this and usually $B < 1000$. In practice, this means that the sonar's pulse power can be restricted by some watts to produce much better tactical and technical characteristics compared to $B = 1$ unit.

Using digital signal processing technology, we can generate scanning signals of any complexity and guarantee adaptive-optimum reception of these spread spectrum signals [18] using acoustic power that is hundreds and thousands of times lower.

Complemetary (Golay) codes [14][19] are another approach to reducing time sidelobes by using two codes with mutually canceling sidelobes. Work done in the 1950s by Welti and Golay introduced the concept of code pairs. Complementary (or Golay) codes yield autocorrelation function with a single spike and zero sidelobes. Let A and B be a complementary code set, each of length L-bits, then

$$(A \lozenge A) + (B \lozenge B) = 2L\delta(t) \,. \tag{5.1.22}$$

The autocorrelation functions $(A \lozenge A)$ and $(B \lozenge B)$ each have sidelobes with magnitudes up to 10% of the $(A \lozenge A)$ or $(B \lozenge B)$ autocorrelation peak. However,

when the complementary autocorrelations are summed, the sidelobe levels are reduced and the base of the autocorrelation spike is narrower resulting in better time resolution. For example, a pair of 16-element code complementary codes given by Golay are

$$A = \{1,0,0,0,1,1,0,1,1,0,0,0,0,0,1,0\}$$
$$B = \{0,1,0,0,0,0,0,1,0,1,0,0,1,1,1,0\}.$$

(5.1.23)

The complementary code is also a way to establish time resolution much shorter than the duration of the signal. Practically speaking, a sonar (or radar) using complementary code modulated baseband signals, i.e., transmitting a waveform as the code, would transmit the two codes simultaneously and then apply each reference code to the returned signal by splitting the signal and using two correlators. We can apply the same technique of phase coding (5.1.10) to the complementary code sequence and
the phase coding does give zero time sidelobes; however, the maximum peak value of the correlator output gives a smaller maximum output value. The time resolution effect is the same; however, the maximum output will be different.

5.2   THE DYNAMICS OF SCANNING SIGNALS IN EQUIVALENT DISTANCE SENSOR ARRAY

Now we must investigate, how these (spread spectrum) signals are act in phased arrays. In general, the equation defines signal processing in the phase compensation array [11]:

$$\overset{0}{y}(\beta,\beta_{\gamma},l) = \sum_{n=0}^{N-1} E_1(\beta) \sum_{k=0}^{KT-1} \overset{0}{A}_{kn}(l,\beta) \overset{0}{C}_n(\beta_{\gamma})$$

(5.2.1)

where

$\quad\overset{0}{y}(\beta,\beta_y,l)$ -array output signal at time moment l,

$\quad\beta_{\gamma}$ -   -the angle the signal falls on the array,

$\quad\beta$ -   -beam steering angle,

$\quad N$ -amount of sensors,

$\quad E_1(\beta) = 1$ -directional pattern of sensors,

$\quad KT$ -amount of total components (chips),

$$\overset{0}{A}_{kn}(l,\beta) = A \cdot a(l - k\tau_e - nd \cdot \sin\beta / c),$$
$$\cdot e^{j\Phi_k} \cdot e^{(-)jn2\pi d \cdot \sin\beta / \lambda}$$

(5.2.2)

$$a(l) = \begin{cases} 1, & \text{if } 0 \leq l \leq \tau_e \\ 0, & \text{if } 0 > l > \tau_e \end{cases} \tag{5.2.3}$$

and

$$\overset{0}{C}_n(\beta_\gamma) = h(n) \cdot e^{-jn2\pi d \sin(\beta_y)/\lambda} \tag{5.2.4}$$

is a complex weight of the n-th sensor with amplitude window $h(n)$. λ is the wavelength, τ_e is the signal chip length and d is the distance between the sensors. If $h(n) = 1 \ \forall z$ and $\tau_e \gg n \cdot d \cdot \sin \beta / c$, then

$$\begin{aligned} \overset{0}{A}_{kn}(l, \beta) &= A \cdot a(l - k\tau_e) \cdot e^{j\Phi_k} \cdot e^{(-)jn2\pi d \cdot \sin \beta / \lambda} = \\ &= \overset{0}{A}_k(l) \cdot \overset{0}{A}_n(\beta) \end{aligned} . \tag{5.2.5}$$

Here

$$\overset{0}{A}_k(l) = A \cdot a(l - k\tau_e) \cdot e^{j\Phi_k} \tag{5.2.6}$$

and

$$\overset{0}{A}_n(\beta) = e^{(-)jn2\pi d \cdot \sin \beta / \lambda} . \tag{5.2.7}$$

Thus, in stationary operating mode, time and directional signal processing of the phase array are independent of one another and the formula (5.2.1) can be rewritten as

$$\overset{0}{y}(\beta, \beta_\gamma, l) = \overset{0}{y}_\Sigma(l) \cdot \overset{0}{y}_\Sigma(\beta, \beta_\gamma) , \tag{5.2.8}$$

$$\overset{0}{y}_\Sigma(l) = \sum_{k=0}^{KT-1} \overset{0}{A}_k(l) , \tag{5.2.9}$$

$$\overset{0}{y}_\Sigma(\beta, \beta_\gamma) = E_1(\beta) \cdot \sum_{n=0}^{N-1} \overset{0}{A}_n(\beta) \cdot \overset{0}{C}_n(\beta_\gamma) . \tag{5.2.10}$$

When substituting formulas (5.2.4) and (5.2.7) into formula (5.2.10), we can rewrite formula (5.2.10) as

$$\overset{0}{y}_\Sigma(\beta, \beta_\gamma) = E_1(\beta) \cdot \left[\sum_{n=0}^{N-1} e^{-j2\pi nd \cdot (\sin \beta - \sin \beta_\gamma)/\lambda} \right] . \tag{5.2.11}$$

Now we can compute the coefficient of the array as

$$D(\beta,\beta_\gamma) = \frac{\left|\overset{0}{y_\Sigma}(\beta,\beta_\gamma)\right|}{\left|\overset{0}{y_\Sigma}(0,0)\right|} =$$

$$= \left|\frac{\sin(\pi N d(\sin\beta - \sin\beta_\gamma)/\lambda)}{N\sin(\pi d(\sin\beta - \sin\beta_\gamma)/\lambda)}\right| \cdot E_1(\beta)$$

(5.2.12)

When $\beta_\gamma = 0$, then from the condition $D(\beta,0)$ we can obtain the main lobe width of the directional pattern at zero level, which can be found from the formula

$$\sin\beta = \frac{\lambda}{N \cdot d},$$

(5.2.13)

where $N \cdot d = L_a$ is the length of the array. In our situation, where $\lambda = 0.006$ (250 kHz), $d = 0.0015\ m$, and $N = 81$, $\beta = 0.049\ rad$ (Fig. 5.2.1).
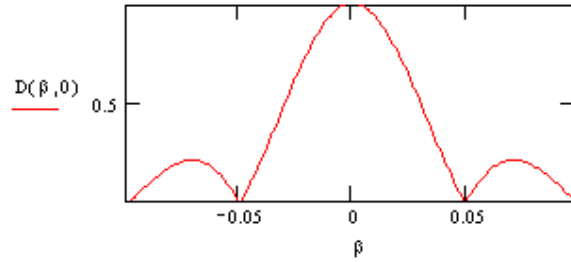
Fig. 5.2.1. Direction diagram $D(\beta,0)$

It is noteworthy that if $\sin\beta_\gamma$ is to vary with step $\sin\beta$, then the array output signal for each discrete direction

$$\sin\beta_\gamma = u \cdot \sin\beta$$

(5.2.14)

can be formed with the Fourier transform. Now complex weight (4) can be rewritten as

$$\overset{0}{C}_n(u) = h(n) \cdot e^{-j2\pi n \cdot u/N}.$$

(5.2.15)

Here

$$u = \frac{\sin\beta_\gamma}{\sin\beta} = \frac{N \cdot d \cdot \sin\beta_\gamma}{\lambda}$$

(5.2.16)

and formula (5.2.10) can be rewritten as

$$\overset{0}{y_\Sigma}(\beta, u) = E_1(\beta) \cdot \sum_{n=0}^{N-1} \overset{0}{A_n}(\beta) \cdot h(n) \cdot e^{-j2\pi nu/N}. \tag{5.2.17}$$

As we can see, discrete β_γ are independent, if the following condition is satisfied

$$\sin \beta_\gamma = \frac{u \cdot \lambda}{L_a}. \tag{5.2.18}$$

If condition

$$\tau_e \gg nd \cdot \sin \beta / c \tag{5.2.19}$$

is not satisfied, then time and space processing of the signals are not independent and formula (5.2.10) can be expressed as

$$\overset{0}{y}(\beta, \beta_\gamma, l) =$$
$$= A \cdot E_1(\beta) \sum_{n=0}^{N-1} \sum_{k=0}^{KT-1} a(l - k\tau_e - nd \cdot \sin \beta / c) \cdot e^{j\Phi_k} \cdot \tag{5.2.20}$$
$$\cdot e^{jn2\pi d \sin(\beta)/\lambda} \cdot$$
$$\cdot h(n) \cdot e^{-jn2\pi d \sin(\beta_y)/\lambda}$$

In general, we are only interested in independent partial directions; that is, $\beta = \beta_\gamma$ and if we assume that

$$A = 1, \; E_1(\beta) = 1, \; h(n) = 1 \; \forall n, \tag{5.2.21}$$

then the array output signal can be expressed by

$$\overset{0}{y}(\beta_\gamma, l) = \sum_{n=0}^{N-1} \sum_{k=0}^{KT-1} a(l - k\tau_e - nd \cdot \sin \beta_\gamma / c) \cdot e^{j\Phi_k}. \tag{5.2.22}$$

It is not difficult to notice, when $\beta_\gamma = 0$, then:

$$\overset{0}{y}(0, l) = N \cdot \sum_{k=0}^{KT-1} a(l - k\tau_e) \cdot e^{j\Phi_k} \tag{5.2.23}$$

and the signal, formed from the sensor, transmits a primary signal without any distortion, as in (Fig. 5.2.2).
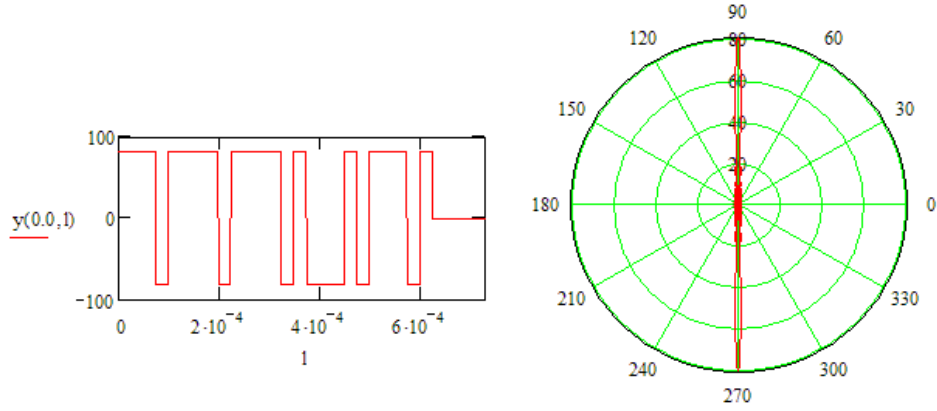
Fig. 5.2.2. Array output at $\beta_\gamma = 0 \; rad$ and corresponding beam pattern

Here we used a simplified version of signal expression (5.2.11) where the amount of total components $KT = 25$ and phase vector is expressed as a nested code

$$\Phi_k = \{+1,+1,+1,-1,+1,+1,+1,+1,-1,+1,+1,+1,$$
$$+1,-1,+1,-1,-1,-1,+1,-1,+1,+1,+1,-1,+1\} \qquad (5.2.24)$$

In other cases, the situation is different. When the time permanence of the signal is T_s, then its spatial length is $L_s = T_s \cdot c$ and it activates on the signal coming on the angle β_γ only part of the whole array with length L_{ef}. The maximal amount N_{ef} of simultaneously activated sensors can be computed as

$$N_{ef} = \frac{L_s}{d \cdot \left| \sin \beta_\gamma \right|} \leq N . \qquad (5.2.25)$$

From equality

$$L_s = N \cdot d \cdot \sin \beta_{kr} , \qquad (5.2.26)$$

we can find the direction of the arriving signal β_{kr}, where at least one space of time $\Delta t_a = d \cdot \sin \beta_\gamma / c$, exists as the equation $N_{ef} = N$

$$\left| \sin \beta_{kr} \right| = \frac{L_s}{L_a} . \qquad (5.2.27)$$

60

For example, if $\tau_e = 25\ \mu s$, $L_s = 25 \cdot \tau_e \cdot c = 94\ cm$ and $L_a = N \cdot d = 12,5\ cm$, then $\beta_{kr} = 0.33\ rad$ (Fig. 5.2.3).
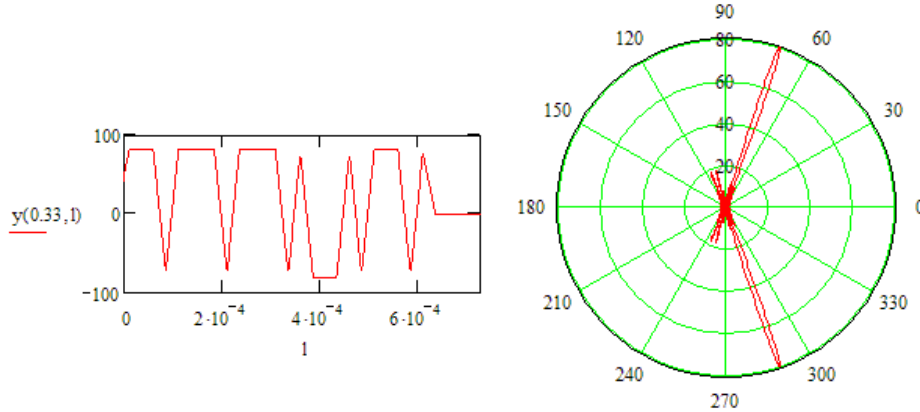
Fig. 5.2.3. Array output at $\beta_\gamma = 0.33\ rad$ and sample beam pattern

Critical angle β_{kr} is a very important parameter for the block-phase compensation algorithm (see Chapter 5.5). When $\beta_y < \beta_{kr}$, then the space in time Δt_v at $N_{ef} = N$ is larger than Δt_a (Fig. 5.2.4).
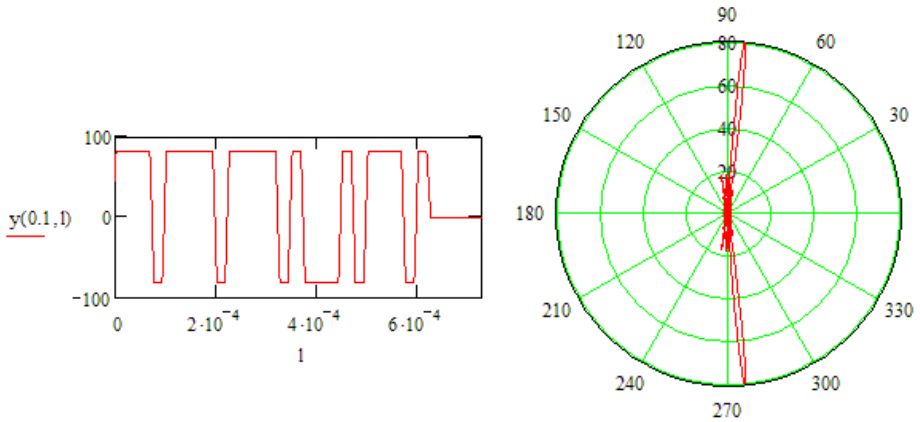
Fig. 5.2.4. Array output at $\beta_\gamma = 0.1\ rad$ and sample beam pattern

However, when, $\beta_y > \beta_{kr}$, then $N_{ef} < N$ and the amplitude of the output signal is proportional to N_{ef} (not to N) and the directional diagram is formed only from signals of the N_{ef} sensors (Fig. 5.2.5 and Fig. 5.2.6).

61
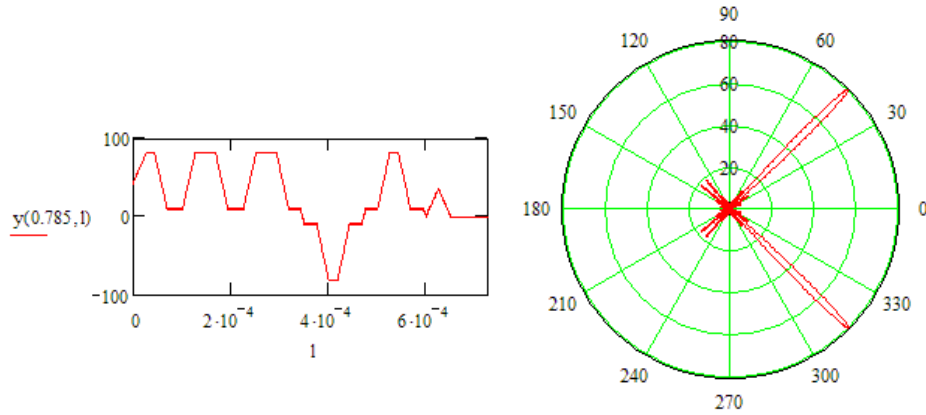
Fig. 5.2.5. Array output at $\beta_\gamma = 0.785\ rad$ and sample beam pattern
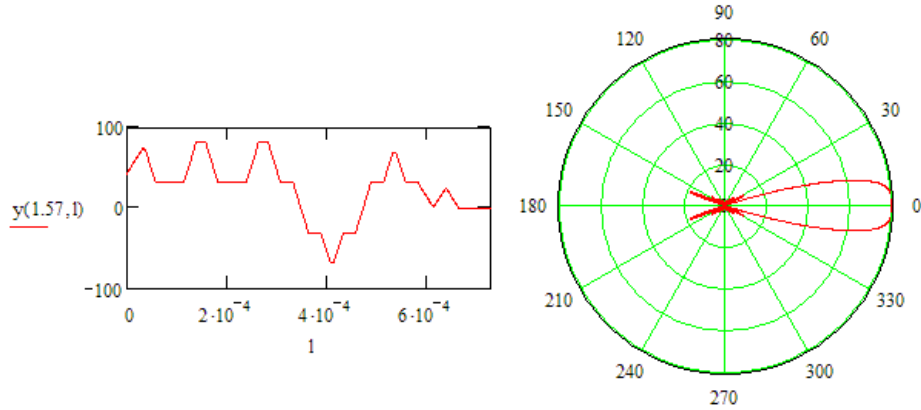
Fig. 5.2.6. Array output at $\beta_\gamma = 1.57\ rad$ and sample beam pattern

As we can see, an increase in the receiving angle of the wave will cause a strong deformation in the form the summary signal. Thereafter, directional diagrams formed by the sensor array using a different $\beta_y \neq 0$, are different if the following condition is not satisfied

$$\frac{L_s}{L_a} << 1 \qquad\qquad (5.2.28)$$

or

$$T_s >> \frac{L_a}{c}. \qquad\qquad (5.2.29)$$

Thus, for signals with a short spatial length, the directional diagrams of the sensor array vary dynamically in time [13] and can be computed at a normalized shape using the formula

$$D_r\left(\beta,\beta_\gamma;n\Delta t_a\right)=\left|\frac{\sin\left(\pi nd\left(\sin\beta-\sin\beta_\gamma\right)/\lambda_o\right)}{n\sin\left(\pi d\left(\sin\beta-\sin\beta_\gamma\right)/\lambda_o\right)}\right|E_1\left(\beta\right).\qquad(5.2.30)$$

Here $n=1,2,...,N_{ef}$, $\Delta t_a=d\cdot\sin\beta_\gamma/c$. Fig. 5.2.7 depicts the beam patterns for $\tau_e\gg d\cdot\sin\beta_\gamma/c$ at different angles, but Fig. 5.2.8 depicts the situation when the condition is not satisfied.
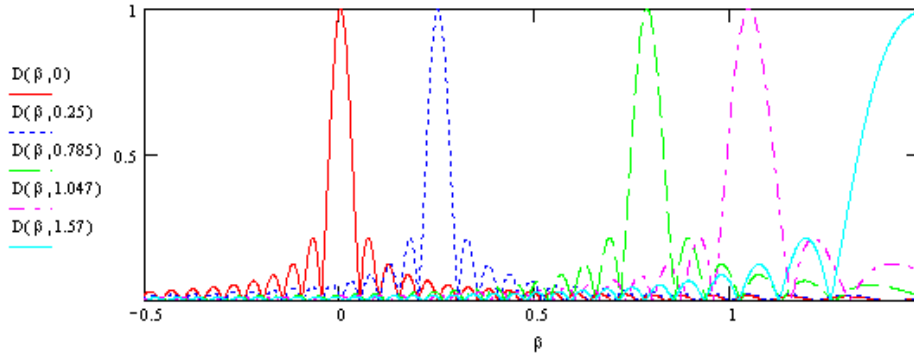
Fig 5.2.7. Beam-patterns in case of $\tau_e\gg nd\cdot\sin\beta/c$ and with angles
$\beta_\gamma=0^0$, $\beta_\gamma=15^0$ $(0,25\ rad)$, $\beta_\gamma=45^0$ $(0,785\ rad)$, $\beta_\gamma=60^0$ $(1,047\ rad)$,
$\beta_\gamma=90^0$ $(1,57\ rad)$
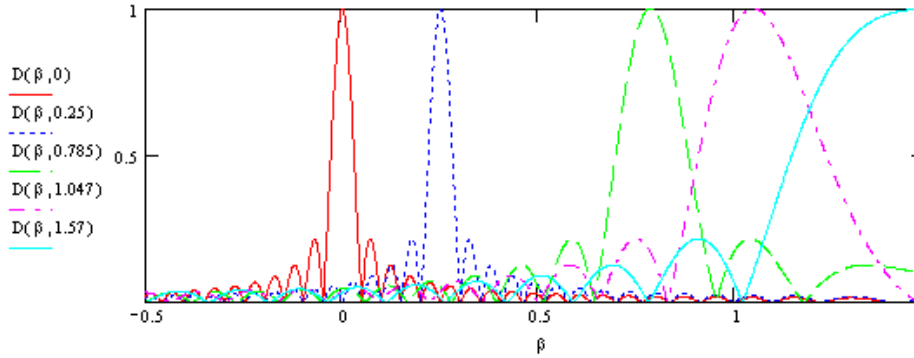
Fig. 5.2.8. Beam-patterns in case of signal with short spatial length $L_s=\tau_e\cdot c=4\ cm$,
$L_a=N\cdot d=12,5\ cm$ and with angles
$\beta_\gamma=0^0$, $\beta_\gamma=15^0$ $(0,25\ rad)$, $\beta_\gamma=45^0$ $(0,785\ rad)$, $\beta_\gamma=60^0$ $(1,047\ rad)$,
$\beta_\gamma=90^0$ $(1,57\ rad)$

Now, about partial direction $\beta_\gamma=60^0$ $(1,047\ rad)$. Here $N_{ef}<N$ and resulting

partial direction prime sheet maximum at zero level is at first 4–5 times larger than at direction $\beta_\gamma = 0^0$, or 2–3 times larger when compared with $\beta_\gamma = 60^0$ (1.047 rad) in Fig. 5.2.7. When signal detection occurs using level comparisons, then a widening of the directional diagram gives rise to the so-called smile effect.

The best estimation of a time delay is achieved using the optimal filter, which maximizes the signal-noise ratio at its output. The phase array output signal is used as an optimal filter input signal and the filter impulse response is defined by a sounding signal [30][34]. The appropriate optimal filter output values for different angles are shown in Figs. 5.2.9-5.2.14.
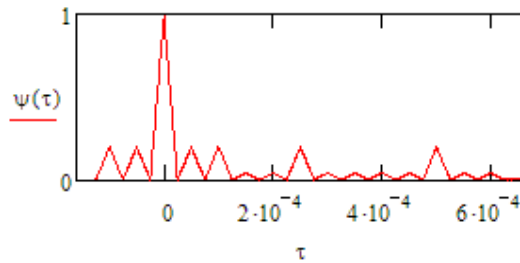
Fig. 5.2.9. Optimal filter output when $\beta_\gamma = 0$
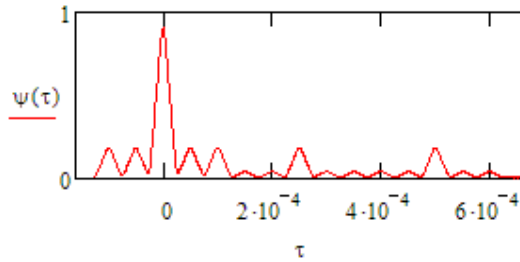
Fig. 5.2.10. Optimal filter output when $\beta_\gamma = 0.1$
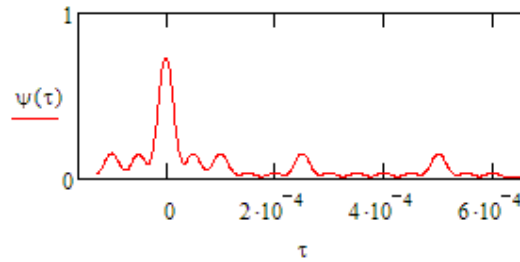
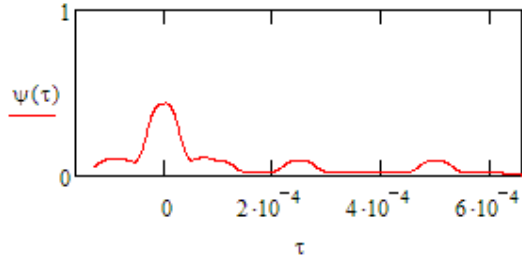Fig. 5.2.11. Optimal filter output when $\beta_\gamma = 0.33$

64

Fig. 5.2.12. Optimal filter output when $\beta_\gamma = 0.785$
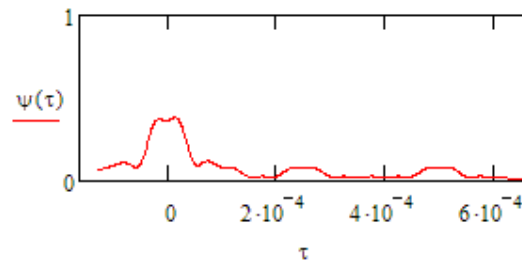

Fig. 5.2.13. Optimal filter output when $\beta_\gamma = 1.047$
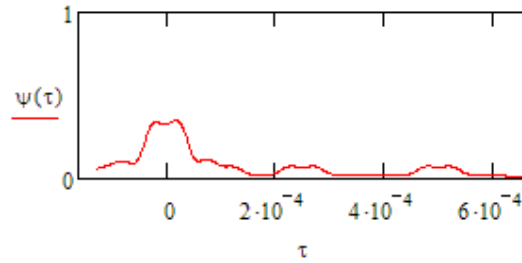

Fig. 5.2.14. Optimal filter output when $\beta_\gamma = 1.57$

It is important to notice that the increase in β_γ results in a decrease in the magnitude of the output signal and an expansion of the maximum area as well as the time shift of a maximum point in the increased direction.

Using digital signal processing technology, we can compensate all delays from signal magnitudes

$$\tau_m = n \cdot d \cdot \sin\left(\frac{\beta_\gamma}{c}\right) \tag{5.2.31}$$

and with that cause a similar situation using $\beta_\gamma = 0$ (Three methods are developed, see Chapters 5.3 – 5.5).

In addition, we must consider that this processing requires a flat wave front, and then we can complete the equation regarding the distance between objects as:

$$D > \frac{L_a^2}{\lambda_0}.$$ (5.2.32)

For example, if $L_a = 12.5\ cm$ and $\lambda_0 = 6\ mm$

$$D > \frac{12.5^2}{0.6}\ cm = 260\ cm = 2.6\ m.$$ (5.2.33)

A sensor array built on the principles viewed earlier, only operates adequately when the sources of the received signals are situated far away. Following the given example, this distance is farther than 2.6m. Otherwise, we must also consider the spherical shape of the wave front, and partial directional diagrams must be formed as a three-argument function $D_r\left(\beta, \beta_\gamma, D\right)$.

5.3   THE MATRIX ALGORITHM FOR THE COMPENSATION OF REFERENCES

Using digital signal processing technology, we can compensate all delays for signal magnitudes

$$\tau_m = n \cdot d \cdot \sin\left(\frac{\beta_\gamma}{c}\right)$$ (5.3.1)

and with that, cause an equivalent situation with $\beta_\gamma = 0$. For this purpose, we can create digital data buffers behind each sensor and as a result obtain a data matrix behind the sensor array. Therefore, the length of the matrix has been fixed using the formula,

$$LB_{max} = L + \max\left(fs \cdot n \cdot d \cdot \sin\left(\beta_\gamma\right)/c\right) - 1$$ (5.3.2)

or

$$LB_{max} = L + \left(fs \cdot N \cdot d \cdot \sin\left(\frac{\pi}{2}\right)/c\right) - 1.$$ (5.3.3)

Here we consider that $\max \beta_\gamma = 90°$. The width of the matrix is fixed according to the number of elements in the sensor array and

fs -sampling rate (Hz),
L -number of signal samples,
N -number of sensors,
d -distance between the sensors (m),
c -wave speed in water (1500 m/s).

As it is shown in formulas (5.3.2) and (5.3.3), the length of the matrix depends on the speed at which the wave is propagated. Finding the optimal sampling rate is also important because the memory requirements for the matrix method depend on this. For example, if the duration of the signal is $L = 25 \cdot 25 = 625$ discrete values, the number of sensors is $N = 81$, and the distance between the sensors $d = 0.0015$, the maximum length of the buffer is 705 discrete values. Thus, the matrix of 81 x 705, involving 57,105 complex numbers, forms behind the sensor array. Using 4 bytes to maintain the complex numbers, we arrive at a memory storage requirement of 228,420.

The signal in the different channels of the sensor array can be expressed using the formula

$$\overset{0}{M}_{l,n} = \sum_{p=0}^{KV-1} \sum_{k=0}^{KH-1} A(l - k\tau_e - fs \cdot n \cdot d \cdot \sin\beta_\gamma / c, k + (p \cdot KH)) \cdot e^{-j|\Phi_p - \Phi_k|} . (5.3.4)$$

Here:

l -sampled time $l = \overline{0, LB_{max}}$,

n -sensor sequence number,

$\overset{0}{M}_{l,n}$ - $LB_{max} \times N$ matrix in memory,

KH -number of signal internal components (amount of chips),
KV -number of signal external components,
$A(n,k) = a(n - k \cdot LDi)$,   (see Chapters 5.1 and 5.2)

$$a(n) = \begin{cases} 1 \rightarrow 0 \le n \le (LDi - n) \\ 0 \rightarrow otherwise \end{cases} . \text{ (see Chapters 5.1 and 5.2)}$$

For example, where the nested code, synthesized on the basis of the 11-element Barker's code was used with a duration of one element, $\tau_e = 25 \, \mu s$ and $fs = 1 \, MHz$, $L = 25 \cdot 11 = 275$, $N = 81$ and $d = 0.0015 \, m$, the maximum length of the buffer is $LB_{max} = 355$ discrete values. Now, corresponding (delayed) signals in different channels (in the matrix columns 0, 40, and 80) are shown in Figs. 5.3.1, 5.3.2 and 5.3.3
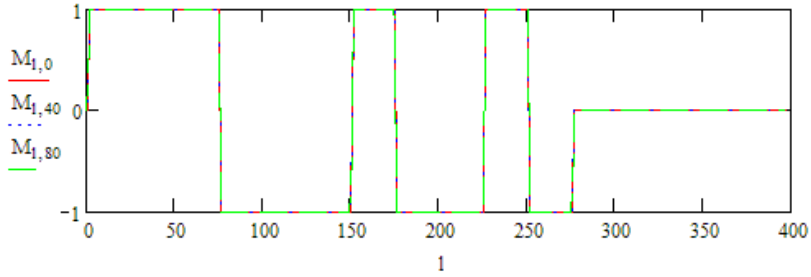
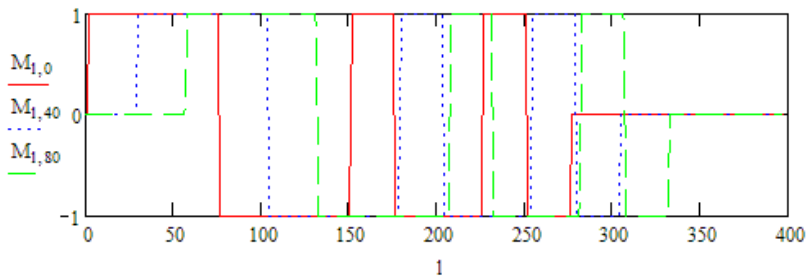Fig. 5.3.1. Magnitudes in different channels (0, 40, 80) at $\beta_\gamma = 0$

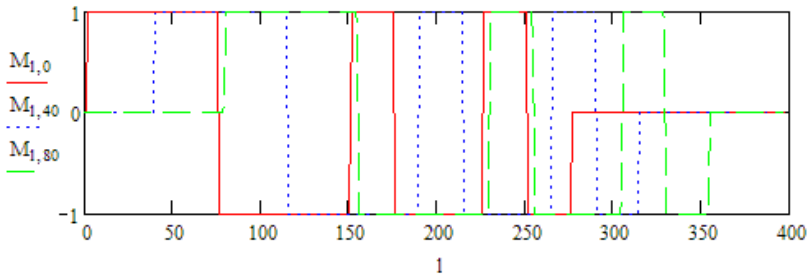Fig. 5.3.2. Magnitudes in different channels at $\beta_\gamma = 0.785 \ rad$

Fig. 5.3.3. Magnitudes in different channels at $\beta_\gamma = 1.57 \ rad$

For compensation we can use the algorithm

$$\overset{0}{y}(l) = \sum_{n=0}^{N-1} M_{f(l,n),n} \ , \tag{5.3.5}$$

where

$$f(l,n) = \begin{cases} g(l,n), & \text{if} \quad g(l,n) \le L-1 \\ h(l,n), & otherwise \end{cases} \tag{5.3.6}$$

and here

68

$$g(l,n) = l + \left(fs \cdot n \cdot d \cdot \sin(\beta_\gamma)/c \right) \qquad (5.3.7)$$

And

$$h(l,n) = l + \left(fs \cdot n \cdot d \cdot \sin(\beta_\gamma)/c \right) - N . \qquad (5.3.8)$$

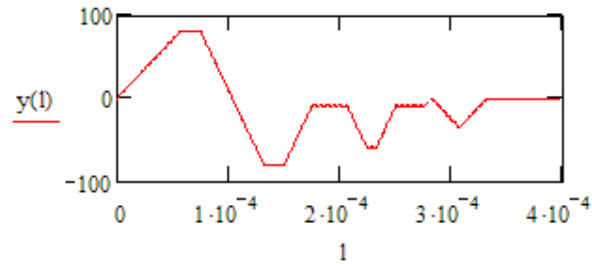The results when $\beta_\gamma = 0.785 \; rad$ are shown in Figs. 5.3.4 – 5.3.5.

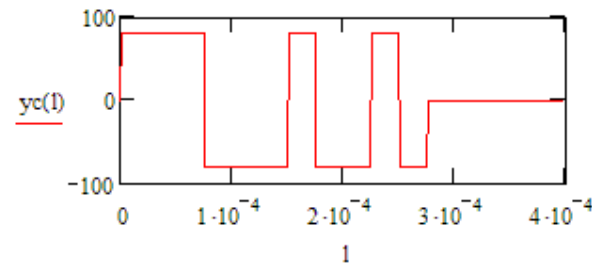Fig. 5.3.4. Signal in the output of the array without compensation at $\beta_\gamma = 0.785 \; rad$

Fig. 5.3.5. Signal in the output of the array with compensation at $\beta_\gamma = 0.785 \; rad$

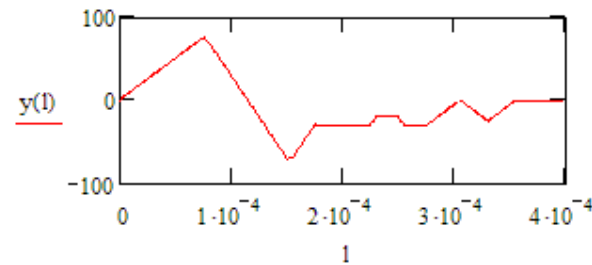On Figs. 5.3.6 – 5.3.7 similar results are shown, but for $\beta_\gamma = 1.57 \; rad$.

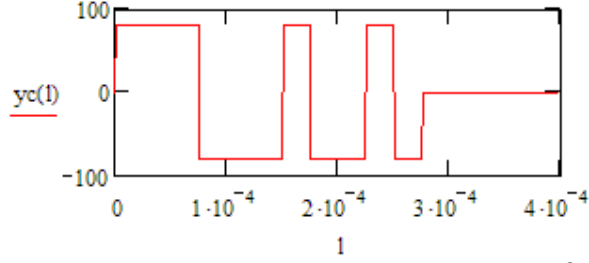Fig. 5.3.6. Signal in the output of the array without compensation at $\beta_\gamma = 1.57 \; rad$

69

Fig. 5.3.7. Signal in the output of the array with compensation at $\beta_\gamma = 1.57\ rad$

The best estimation of a time delay is achieved using the optimal filter, which maximizes the signal-noise ratio at its output. The array (matrix) output signal is used as an optimal filter input signal and the filter impulse response is defined using a sounding signal. It is important to notice that an increase in β_γ results in a decreased output signal and an expansion of the maximum area as well as the time shift of the maximum point in the increasing direction. The compensation mechanism resolves these problems well (theoretically), but the problem lies in the fact that the wave propagation speed may vary, which causes distortions in the output of the compensator. Finding the optimal sampling rate is also important. The given problems are dealt with in depth in Chapter 5.8.1 of the present paper.

5.4   DELAY COMPENSATION IN THE FREQUENCY DOMAIN

In order to produce the correct time delay, we can use characteristics of the Fourier transform [9]. When switching to a complex envelope, we can find the output signal from sensor n at time l using the formula:

$$\overset{0}{M}_{l,n} = \sum_{p=0}^{KV-1} \sum_{k=0}^{KH-1} A(l - k\tau_e - round\left(fs \cdot n \cdot d \cdot \sin\beta_\gamma / c\right), k + (p \cdot KH)) \cdot$$
$$\cdot \exp\left(-j\left(\left|\phi_p - \phi_k\right| + \left(\omega_0 \cdot \frac{n \cdot d \cdot \sin\beta_\gamma}{c}\right)\right)\right)$$

.(5.4.1)

First, we must compute the complex frequency spectrum from M. Since the complex weight is a function of frequency q, an appropriate complex weight must be applied to each frequency component contained in the signal spectrum. This must be done at each sensor n in the array, as follows:

$$\overset{0}{Y}_{n,(q+Lp)} = C(n,q) \cdot \frac{1}{L-1} \sum_{l=0}^{L-2} M_{l,n} \cdot \exp\left(-j\frac{2\pi \cdot q \cdot l}{L-1}\right),$$

(5.4.2)

70

where q is sampled frequency $q = \overline{-Lp, Lp}$ and

$$Lp = \frac{L-2}{2}. \qquad (5.4.3)$$

The complex weight $C(n,q)$ is expressed using the formula:

$$C(n,q) = \begin{vmatrix} 0 \; if \; |n| > N-1 \\ a(n,q) \cdot \exp(j\theta(n,q)) \cdot \exp(j\varphi(n)) \end{vmatrix}, \qquad (5.4.4)$$

where $a(n,q)$ is the frequency dependent amplitude window. $a(n,q) = 1, \forall n, \forall q$ for our purposes. To compensate for the time delay, we will use the weight:

$$\theta(n,q) = \frac{2\pi q}{(L-1)} \cdot round\left(\frac{n \cdot d \cdot fs \cdot \cos(\beta_\gamma)}{c} \right) \qquad (5.4.5)$$

and to compensate for the phase, we will use the weight:

$$\varphi(n) = 2\pi \cdot n \cdot d \cdot \frac{\cos(\beta_\gamma)}{\lambda_0}. \qquad (5.4.6)$$

It is important to notice that both weights (5.4.5), (5.4.6) must be used in order to achieve the correct time delay and phase compensation. The complex weighted frequency spectrum $Y_{n,(q+Lp)}$ in all 81 channels is depicted in Fig.5.4.1. The centre frequency is 250 kHz.
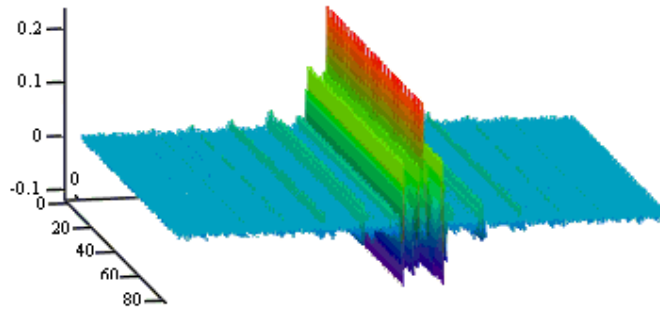

Fig. 5.4.1. Complex weighted frequency spectrum $Y_{n,(q+Lp)}$

Taking the inverse Fourier transform with respect to frequency q, we get:

$$CM_{n,l} = \sum_{q=-Lp}^{Lp} \overset{0}{Y}_{n,(q+Lp)} \cdot \exp\left(j\frac{2\pi \cdot q \cdot l}{L-1} \right), \ 0 \le l \le L-2, \qquad (5.4.7)$$

where the output electrical signals in each channel are now in phase. Resulting from this, the total signal in the output of the array can be expressed using the formula:

$$\overset{0}{y}(l) = \sum_{n=0}^{N-1} CM_{l,n} . \qquad (5.4.8)$$
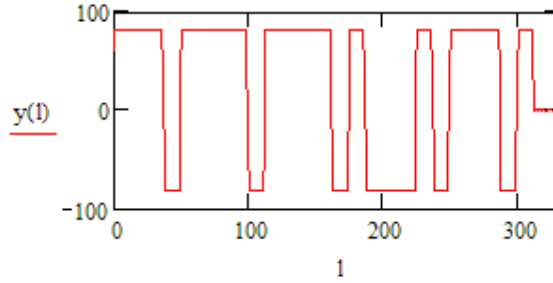
The array output in this case is visualized in Fig. 5.4.2

Fig. 5.4.2. Array output signal at $\beta_\gamma = 0.785 \ rad$ after compensation

As we can see from Fig. 5.4.2, we obtain practically the same situation with $\beta_\gamma = 0$.

This method enables immediately to perform an optimal reception to evaluate the actual round-trip time delay (optimal receiver must carry out pattern of the function of uncertainty). In this case, taking the inverse Fourier transform (5.4.7) is really not necessary and it helps to save the system resources. Optimal reception in a frequency-domain is expressed with the formula

$$\psi(\tau,0) = \sum_{q=-Lp}^{Lp} \left[YS_{(q+Lp)} \cdot SKV_{(q+Lp)} \right] \cdot \exp\left(j\frac{2\pi \cdot q \cdot \tau}{L-1} \right), \qquad (5.4.9)$$

Where

$$YS_{(q+Lp)} = \sum_{n=0}^{N-1} \overset{0}{Y}_{n,(q+Lp)} \qquad (5.4.10)$$

And

$$SKV_{(q+Lp)} = \frac{1}{L-1} \sum_{l=0}^{L-2} \overset{0}{VTV}_l \cdot \exp\left(j\frac{2\pi \cdot q \cdot l}{L-1} \right) \qquad (5.4.11)$$

and

$$VTV_l^0 = N \cdot \sum_{p=0}^{KV-1} \sum_{k=0}^{KH-1} A(l - k\tau_e, k + (p \cdot KH)) \cdot \exp\left(-j\left(\left|\phi_p - \phi_k\right|\right)\right). \quad (5.4.12)$$

is the support signal. All values of $SKV_{(q+LP)}$ can be previously recorded into the processor memory. The appropriate optimal filter output is shown in Fig. 5.4.3.
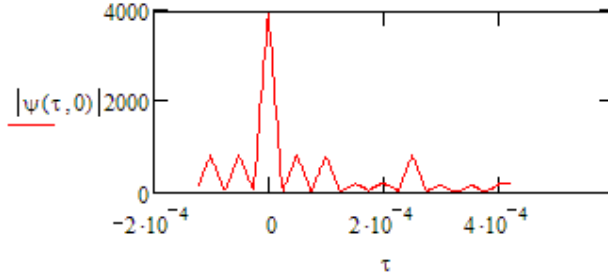

Fig. 5.4.3. Vertical cut of the ambiguity function of the optimal filter at $\beta_\gamma = 45^0$

It is important to notice that with the proposed method, each frequency in the signals is weighted with complex weights (5.4.4). The imaginary parts of the complex weights can be selected independently and appropriately so that the beam-pattern of the beamformer is constant over the frequency band (i.e. frequency-invariant beamformer), while the amplitudes $a(n,q)$ in the complex weights are used to control the beam-pattern characteristics. The proposed method is able to control the main-beam width and sidelobe levels of the beam-pattern in a wide range of frequencies, providing a wideband non-adaptive method for reducing interference. With the use of a frequency-domain structure, it is insensitive to the sampling rate (required only at the Nyquist frequency).

5.5   BLOCK-PHASE METHOD

Here we take into consideration that the amount of simultaneously activated sensors is determined by the spatial length of the signal's smallest element. The sensor array is divided into subarrays [39] where the amount of sensors within the subarray is less than or equal to $N_{ef}(\beta_\gamma)$.

$$N_{ef}(\beta_\gamma) = \begin{vmatrix} z = round\left[\dfrac{\tau_e \cdot c}{d \cdot 0.9 \cdot |\cos(\beta_\gamma)|}\right] - round\left[\dfrac{\tau_e \cdot c}{d}\right] & if \ \cos(\beta_\gamma) \neq 0 \\ v = z \ if \ z \leq N \\ v = N \ otherwise \\ h = v \ if \ v > 0 \\ h = 1 \ otherwise \\ h \end{vmatrix} \tag{5.5.1}$$

Fig. 5.5.1 shows relationship between amount of simultaneously activated sensors and partial directions β_γ.
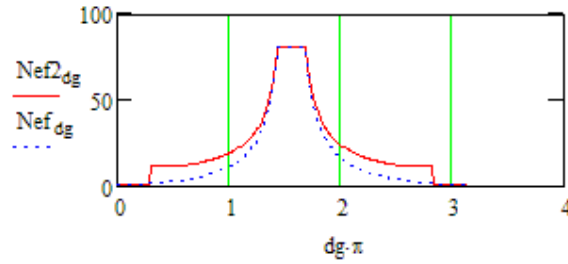

Fig. 5.5.1. Relationship between amount of sensors and partial directions

Dotted line on Fig 5.5.1 is calculated by using the formula 5.5.1. Solid line on the Fig. 5.5.1 is calculated by using formula 5.5.2.

$$N_{ef}(\beta_\gamma) = \begin{vmatrix} z = round\left[\dfrac{\tau_e \cdot c}{d \cdot |\cos(\beta_\gamma)|}\right] & if \ \cos(\beta_\gamma) \neq 0 \\ v = z \ if \ z \leq N \\ v = N \ otherwise \\ h = v \ if \ v > \dfrac{\tau_e \cdot c}{d} \\ h = 1 \ otherwise \\ h \end{vmatrix} \tag{5.5.2}$$

Formula 5.5.2 is more close to the theoretical result (5.2.25) but in practice, it is still better to use formula 5.5.1 because it does not have rapid transition of the amount of sensors in the case of big angles.

The output signal in different partial directions β_γ can be computed using the formula

$$\overset{0}{y}(l,\beta_\gamma) = \sum_{i=0}^{grp(\beta_\gamma)-1} \sum_{n=\frac{i\cdot N}{grp(\beta_\gamma)}}^{\left(\frac{N\cdot(i+1)}{grp(\beta_\gamma)}\right)-1} \overset{0}{M}_{l+d(i,\beta_\gamma),n} \cdot \exp\left(j\frac{2\pi\cdot n\cdot d\cdot\cos(\beta_\gamma)}{\lambda_0} \right). \quad (5.5.3)$$

where $grp(\beta_\gamma)$ is the amount of subarrays corresponding to different partial directions β_γ and i is the index of subarrays. In the case of $N=81$

$$grp(\beta_\gamma) = \begin{vmatrix} 1 & if & N_{ef}(\beta_\gamma) \geq N \\ 3 & if & 27 \leq N_{ef}(\beta_\gamma) < N \\ 9 & if & 9 \leq N_{ef}(\beta_\gamma) < 27 \\ 27 & if & 3 \leq N_{ef}(\beta_\gamma) < 9 \\ N & otherwise \end{vmatrix} \quad (5.5.4)$$

A delay (in samples) of the i-th subarray corresponding to partial direction β_s is fixed by formula:

$$d(i,\beta_\gamma) = round\left(fs \cdot \frac{i\cdot N}{grp(\beta_\gamma)} \cdot \frac{d\cdot\cos(\beta_\gamma)}{c} \right). \quad (5.5.5)$$

Fig. 5.5.2 shows the output signal of the sensor array if the falling angle of the signal is $\beta_\gamma = 0.524 \; rad$.
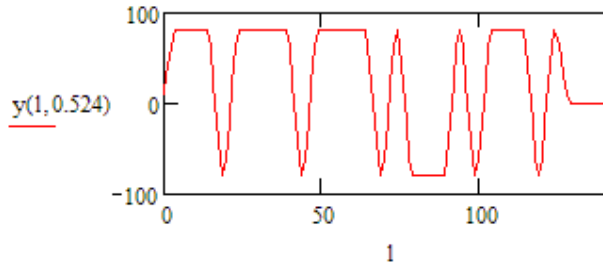

Fig. 5.5.2. Array output after the block-phase compensation

Fig. 5.5.3 shows the output signal after performing an optimal reception for $\beta_\gamma = 0.524 \; rad \quad \beta_\gamma = 0.524 \; rad$ ($\beta_\gamma = \beta_{kr}$) and with a support signal (5.4.12)
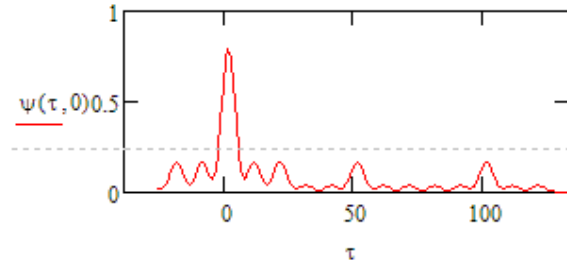
(see also figs. 5.5.31-5.5.34).

Fig. 5.5.3. Vertical cut of the ambiguity function of the optimal filter after block-phase compensation

Fig.5.5.4 illustrates the phase planes in the sensor array. In the given example, the sensor array is divided into 26 subarrays where in each subarray classical phase compensation is performed, although taking into account that $\beta_\gamma \leq \beta_{kr}$. In the next processing steps, compensations of the time lags of the phase planes are performed according to $d(i, \beta_\gamma)$. In principle, this figure shows how the formula works (5.5.3).
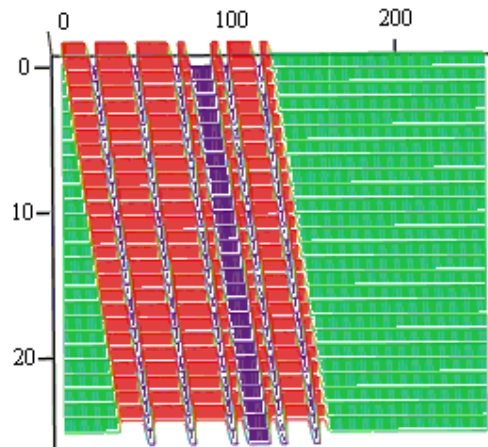

Fig 5.5.4. Phase planes in sensor array

To minimise the amount of mathematical operations in real time, we can pre-record all values of $d(i, \beta_\gamma)$ and $grp(\beta_\gamma)$ into the system memory. A three-dimensional image of the two-dimensional delay array $d(i, \beta_\gamma)$ is shown in Fig. 5.5.5.
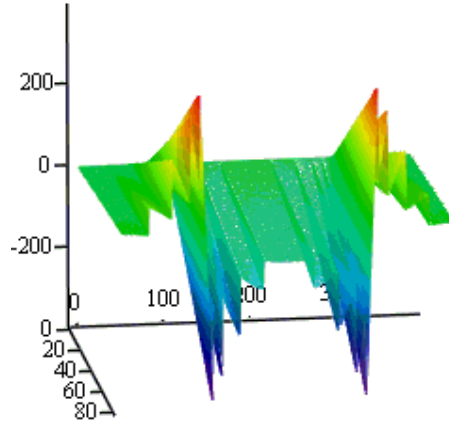
76

Fig. 5.5.5. Three dimensional image of $d(i, \beta_s)$

The vertical axis represents the subarray delays in the samples, and the horizontal axes represents the subarray indices and sampled directions. Thus, we can create the following arrays beforehand:

$$DL_{i, \frac{\varphi \cdot pa}{\pi}} = d(i, \varphi), \tag{5.5.6}$$

$$GRP_{\frac{\varphi \cdot pa}{\pi}} = grp(\varphi), \tag{5.5.7}$$

$$GRPK_{\frac{\varphi \cdot pa}{\pi}} = \frac{N}{grp(\varphi)}, \tag{5.5.8}$$

Hereby:

$i = \overline{0..(N-1)}$

φ angles in rad $\varphi = \overline{0, (\pi / pa)...\pi}$,

pa amount of points in beam-pattern $(pa = 384)$,

dg sampled partial directions $dg = \overline{0,1...pa}$.

Also, depending on the computing method, either of the following arrays can be created:

$$FCOM_{\frac{\varphi \cdot pa}{\pi}} = 2\pi \cdot d \cdot \frac{\cos(\varphi)}{\lambda_0}, \tag{5.5.9}$$

77

$$b(l,i,dg) = \begin{vmatrix} l + DL_{i,dg} & if & 0 \le DL_{i,dg} \le L-1 \\ 0 & if & DL_{i,dg} < 0 \\ L-1 & otherwise \end{vmatrix} \qquad (5.5.10)$$

and formula 5.5.2 can be rewritten as:

$$\overset{0}{S}(l,dg) = \sum_{i=0}^{GRP_{dg}-1} \sum_{n=i\cdot GPRK_{dg}}^{\left(GPRK_{dg}(l+i)\right)-1} \overset{0}{M}_{b(l,i,dg),n} \cdot \exp\left(j \cdot n \cdot FCOM_{dg}\right). \qquad (5.5.11)$$

The horizontal far-field beam pattern can be expressed using the formula:

$$LX_{l,dg} = \mathrm{Re}\left(\overset{0}{y}\left(l, \frac{dg \cdot \pi}{pa} \right) \right), \qquad (5.5.12)$$

where

pa- amount of points in direction diagram (pa=384),

dg- sampled partial directions $dg = \overline{0,1,.., pa}$,

$$\beta_\gamma = \frac{dg \cdot \pi}{pa}. \qquad (5.5.13)$$

A three-dimensional image of two-dimensional signal array *LX* is shown in Fig. 5.5.6.
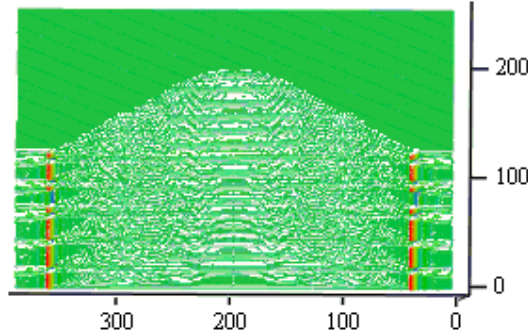

Fig. 5.5.6. Three-dimensional image of *LX*

Here, the horizontal axis represents the sampled partial directions *dg* and the vertical axis (0-400) represents the signal samples (see also figs. 5.5.27 to 5.5.30).

As we can see in Figs. 5.5.2 and 5.5.3, the block-phase method does not give such good results as the previous method, but the results are good enough and the required computing power is much less compared with previous methods. See also Chapter 5.3.

Figs. 5.5.7 to 5.5.26 presents the horizontal far-field beam patterns in the case of block-phase and conventional beamforming ($N=81$).

Fig.5.5.7. Block-phase beamf. at $\beta_\gamma = 90^0$ Fig 5.5.8. Conventional beamf.at $\beta_\gamma = 90^0$

Fig.5.5.9. Block-phase beamf. at $\beta_\gamma = 80^0$ Fig 5.5.10. Conventional beamf. at $\beta_\gamma = 80^0$

79
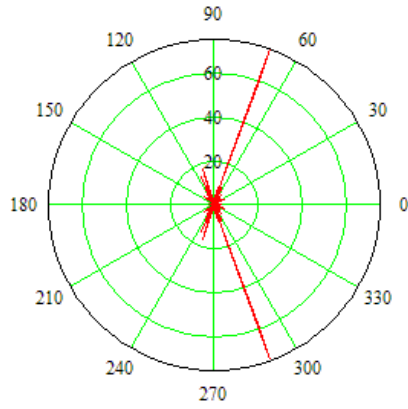
Fig.5.5.11. Block-phase beamf. at $\beta_\gamma = 70^0$
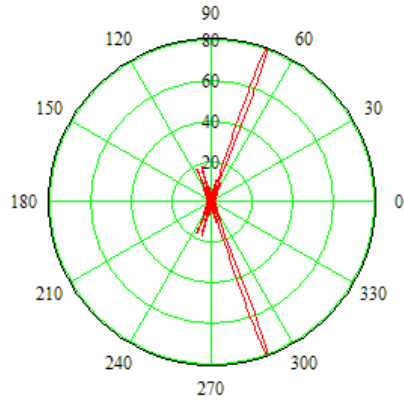
Fig 5.5.12. Conventional beamf. at $\beta_\gamma = 70^0$
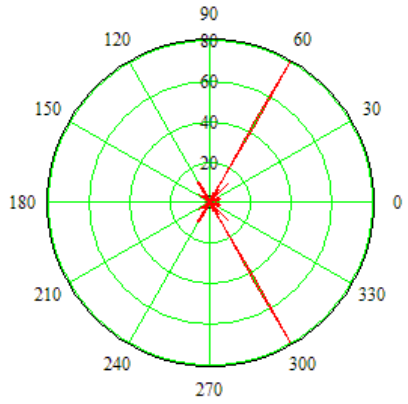
Fig.5.5.13. Block-phase beamf. at $\beta_\gamma = 60^0$
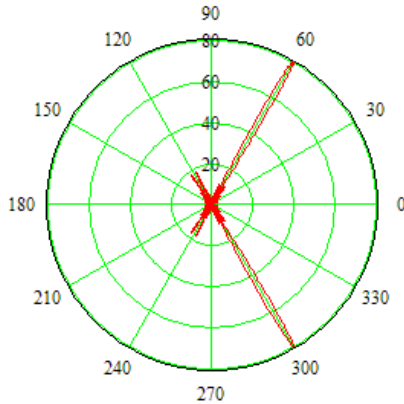
Fig 5.5.14. Conventional beamf. at $\beta_\gamma = 60^0$
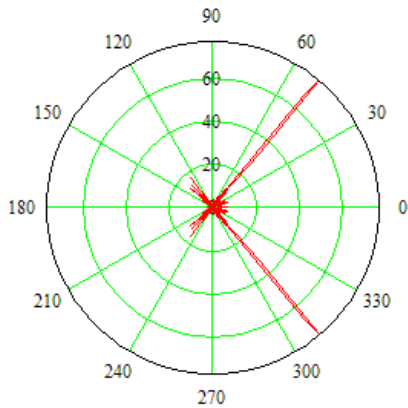
Fig.5.5.15. Block-phase beamf. at $\beta_\gamma = 50^0$
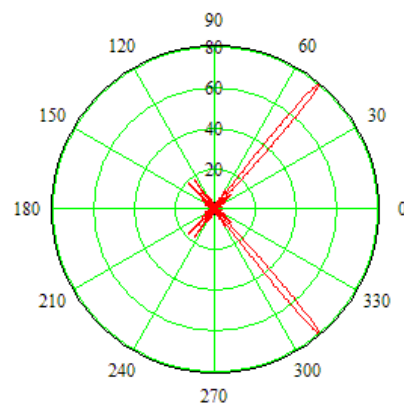
Fig 5.5.16. Conventional beamf. at $\beta_\gamma = 50^0$

80
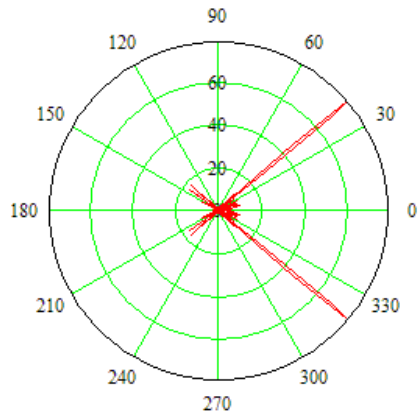
Fig.5.5.17. Block-phase beamf. at $\beta_\gamma = 40^0$ Fig 5.5.18. Conventional beamf. at $\beta_\gamma = 40^0$
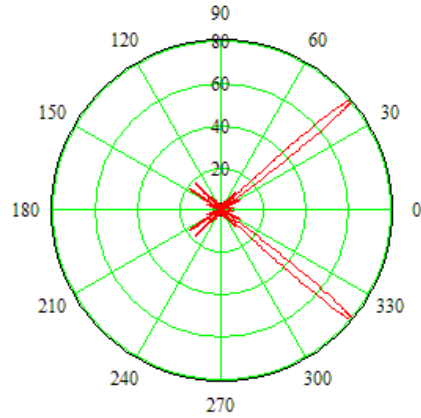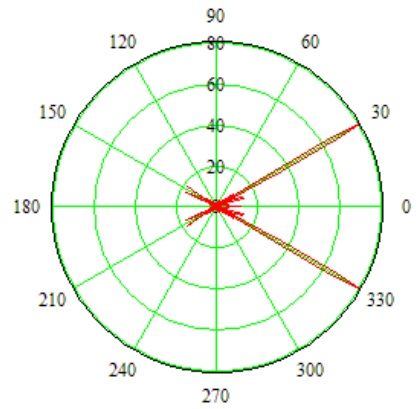
Fig.5.5.19. Block-phase beamf. at $\beta_\gamma = 30^0$ Fig 5.5.20. Conventional beamf. at $\beta_\gamma = 30^0$
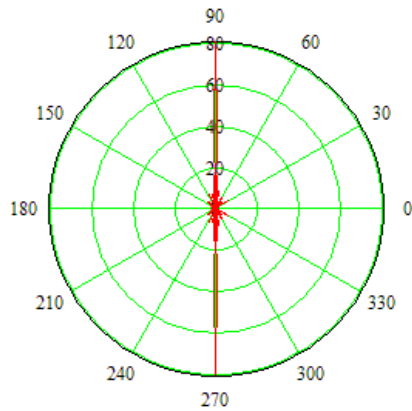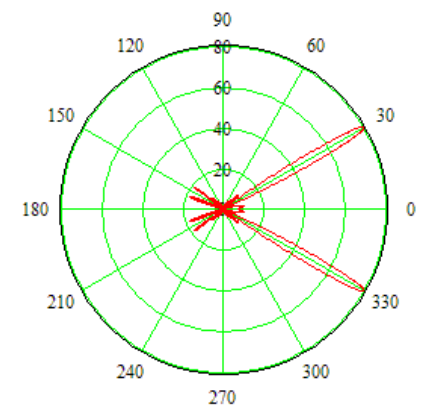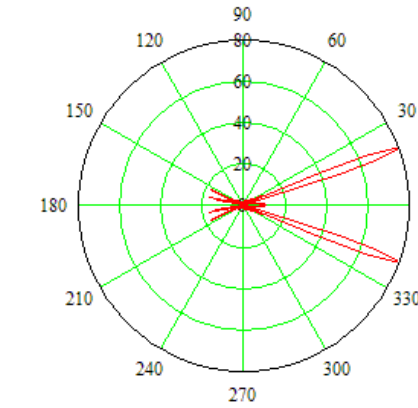

Fig.5.5.21. Block-phase beamf. at $\beta_\gamma = 20^0$ Fig 5.5.22. Conventional beamf. at $\beta_\gamma = 20^0$
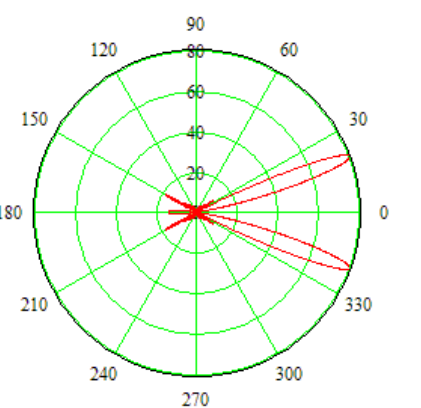
81

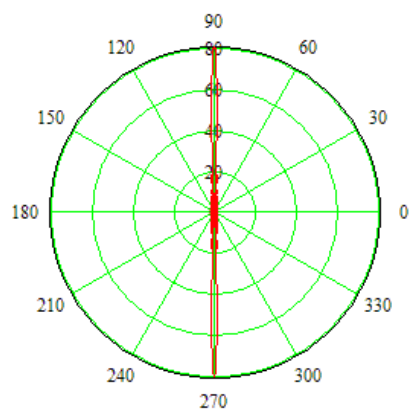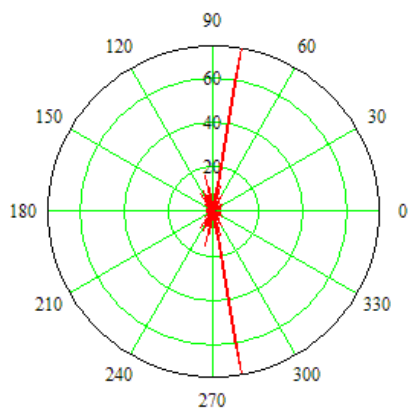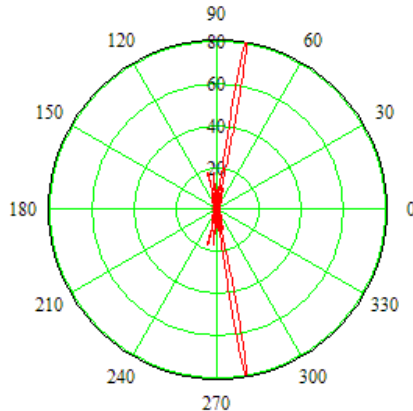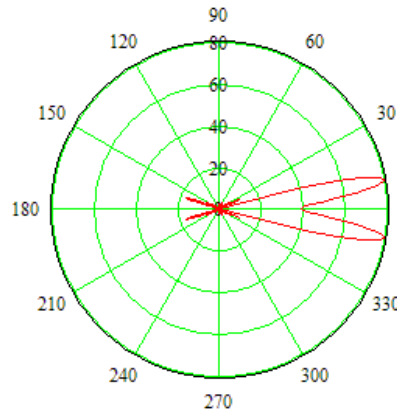Fig.5.5.23. Block-phase beamf. at $\beta_\gamma = 10^0$ Fig 5.5.24. Conventional beamf. at $\beta_\gamma = 10^0$
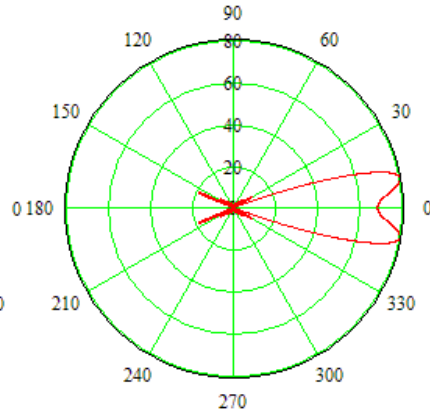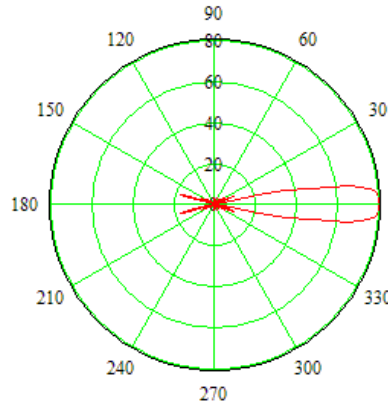
Fig.5.5.25. Block-phase beamf. at $\beta_\gamma = 0^0$ Fig 5.5.26. Conventional beamf. at $\beta_\gamma = 0^0$
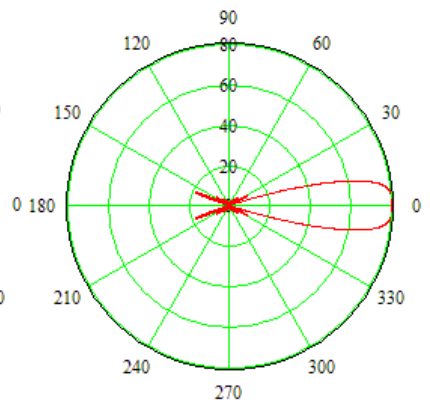
As we can see from Figs. 5.5.7 to 5.5.26, the Block-phase beamformer has narrower beam pattern compared with the conventional (phased array) beamformer.

A three-dimensional images of two-dimensional signal array *LX* in case of different angles are shown in Fig. 5.5.27 to 5.5.30.

82
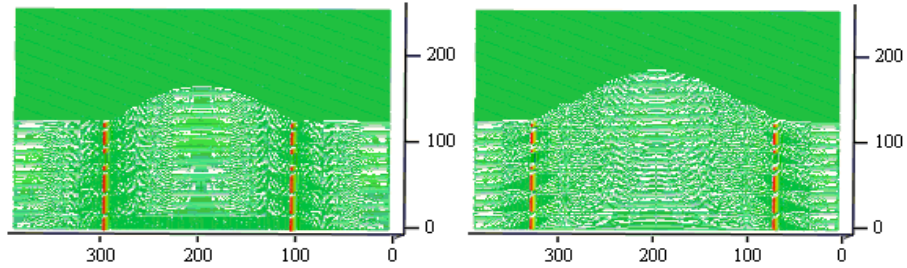
Fig.5.5.27. 3D. image of LX at $\beta_\gamma = 90^0$ Fig 5.5.28. 3D image of LX at $\beta_\gamma = 60^0$
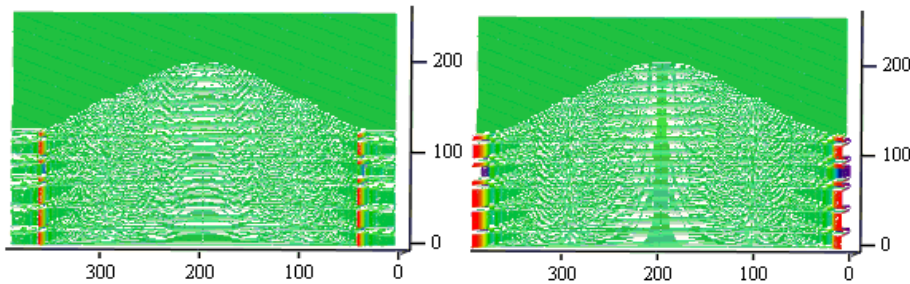
Fig.5.5.29. 3D. image of LX at $\beta_\gamma = 30^0$ Fig.5.5.30. 3D. image of LX at $\beta_\gamma = 0^0$

Fig. 5.5.31 to 5.5.33 shows the output signals after performing an optimal reception in case of different angles.

$\psi(\tau, 1.5707)$
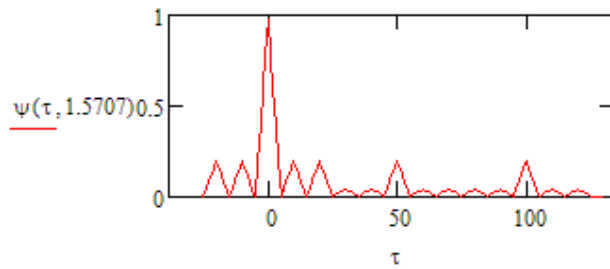
Fig. 5.5.31. Vertical cut of the ambiguity function of the optimal filter at $\beta_\gamma = 90^0$

$\psi(\tau, 1.047)$
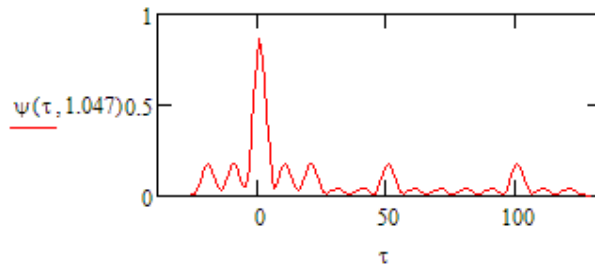
Fig. 5.5.32. Vertical cut of the ambiguity function of the optimal filter at $\beta_\gamma = 60^0$

83
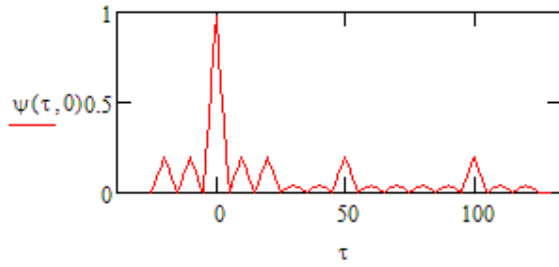
Fig. 5.5.33. Vertical cut of the ambiguity function of the optimal filter at $\beta_\gamma = 0^0$

Figs.5.5.34 to 5.5.37 illustrates the phase planes in the sensor array in case of different angles.
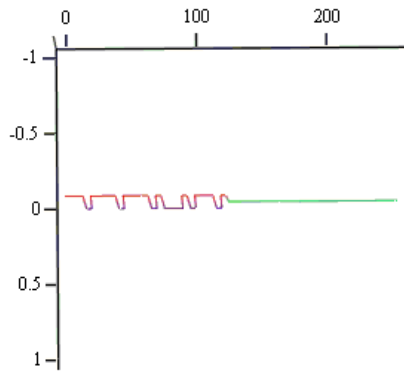
Fig.5.5.34. Phase planes in array at $\beta_\gamma = 90^0$ Fig.5.5.35. Phase planes in array at $\beta_\gamma = 60^0$
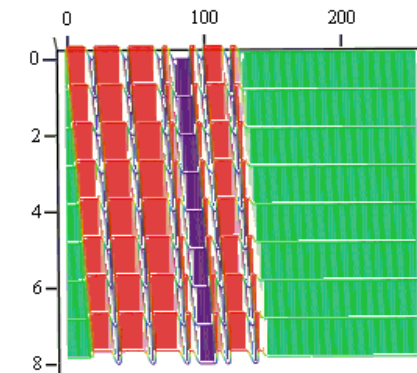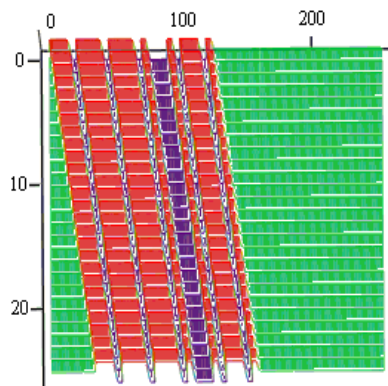
Fig.5.5.36. Phase planes in array at $\beta_\gamma = 30^0$ Fig.5.5.37. Phase planes in array at $\beta_\gamma = 0^0$
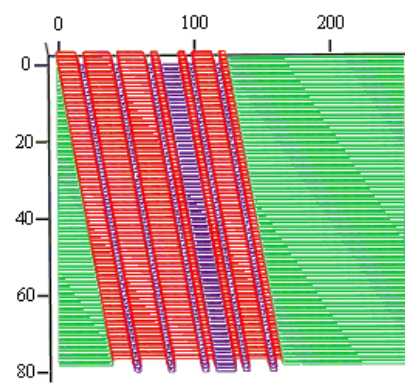
Fig. 5.5.38 to 5.5.42 shows the output signal of the sensor array in case of different

84

angles
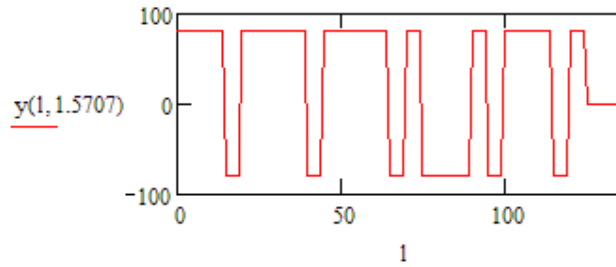
Fig. 5.5.38. Array output after the block-phase compensation at $\beta_\gamma = 90^0$
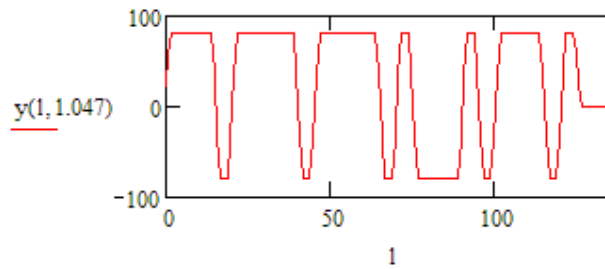
Fig. 5.5.39. Array output after the block-phase compensation at $\beta_\gamma = 60^0$
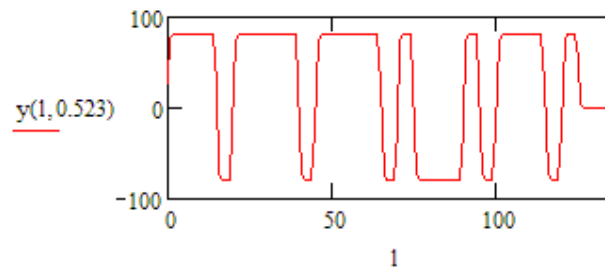
Fig. 5.5.40. Array output after the block-phase compensation at $\beta_\gamma = 30^0$
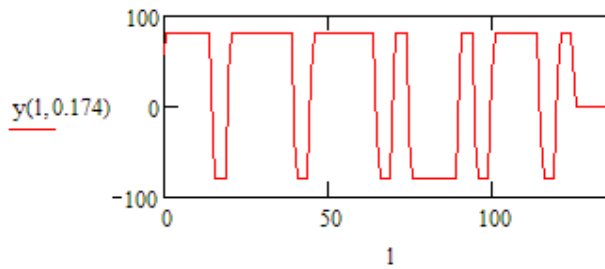
Fig. 5.5.41. Array output after the block-phase compensation at $\beta_\gamma = 10^0$
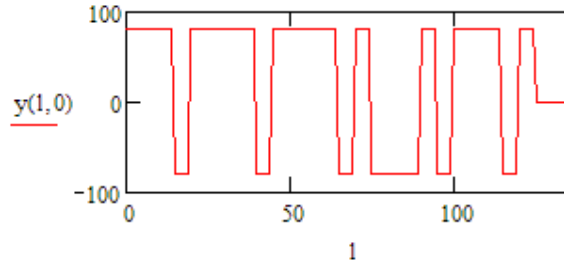
Fig. 5.5.42. Array output after the block-phase compensation at $\beta_\gamma = 0^0$

5.6 MODIFIED OPTIMAL RECEIVER

When impulse signals using binary phase manipulation are often used in modern sonar systems, we are not concerned with the initial phase of the signal and it is essential to eliminate the influence of the initial phase on the amplitude of the received signal [15] [16].

An example of the signal, where changes to the phases are made according to the values of five-element Barker's codes, is depicted in Fig. 5.6.1. Every element of the code includes 3 periods of harmonic oscillation, perhaps $N = 3 \cdot 5 = 15$.
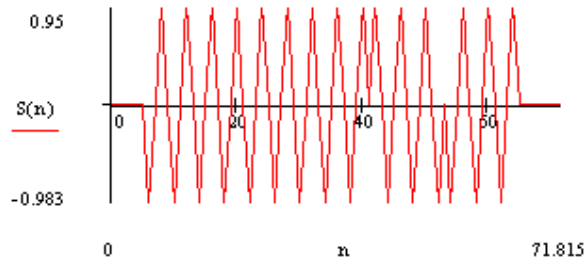
Fig. 5.6.1. Phase-manipulated signal based on the five-element Barker's code

The power of the harmonic signal P_s is independent from the phase and can be found through the one signal period T_0 as:

$$P_s = \frac{1}{T_0}\int_0^{T_0} s^2(t)dt = \frac{A_0^2}{T_0}\int_0^{T_0}\cos^2\left(\frac{2\pi}{T_0}t + \varphi_0\right)dt = \frac{A_0^2}{2}. \qquad (5.6.1)$$

Thus, the separation of quadrature components is not necessary to ensure invariance in the initial phase, and this enables us to abandon the rather complicated receiver with the quadrature correlator.

86

Instead, coherent collection of the signal energy must take place inside the optimal receiver in the course of time T_0 and therefore, we can determine the signal power P_s directly by summing the squares of the signal samples during the signal period T_0

$$P_s = \sum_{n=0}^{M-1} s^2(n),$$ (5.6.2)

where M is the amount of signal samples per one period T_0.
From here we obtain the signal energy:

$$E_s = P_s T_0 = \frac{A_0^2 T_0}{2}.$$ (5.6.3)

The structural scheme of the coherent optimum collection receiver is depicted in Fig. 5.6.2.
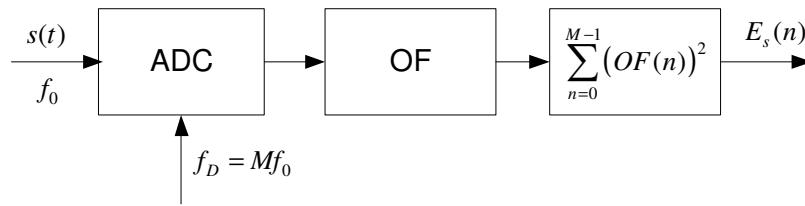
Fig. 5.6.2. Coherent optimum collection receiver

Reception occurs at the intermediate frequency without preliminary detection and accordingly, we must sample the signal at the intermediate frequency f_0 at first. Consequently, when using digital technology, it is advisable that the amount of samples per one signal period is expressed using the power of two. Taking into account, that the computing resources needed for processing increased proportionally with the amount of samples per period and considering the required quality indicators, the optimal sample rate is four samples per period, so $M = 4$ [10]. The general structural scheme of the optimal filter (OF) is depicted in Fig 5.6.3.
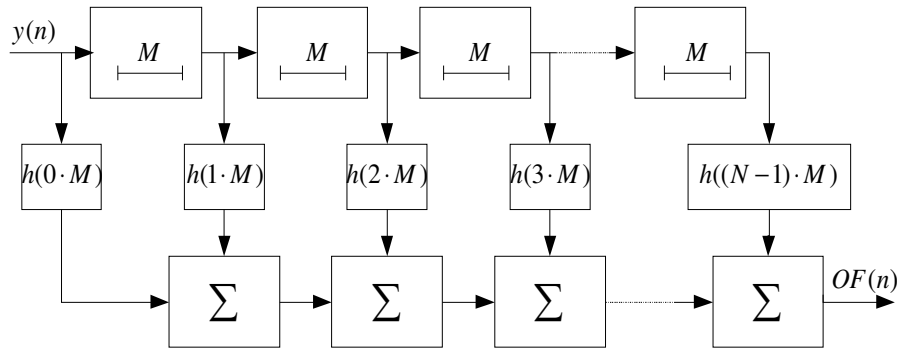
Fig. 5.6.3. Optimal filter

Its output signal is expressed as:

$$OF(n) = \sum_{j=0}^{N-1} h(j \cdot M) y(n + j \cdot M).$$ (5.6.4)

Presumably, only the pure signal exists in the input of the filter (Fig. 5.6.1) perhaps:

$$y(n) = s(n).$$ (5.6.5)

The required impulse response for the optimal filter is depicted in Fig. 5.6.4.
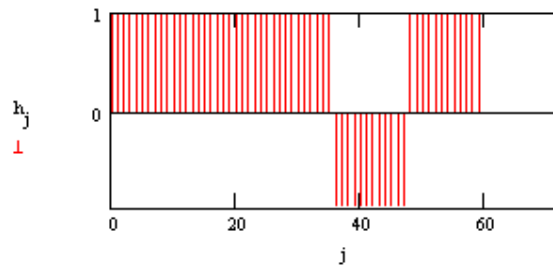
Fig. 5.6.4. Impulse response for the optimal filter in case of five-element Barker's code

In the structural scheme depicted in Fig. 5.6.3 and formula (5.6.4), only one sample per period is considered in the optimal filter and actually the expanded impulse response is used according to Fig. 5.6.5.
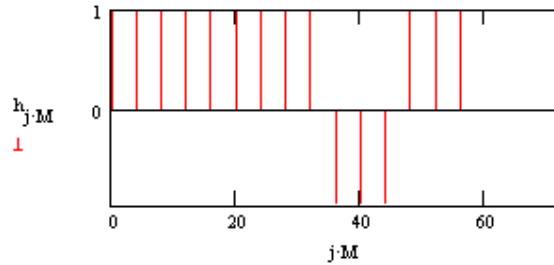
Fig. 5.6.5. Expanded impulse response of the optimal filter

The signal in the optimal filter output is depicted in Fig. 5.6.6.
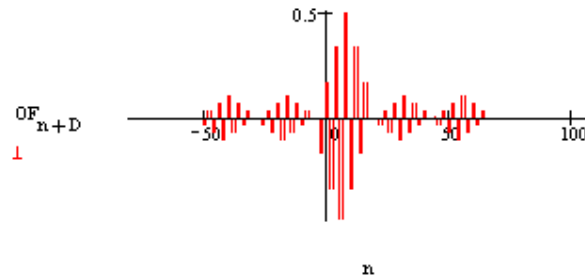
Fig. 5.6.6. Output signal of the optimal filter with coherent collection

The acquired output signal for the optimal filter directed to the input of the coherent collector, where the structural scheme of which is depicted, can be seen in Fig. 5.6.7. The required number of mathematical operations for this kind of receiver is:

$sum = (N-1)+(M-1)$ summing operation, in case of our example

$sum = 14+3 = 17$,

$mult = N + M$ multiplications, in case of our example $mult = 15+4 = 19$.

It is worth noting that the output signal of the optimal receiver actually described a vertical section of the ambiguity function of the scanning signal $F_v = 0$ so $\psi(\tau)$. The scanning signals and their ambiguity functions are dealt with in depth in Chapter 5.1.
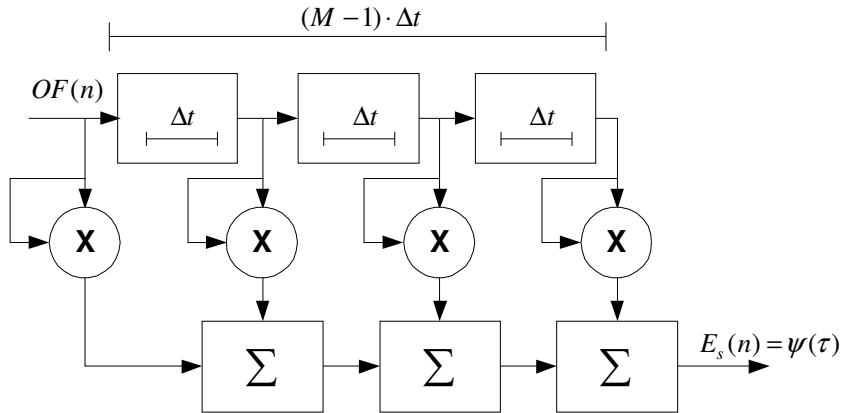
Fig. 5.6.7. Coherent collector of the signal energy

The output signal of the optimal receiver can be expressed as:

$$E_s(n) = \sum_{i=0}^{M-1}\left(\sum_{j=0}^{N-1} h(j \cdot M)\, y(n+i+j \cdot M) \right)^2 \qquad (5.6.6)$$

and the graph of the output signal is depicted in Fig. 5.6.8 (modelled using the MathCad package).
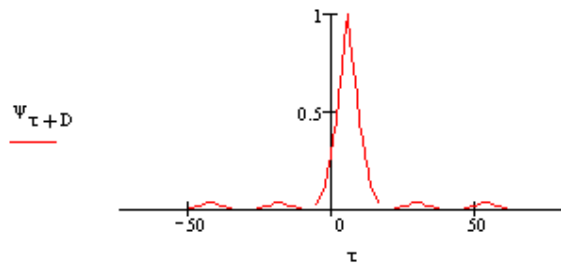
Fig. 5.6.8. Output signal of the optimal receiver for five element Barker's codes

We draw attention to the fact that the output signal of the receiver in Figure 5.6.8 (the section of the ambiguity function) has shifted against point 0 since the scanning signal (Fig.5.6.1) has also been delayed.

Such an optimal receiver produces the same result as the quadrature algorithm, but is considerably simpler and needs less computing power. Figure 5.6.9 gives an example of the output signal of the optimal filter, based on the quadrature modulator.
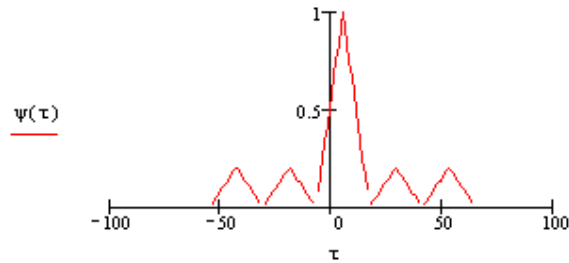
Figure 5.6.9 The output signal of the five-element Barker's code receiver when the quadratic algorithm is applied

Applying the quadrature transform on the output signal given in Figure 5.6.9 , we would obtain exactly the same graph as given in Figure 5.6.8.

At the same time, processing sonar signals requires a lot of computing power and in order to get satisfactory scanning results some methods must be applied to optimise filtering operations[21][28]. One of the most efficient methods is filtering of the scanning signal using elements and the application of the sliding average algorithm to each element. The Barker's code elements are rectangular radio impulses and if the time for averaging is chosen equal to the duration of one impulse, we can obtain a filter that is optimal for the element. The structural scheme of the sliding average algorithm [32] of one element is presented in Figure 5.6.10.
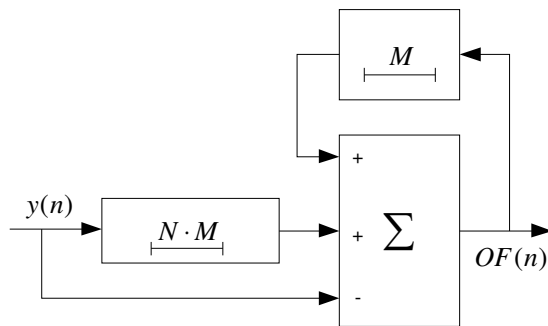
Figure 5.6.10 Optimal filter for the Barker's code element with sliding averaging

The architectural features of digital signal processors can be used, centralising, for example, the part of the optimal filtering into one block and the coherent collector into the other block working parallel. It is also possible to use the distribution of input data into odd and even channels and later sum up the results. The latter causes a halving of the decomposition capacity since the distance between the discretes doubles. Developing the parallel processing idea given above and considering the periodicity of input signals we can increase the efficiency of the

91

processing using only two discretes per period. Since in such a case only one discrete remains in both channels, processing within the period reduces to taking a square of the output signal of the optimal filter. At the same time, the decomposition ability decreases four times compared to the so-called clean direct processing. Considering the working speed of state-of-the-art signal processors, the reduction of the decomposition ability is not significant.

Since the optimal reception of sonar signals does not constitute the main topic of the present paper, I will not go into it in-depth here. Further reading on the above-mentioned topics is available in the literature [15], [16] and [17]. It is naturally also possible to implement optimal processing in the frequency domain. Some examples on the topic are viewed in Chapter 5.4 of the present paper.

5.7   COMPARISON OF RESULTS, SELECTING THE SCANNING SIGNAL

The analysis of scanning signals has been elaborated upon in Chapter 5.1 of the present thesis. According to the requirements, to reduce the impulse power and increase the precision of evaluating the time lag, the most effective method is to use signals based on Barker's codes. It is possible to use m-sequences, but in this case longer code sequences must be used to achieve the results equal to the Barker's codes. This aggravates the discovery of objects within shorter distances to the sensor array. We can get the most effective scanning signals when we use the nested codes, synthesized on the basis of Barker's codes, since these ensure extraordinarily narrow extremal areas and the same levels for the side lobe as for classical Barker's codes. A problem may arise with the spatial length of signals, which increases the minimal operating radius of the system. Therefore, when realising the system in practice, it is reasonable to make the configuration of the choice of a scanning signal simpler.

Concerning the dynamics of the scanning signals in the sensor array surveyed in the present work (Chapters 5.2), we observed that the general behavioural model is the same and still connected with the duration of the shortest element of the signal. Some differences appeared when using very long nested codes (the average amplitude of the output signal of the sensor array remained somewhat higher for large angles than when using traditional signals) but for the dynamics, the choice of scanning signals is not an essential factor. The choice of scanning signal is rather determined by the minimal and maximal operating radiuses and the correlation features of the signal.

The choice of algorithm depends on concrete situations, available hardware, etc. Comparing the theoretical results (Chapters 5.3, 5.4 and 5.5) it can be stated that they are all realizable and provide very good results theoretically. Essentially, the

whole angular interval $\beta_\gamma = \pm 90^0$ can be reduced to the equivalent situation $\beta_\gamma = 0$. The compensation of lags in the frequency domain can be considered the most accurate variant, but still this method is quite resource consuming. The matrix algorithm is the simplest in principle; however, it requires quite a high sampling rate to achieve the adequate precision (see Chapter 5.8) and the entire optimal reception must be realised separately. Hence, it must be admitted that in the case of the matrix algorithm it is reasonable to use the optimal receiver, working on the basis of the coherent collection principle (Chapter 5.6). This enables us to abandon the separation of the quadrature components from the algorithm. The minimal sampling rate should be at least 4 discretes per period (Chapter 5.8).

The block phase method provides good enough results if we stick to the rule that the relation $\beta_\gamma \le \beta_{kr}$ is valid according to the spatial length of one element (chip) of the signal and the length of the subarray. We are losing a little in the level of the main lobe of the output signal of the optimal receiver, but this loss is insignificant. It is essential that the main lobe width and general shape of the optimal receiver do not change. The level of the side lobes remains the same.

It must also be noted that the block phase method is not invariant to the scanning signal. Its concrete realisation (the number of subarrays formed) is dependent upon the scanning signal (to be more exact upon the duration/spatial length of its shortest element).

5.8 QUALITY MEASURES

5.8.1 The influence of sampling rate and initial phase on the quality of compensation

In order to find an optimal sampling rate for the system and evaluate its figures of merit, it is essential to preserve the oscillating component of the signals when modelling. The signal in the different channels of the sensor array can be expressed with the formula

$$M_{l,n} = \sum_{p=0}^{KV-1} \sum_{k=0}^{KH-1} A(l - k\tau_e - \tau_\xi, k + (p \cdot KH)) \cdot W(l - \tau_\xi, p, k), \qquad (5.8.1)$$

where

$$\tau_\xi = \frac{fs \cdot n \cdot d \cdot \sin(\beta_\gamma)}{c + \Delta c} \qquad (5.8.2)$$

93

and

$$W(l, p, k) = \cos\left(\frac{2\pi f_0 \cdot l}{fs} + \left|\phi_p - \phi_k\right| + \Delta\phi\right). \tag{5.8.3}$$

Here

Δc - distortion in the wave propagation speed,
$\Delta\phi$ - distortion in the scanning signal phase.

Resulting from this, the total signal in the output of the array can be expressed with the formula

$$y(l) = \sum_{n=0}^{N-1} M_{f(l,n),n}. \tag{5.8.4}$$

The signal's "ideal" ambiguity function $\psi(\tau, 0)$ that we viewed is depicted in Fig. 5.8.1. Here a high sampling rate has been used (16 samples per period). The use of this is not expedient in practice. Fig. 5.8.2 shows a case in which the source has been sampled according to the Nyquist theorem or, in other words, 2 samples per period and $\beta_\gamma = 0$.
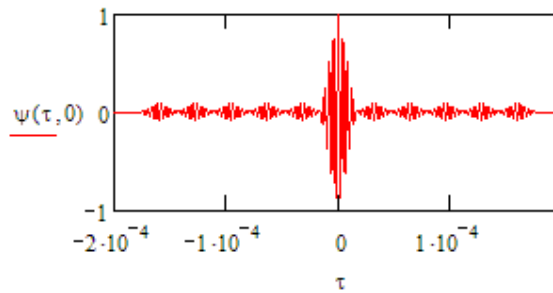
Fig. 5.8.1. $\psi(\tau, 0)$ with $fs = 4MHz$
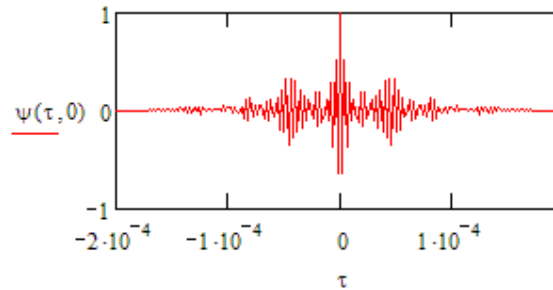
Fig. 5.8.2. $\psi(\tau, 0)$ with $fs = 500kHz$

Here the frequency of the oscillation component is $f_0 = 250\ kHz$. As Fig. 5.8.2 shows, option $fs = 500\ kHz$ falls out immediately due the discrete errors. Therefore we focus on the option 4 samples per period.

If $\beta_\gamma = 0$, the function $\psi(\tau, 0)$ in the compensator output is similar to that depicted in Fig. 5.8.1. Fig. 5.8.3 shows function $\psi(\tau, 0)$ in the output of the array if $\beta_\gamma = 40°$ and Fig. 5.8.4 the corresponding $\psi(\tau, 0)$ in the compensator output if $\beta_\gamma = 40°$.
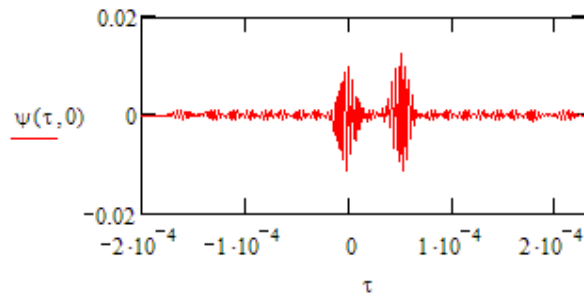
Fig. 5.8.3. $\psi(\tau, 0)$ with $fs = 1\ MHz$
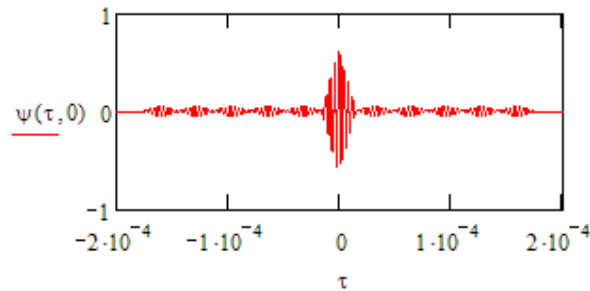
Fig. 5.8.4. $\psi(\tau, 0)$ +comp. $fs = 1\ MHz$

Therefore, we can see that the compensation is not complete. The amplitude of the function of uncertainty is primarily affected which can cause problems in case of bad signal/noise ratio.

Figs. 5.8.5 and 5.8.6 show the results in the same conditions $\beta_\gamma = 40°$; however, the sampling rate has been increased to $fs = 2\ MHz$ (8 samples per period). Therefore, the higher the sampling rate, the more precise is the result of compensation because possible discrete errors which are arised from different signal delays in different channels are less. The results show that 8 samples per

95

period should be enough to reach a satisfactory outcome. The random initial phase of the scanning signal also has an influence on the quality of compensation. The extent and nature of the influence is equivalent to effects caused by the different falling angles. This does not worsen the system's behaviour
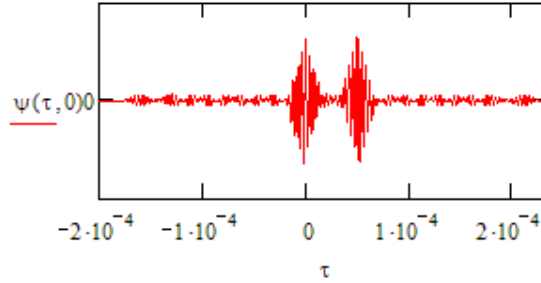
Fig. 5.8.5. $\psi(\tau,0)$ with $fs = 2\ MHz$
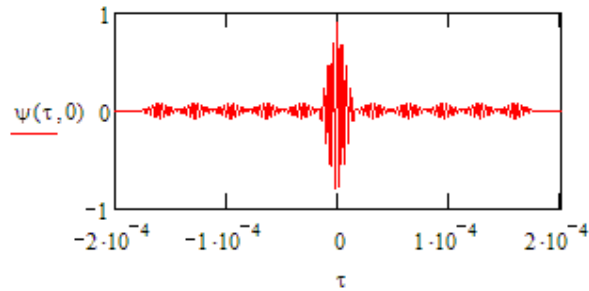
Fig. 5.8.6. $\psi(\tau,0)$ +comp. $fs = 2\ MHz$

Fig. 5.8.7 shows the fluctuations in the maximum values of the functions of ambiguity when $fs = 1\ MHz$ (red solid line) and $fs = 2\ MHz$ (blue dotted line).

Fig. 5.8.8 shows the influence of phase changes when $\beta_\gamma = 40°$.

Fig. 5.8.7. max $\psi(\tau,0)$ $\beta_\gamma = 0 - 90°$
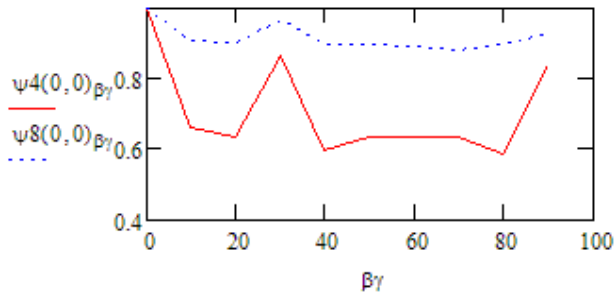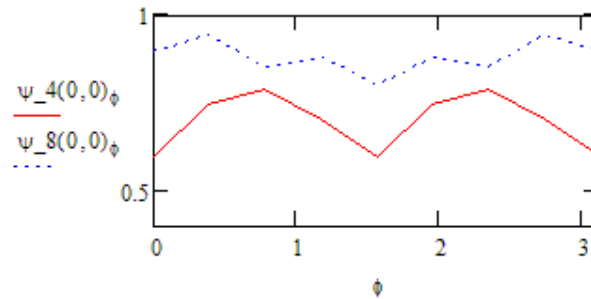
Fig. 5.8.8. max $\psi(\tau,0)$ $\beta_\gamma = 40°$

Subsequently, we will look at the influence of the changes of wave propagation speed on the quality of compensation. For that we will use the sampling rate $fs = 2\ MHz$.

5.8.2 The influence of the changes of wave propagation speed on the quality of compensation

As formula 5.2.31 shows, the extent of the signals delay in each channel of the sensor array depends on the wave propagation speed. If the wave propagation speed has been fixed in the compensation algorithm, but the wave propagation speed of the signal that falls on the sensor array differs from it due to the influence of the environment, the quality of compensation may worsen. In order to evaluate this, we change the propagation speed of the signal that falls on the array in the interval of $\pm 50\ m/s$ ($c = 1450..1550\ m/s$). Figs. 5.8.9 and 5.8.10 show the images of function $\psi(\tau,0)$ in the compensator output when $\Delta c = -20\ m/s$ and $\Delta c = 50\ m/s$. Here we note that $\beta_\gamma = 30°$ and $fs = 2\ MHz$.
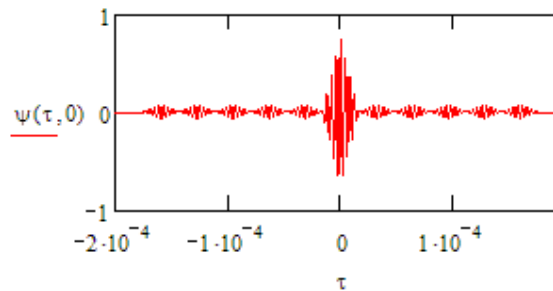
Fig. 5.8.9. $\psi(\tau,0)$ +comp. when $\Delta c = -20\ m/s$

97
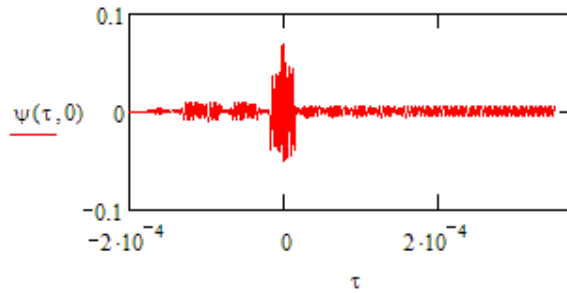
Fig. 5.8.10. $\psi(\tau,0)$+comp. when $\Delta c = 50 \ m/s$

As Fig. 5.8.10 shows, in case of $\Delta c = 50 \ m/s$ the compensator has lost its effect. Fig. 5.8.11 shows the maximum values of function $\psi(\tau,0)$ in case of different distortions. We can see that the compensation algorithm we looked at $f_0 = 250 \ kHz$ works adequately if $fs = 2 \ MHz$ and $\Delta c = \pm 20 \ m/s$. In the opposite case further measures have to be implemented.
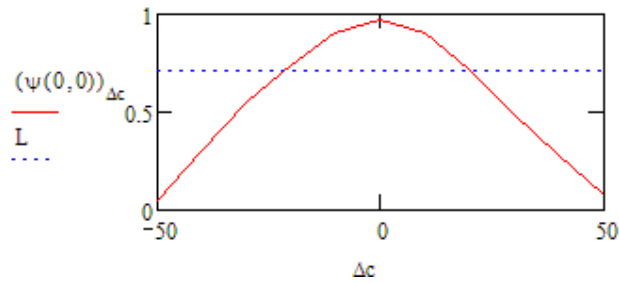
Fig. 5.8.11. Max $\psi(\tau,0)$ values with $\beta_\gamma = 30°$ and $c = 1450 - 1550 \ m/s$

6 ANALYSIS AND ESTIMATES OF THE REALIZATION OPPORTUNITIES

6.1 IN GENERAL

Nowadays, it is possible to use all the advantages of digital signal processing and high-level integration in designing systems. At the moment, digital-analogue converters are produced with sampling frequencies exceeding 250 *MHz*. Signal processors are able to perform billions of operations per second and memory capacities range to gigabytes. At the same time, the cost of the hardware has remained at the same level or even decreased. The high level of integration enables the production of small lightweight systems. Thus, equipment does not pose a problem nowadays, as it may have some years ago. The problems connected to software and algorithms are becoming increasingly important. Radio technology is becoming fully digitalised. SDR (Software Defined Radio) is developing with the aim of digitising the signal as close to the antenna (sensor) as possible.

As a rule, a sonar system consists of a digital part and an analogue part. The analogue part comprises transmitters and receivers; and the digital part signal processors, memory storage devices and analogue-to-digital and digital-to-analogue converters. The formation of the beam pattern is implemented completely digitally. A PC-based computer, which primarily fulfils the steering and presentation function, is also integrated into the sonar system. The transmission of data between specialised hardware and the PC is implemented by means of USB or RS232 ports. It is also possible to use more up-to-date interfaces meant for video transmission. If the specialised hardware has been realised as a computer card, PCI or PCI Express can act as the coupling. The steering and presentation role can be executed by any modern PC if it has a processor with a clock rate of at least 1.4 *GHz* and an operative memory of 512 *MB*. These requirements are first of all related with the requirements of the specialised hardware described above.

6.2 ESTIMATION OF REQUIED COMPUTING POWER

In the present chapter, a rough estimate is given on the basis of concrete examples, with the aim to evaluate the overall technical feasibility of the algorithms. The concrete computing power is nevertheless dependent upon the signals used, the required range of activity, the number of the channels of the sensor array and many other factors.

6.2.1 Phase compensation

Classical phase compensation reduces to calculating the fast Fourier transform (FFT), and so we must consider that with the fast Fourier transform, the

transformation period must be presented by means of levels of two. Thus, with an element array of $N = 81$ we must take the length of the Fourier transformations as being 128. Using the classical FFT algorithm with power of two, we get 896 for the number of summing operations of complex numbers and 448 for multiplication operations of complex numbers. The resources required by the optimum receiver is related to the length of the optimum support signal. If the length of the support signal is, for example, 100 discrete values, the necessary computing power is 100 summing and multiplication operations together, involving memory operations.

6.2.2 Matrix algorithm

Proceeding from the case given in Chapter 5.3, where the nested code, synthesized on the basis of the 5-element Barker's code, was used with a duration of one element $\tau_e = 25 \, \mu s$, when the sampling frequency is $fs = 1 \, MHz$, the duration of the signal is $L = 25 \cdot 25 = 625$ discrete values. When the number of sensors is $N = 81$ and the distance between the sensors $d = 0.0015$, the maximum length of the buffer is 705 discrete values. Thus, the matrix of 81 x 705, involving 57,105 complex numbers, forms behind the sensor array. Using 4 bytes for storing the complex numbers, we obtain the required memory storage capacity of 228,420 bytes. Hence, it follows that in any case it would be functional to use systems of at least 32 bytes for processing the signals. If the system has been realised on the basis of circular buffers, it means that the signal processor must be able to perform external memory operations of 228,420 bytes during $1 \, \mu s$. As a rule, memory operations are realised by means of a special instruction set in the signal processors, which realise the shift of data in the memory during one machine cycle or even faster. In the case of the 32-byte system, it would make 57.1×10^9 memory operations per second if it were necessary to transfer the whole contents of the matrix using every next discrete value. In addition, it is necessary to implement N=81 summing operations of complex numbers, 81 summing operations of indexes and 81 comparison operations during $1 \, \mu s$. If one wants to use an amplitude window of a special shape, 81 more multiplying operations of complex numbers are added. If the magnitudes calculated on the basis of formulae 5.3.7 and 5.3.8 have been calculated previously and stored in the memory of the processor, there will not be any additional multiplication operations.

It must be considered that summing complex numbers requires two operations with real numbers and multiplication of complex numbers requires two summing and four multiplication operations with real numbers. Implementing comparisons is equivalent to two mathematical operations (uses two machine cycles of the processor). Thus, in the case of the unit amplitude window, the system must implement 405 operations during $1 \, \mu s$ (or 405 million summing operations per second). Using other amplitude windows, 162 summing operations and 324 multiplication operations are added during $1 \, \mu s$. Considering that in modern signal

processors there is no difference between the temporal duration of summing and multiplication operations, it results in 891 operations in total during $1\,\mu s$ (891 million operations per second).

For a signal consisting of 625 discrete values, at least 1,250 operations are performed to achieve optimum reception (if the optimum receiver has been realised considering classical principles) of the signal during $1\,\mu s$ (1,250 million operations per second). A rough estimate of the computing power of the whole system is 2,141 million operations per second. Such efficiency is ensured, for example, by the general-purpose TigerSHARC processor ADSP-TS101S.E.

It is also possible to realise the system so that the whole reflected signal is stored in the vast scale array of the memory storage. When the recording has finished, the post processing does not take place in real time. The parallel processor systems, which are interconnected, can also be applied. An estimate of the memory capacity necessary for post processing is given in the next chapter.

6.2.3   Delay compensation in the frequency domain

According to Chapter 5.4, the nested code, synthesized on the basis of the 5-element Barker's code, is used with a duration of $\tau_e = 25\,\mu s$ of a unit element. When the quadrature components have been separated, we can use the reduced sampling frequency of $fs = 0.5\,MHz$. The duration of the signal will be $L = 313$ discrete values. Using the number of sensors $N = 81$ and a mutual distance between the sensors of $d = 0.0015$, the maximal length of the buffer will be 353 discrete values if a system based on circular buffers is used. Thus, a matrix of 81×353 is formed behind the sensor array, which consists of 28,593 complex numbers. In the 32-byte system, it would perform $28.6 \times E9$ memory operations per second if the whole contents of the matrix need to transfer for every following discrete value.

In the case of the given method, it is necessary to find the fast Fourier transform in every channel. Since the number 512 is the level of two nearest to 353, the FFT must be used with a period of 512. The necessary number of summing operations in one channel is 4,608 and the number of multiplication operations 2,304. In addition, the multiplication of 512 complex weight coefficients must be implemented if the values of the expression 5.4.4 have been previously calculated for all the array channels and discrete frequencies. Since the number of sensors is 81, the numbers mentioned above must be multiplied by 81. For optimum reception, all spectrum values must be summed, which adds to the total number of operations – $81 * 512 = 41472$ summing operations.

The number of operations preceding the optimum reception will be $81*(4608+2301+512+512)=642573$ complex operations. If the complex conjugated spectrum of the support signal has been previously stored in the memory, the optimum reception adds $4608+2301+512=7421$ operations and the total number of operations will be 649,994 complex operations during $2\ \mu s$ or 324 billion operations per second. It is clear that by using such a method it is not necessary to apply processing based on circular buffers, but to collect the reflected signal into the vast array of the memory and conduct post processing later. Considering that the wave propagation speed in the water is $c=1500\ m/s$ and the sampling frequency is $fs=0.5\ MHz$, then in order to achieve a 200-metre range of activity, the capacity of the memory array must be 81×133333 discrete values. If every discrete value were presented by a 32-byte number, the necessary memory capacity would be 44 MB. Considering that coefficient arrays must also be stored, the estimated memory capacity will be 128 MB, which poses no problem nowadays. Certainly, in this case the capacity of the Fourier direct and inverse transforms will increase, but since there is no need to perform this during the period following two consecutive discrete values, the general demand for computing power decreases. If necessary, it is possible to apply the commuted processing systems, which increases the scanning speed.

6.2.4 Block method

As mentioned above, the block method integrates the phase compensation and the matrix algorithm. By compiling the signal buffers, we can proceed from the principles given in point 6.2.2. To estimate the required computing power we proceed from the expression 5.5.10 and the internal sum reduces to the fast Fourier transform. Since by dividing the sensor array into sub-arrays, the lengths of the Fourier transforms decrease, the processing of the whole array occurs more rapidly compared with when the Fourier transform is calculated simultaneously for all the array elements. For example, for the 81-element sensor array we should apply the 128-point Fourier transform, which presumes summing 896 complex numbers and the multiplication of 488 complex numbers. Dividing the array into 9 sub-arrays with a length of 9 elements, we can use the 16-point Fourier transform, which can be executed by 64 summing and 32 multiplication operations. Considering that the number of sub-arrays is 9, we can get a total of 576 summing operations of complex numbers and 288 multiplications. In addition, 9 summing operations of complex numbers, 54 indexing operations and 128 comparison operations must be implemented at every moment. Considering the number of operations for executing complex operations, we can get 1,836 summing operations for real operations (the comparison operation is equal to two operations) and 1,152 multiplications, which makes 2,988 operations in total necessary during $2\ \mu s$ if $fs=0.5\ MHz$ (1,494 million operations per second). For a signal consisting of 313 discrete values, 626 operations are added for optimum reception during $2\ \mu s$ (313 million operations

per second). According to our rough estimate, the computing power of the whole system will be 1,807 million operations per second. Such efficiency is ensured by, for example, the general-purpose TigerSHARC processor ADSP-TS101S.

7 CONCLUSIONS

The main problem the present doctoral thesis described is the fact that there are problems steering the beam pattern of the sensor array using spread-spectrum signals. In addition, the qualities of the scanning signals and problems with steering the optimum reception of signals have also been observed.

Chapter 4 presented the theoretical foundation of this paper, the propagation of acoustic waves in the modelling environment, the theory of complex aperture, array theory and classical methods of signal processing in arrays. These chapters were reviews and intended primarily to bring the reader up-to-date with the basics of the present work. At the same time, many of the principles presented have been modelled by the author and the results presented graphically. On the one hand, it was possible to discover that the theoretical results are valid, but modelling was primarily necessary at this stage in order to create a proper modelling environment to deal with the central problems. The mathematical package MathCad version 13.1 was chosen for the modelling environment. The choice in favour of MathCad was made because the realisation of complicated (non-standard) mathematical expressions is much simpler with this program compared to, for example, MATLAB [27]. At the same time, calculations are performed quite slowly in the MathCad environment, resulting in the need for more up-to-date computing equipment.

Chapter 5.1 deals with scanning signals and the functions of their ambiguity. The focus is on the phase manipulated scanning signals based on the Barker's code. The signals of such type are good in terms of measuring the delay duration. At the same time, we recognised that while the m-sequence based phase manipulated signals are in place in communication systems, in relation to locating, they do not match the Barker's codes (primarily due to the higher level of the correlation functions of the side lobes). The Barker's codes reportedly range to a length of 13 elements, which on the one hand does not allow us to make the extremal area of the correlation too narrow. The solution to this problem is to use nested codes synthesized on the basis of the Barker's codes. The result of modelling showed that by nesting the Barker's codes in this way, it is possible to obtain a narrower extremal area and reduce the power of the signal. At the same time, the level of the side lobes (the minimal residue) remains at the same level as for the non-nested Barker's codes. It is possible to generate the nested codes on the basis of m-sequences but since their minimum residue is larger, it is not practical to use them. Using the nested codes may be restricted by the range of the activity of the system. Discovering objects in the vicinity may become problematic when using very long codes.

Either, the problems of reducing the power of the scanning signal are dealt with. The conclusions that were made suggested that by the same non-energetic indicators it is possible to reduce the power of the signals by B^2 (B stands for the

signal base). In practical solutions, it will enable a reduction in the power of the sonar system by down to some watts.

Chapter 5.2 deals with the practical solutions to using spread-spectrum signals as scanning signals in sensor arrays. It is known that by using narrow-band scanning signals with a long duration, the beam pattern of the sensor array changes when the angle of the arrival on the array becomes to a certain extent wider (against the norm for the sensor array). One of the goals of this paper is to investigate the dynamics of wide-band spread-spectrum signals with a short equivalent duration in sensor arrays. To better reveal the nature of the problem, the research was started out by studying the behaviour of a single short-duration impulse (i.e. the spatial length of the impulse was considerably smaller compared to the spatial length of the sensor array). As discovered, the sensor array started to change temporally; and in addition, the width of the beam pattern also increased, primarily because an impulse with a short spatial length is able to activate only a certain part of the sensor array. The critical β_{kr} appeared to be an essential parameter in the case of at least one moment when all the sensors of the sensor array are activated. This critical angle formed the basis for working out the block-phase method, since for such an angle the maximum value of the output signal of the optimum receiver is still acceptable. After that, the dynamics of the phase-manipulated signals based on the Barker's codes and m-sequences were studied on the sensor arrays. It appeared that the model of their behaviour is generally similar and related to the duration of the shortest element of the scanning signal (chip). The results of modelling showed that when using the critical angle β_{kr}, the width of the major lobe of the output signal of the optimum receiver does not change and their influence is only expressed in their amplitude. When the angle of the arriving signal on the array exceeds the critical angle, the width of the major lobe of the output signal of the optimum receiver began to increase, which has a direct negative impact on the precision of the time delay assessment. In the case of the nested codes, it was significant that when the angle of the arriving signal on the array increased, the distortion of the output signal of the array also increased, but its maximum value did not decrease. This phenomenon is caused by the fact that the nested code is quite long itself. It is interesting that when the angle of the arriving signal on the array exceeds the β_{kr} value, the shape of the output signal of the optimal receiver did not change. At the same time, the width of the major lobe of the output signal of the optimal receiver has increased so the precision of the time delay assessment will suffer anyway. One idea was to use a separate support signal for every angle, perhaps use the really distorted output signal of the array, but modelling showed that it would not have any effect.

In Chapter 5.3, the author dealt with the matrix algorithm for delay compensation, which is principally the simplest method for processing spread-spectrum signals in sensor arrays. The advantage of the system lies in its principal simplicity, but at the same time it is sensitive to the sampling frequency. This research has shown that

the method works normally at the sampling frequency, which ensures 4 discrete values per signal period. In a properly working system, if the angle of the arriving signal on the array is $\beta_\gamma = \pm 90^0$, this ensures the equivalent situation to $\beta_\gamma = 0^0$ (to the norm of the sensor array). The change in the wave propagation speed also has an effect, which may result from changes in the temperature of the environment or other factors. Analysis showed that the algorithm works adequately within the interval of $\Delta c = \pm 20 \, m/s$. Because of the computing power required, the algorithm may also be realised on the basis of circular buffers, which enables us to considerably increase the range of activity without the need to increase the memory capacity.

Chapter 5.4 looks at the delay compensation and formation of the beam pattern in the frequency domain. First, a transition was carried out to the complex amplitude of the scanning signals and a precise mathematical model was created for delayed scanning signals in the different channels of the sensor array. The validity of the model was checked by restoring the real signal from its complex amplitude and also applying the classical phase compensation to its array (the shape of the output signal was previously known). In modelling, it turned out that when using complex amplitudes it is essential to compensate the temporal delays and also the phase of signals at all frequencies. Thus, in the case of the algorithm observed, the individual complex weights are selected for each frequency, which means that it is possible for us to construct the beam pattern independent of the frequency. It also essential that the amplitude weights only determine the shape of the beam pattern, and the level of the side lobes and the beam patterns of any shape can be construed, independent of the frequency. In principle, this method is an alternative to the adaptive methods of forming beam patterns. This method is not very sensitive to the sampling frequency either. The modelling also showed that on the condition that the system works accurately, with an angle of the arriving signal on any array of $\beta_\gamma = \pm 90^0$, it ensures the equivalent situation to $\beta_\gamma = 0^0$ as in the case of the matrix algorithm. The advantage of this method is the possibility of instantly realising the optimum reception in the frequency domain. The disadvantage of the system is the very large number of calculations if it is realised on the basis of circular buffers. Here it is practical to record the entire reflected signal in the memory of the processor and realise the system by means of post processing.

In Chapters 5.5 a survey is given of the block-phase method, which integrates the phase compensation and the matrix algorithm. The method gives enough good results if we stick to the rule that there is a relation $\beta_\gamma \le \beta_{kr}$ for the spatial length of one element of the signal (chip) and the concrete length of the subarray. The level of the main lobe of the output signal of the optimal receiver is decreasing, but the loss is insignificant. The width and the general shape of the main lobe of the output signal of the receiver do not change and the level of the side lobes remains the same. At the same time the block phase method is not invariant to the scanning

signal. Its concrete realisation (the number of subarrays formed) is dependent upon the concrete scanning signal (to be more precise upon the duration/spatial length of its shortest element). The analysis has also shown that in the optimal receiver it is not reasonable to record supporting signals separately for each partial direction. It is possible to reduce the number of mathematical operations and hence the required computing power if the values of lags and other parameters are recorded previously for all partial directions in the memory. In order to find the direction diagram, the output signals of the sensor array were found for all discrete angles. The modelling results showed that unlike for classical phase compensation the main lobe width of the direction diagram does not increase at large angles. This is also valid for the matrix and FFT algorithm. The advantages of the block-phase method can be considered the reasonable number of mathematical operations, which allows us to also realise the system on the basis of circular buffers. When the scanning signal falls onto the array from the normal direction, only the summing up of signal elements occurs in the system. When the signal falls onto the array at some abnormal angles, the sensor array is divided into sub- (phase) arrays. Thereby, the required computing power even decreases compared to the classical phase arrays since the calculation of the Fourier transform is executed using smaller blocks.

In Chapter 5.6, the problems related to optimal filtering were dealt with in-depth. An optimal filter was modelled for the five-element Barker's code. When impulse signals with binary phase manipulation are used for the scanning signal, we are not concerned with the initial phase of the signal and it is essential to eliminate the influence of the initial phase on the amplitude of the received signal. It was discovered in this chapter that the separation of quadrature components is not necessary to ensure invariance from initial phase and this enables us to abandon the rather complicated receiver with the quadrature correlator. The innovative structural scheme of the coherent optimum collection receiver and the results of the modelling have been highlighted. This type of optimum receiver gives the same results as the quadrature algorithm, but is considerably simpler than the latter and enables the performance of optimum reception directly at intermediate frequencies. It is practical to use the receiver together with the matrix algorithm for lag compensation. For normal operation, both of them need the sampling frequency of 4 discrete values per period.

In summary, it can be said that using the scanning signals formed on the basis of the Barker's codes enables a reduction of the impulse power of the sonar systems and at the same time an increase in the precision of evaluating the time lag. Using the signal processing algorithms given in the present paper it is possible to achieve the comparable decomposition ability to the situation $\beta_\gamma = 0^0$ for all the angles of the signal falling onto the array. The selection of the scanning signal should be configurable on-the-fly. All the given algorithms are realisable with up-to-date microprocessor equipment. The system can be realised on the basis of a

TigerSHARC processor ADSP-TS101S. The predicted memory capacity would be 128-256 *MB*.

Statements presented for public defence:

1. It is possible to reduce the power of the impulse using spread-spectrum signals of the sonar or radar system by 3 to 169 times and at the same time enhance the precision of the time lag estimation by factor $KV \cdot KH$ (3-169) if compared with the signal of the same duration but without intra pulse modulation . The codes based on novel nested codes remarkably enhance the operating range of the sonar or radar.
2. Classical phased array in sonar systems is not applicable for steering beam patterns using spread-spectrum signals because its smallest element (chip) activates only part of the whole array when the signal arrival angle is different from normal.
3. In order to solve the problem, three different signal-processing algorithms for steering the beam pattern of the sensor array are composed and modelled:

    a. MATRIX algorithm,
    b. Advanced FFT algorithm,
    c. Block-phase algorithm where dynamically variable sub-arrays are used.

4. Using the Block-phase method developed by the author, it is possible to enhance the precision of the measurement of the distance, while the power of the impulse of the sonar system is reduced as mentioned above , the radial resolution increased at least 2-3 times in the case of large angles and required computing power is decreased.

8 LAIENDATUD KOKKUVÕTE

Käesolev kokkuvõte on koostatud eesti keeles ja kajastab töö olemust, eesmärke ning põhilisi järeldusi.

8.1 SISSEJUHATUS

Merepõhja kaardistamine ja navigatsioon on olnud ajalooliselt üheks sonarsüsteemide põhiliseks kastusvaldkonnaks. Tänapäeval on lisandunud ka tehniliste objektide lokaliseerimine nagu õliplatvormid, merealused gaasijuhtmed jne. Militaarvaldkonnas on oluline tähtsus miinitõrjel. Samuti on olulisel kohal katastroofipiirkondade uurimine. Olulistemaks parameetriteks on seejuures kauguse mõõtetäpsus ja radiaallahutusvõime [31][35].

Radarite ja sonarite algaastatel kasutati sondeerivate signaalidena lihtsa struktuuriga nn. monopulss tüüpi signaale. On teada, et kauguse mõõtetäpsust saab suurendada lühendades keskkonna aktiviseerimiseks kasutatava sondeeriva signaali ajalist kestvust. Samas tuleb jälle suurendada signaali akustilist võimsust, et oleks tagatud piisav tööraadius ning häirekindlus. Tavasonaritel võib keskkonna aktiviseerimise akustiline võimsus ulatuda mitme *kW*-ni. Sellised signaalid on aga keskkonnale ohtlikud, kaasaarvatud inimestele, kes võivad viibida sonarsüsteemide vahetus läheduses. Hiljem (al. 1958) leiti, et on võimalik kasutada ka keeruka struktuuriga signaale (Barkeri koodid, M-jadad) väljakiiratava võimsuse vähendamise eesmärgil. Samas ei võimaldanud tolleaegne tehniline tase uusi ideid realiseerida. Seoses digitaaltehnika arenguga tekkis võimalus võtta keeruka struktuuriga hajaspektersignaalid kasutusele kuid reaalselt sai neid kasutada vaid mehhaanilise skaneerimise korral.

Sonarsüsteemi radiaallahutusvõime on määratud sensorsüsteemi suunadiagrammi pealehe laiusega. Mida kitsam, seda parem. Klassikalise faasivõre korral on suunadiagrammi pealehe laius määratud sensorvõre ruumilise pikkusega ning tüüpiliselt arvutatakse sensorivõre suunadiagramm lõpmatu kestusega püsiva magnituudiga harmoonilise võnkumise korral. On teada, et suunadiagrammi elektrilisel juhtimisel muutub suunadiagramm signaali võrele langemise nurga suurenemisel (sensorvõre normaali suhtes) laiemaks.

Antud töö põhilisteks eesmärkideks ongi kauguse mõõtetäpsuse suurendamine üheaegselt sonarsüsteemi impulssvõimsuse alandamisega ning radiaallahutusvõime suurendamine suurte nurkade korral. Lähtuvalt eelnevast on käsolevas töös põhitähelepanu pööratud keeruliste signaalide käiumisele sensorvõredes ning suunadiagrammide formeerumisele sellist tüüpi signaalide korral. Reeglina vaadeltakse keerulisi signaale kui laiaribalisi signaale ning ka signaalitöötlus sensorvõres taandatakse sensorvõre ribalaiusele (*Ultra Wideband Array*). Ka sensorvõrede jaotamist alamvõredeks vaadeledakse reeglina kas sensorvõre

ribalaiuse suurendamise eesmärgil või siis suunadiagrammide kõrvallehtede mahasurumise eesmärgil (nn. suvalise sutruktuuriga alamvõred). Käesolevas töös on valitud teine lähenemine, kus vaadeldakse sensorvõre dünaamikat ajalises mastaabis. Selline lähenemine võimaldab väga detailset uurida sensorvõres toimuvaid protsesse.

Töö koosneb teoreetilisest ja praktilisest osast. Teoreetiline osa on suures osas referatiivse iseloomuga ning kõigepealt käsitletakse akustiliste lainete levimist keskkonnas. Seejärel käsitletakse kompleksapertuuri teooriat, võre teooriat, signaalitöötluse klassikalisi meetodeid ning optimaalse vastuvõtuga seotud küsimusi. Sensorvõred võivad teatavasti olla ühemõõtmelised, planaarsed või ka kolmemõõtmelised. Antud töös on vaatluse all ühemõõtmeline ekvidistantne sensorvõre, kus kasutusel on isotroopse suunitlusega sensorid. Samuti eeldatakse, et nii akustiliste lainete levikeskkond kui ka sensorid on toimelt lineaarsed ning eeldatakse tasapinnalist lainefronti (Peatükk 4.1). Põhitähelepanu on pööratud sensoritele rakendavate ja nende poolt tekitavate elektriliste signaalide genereerimisele ja töötlemisele. Lihtsat tüüpi sensorvõre on valitud seetõttu, et signaalide käitumine (dünaamika) sensorvõres hästi välja tuleks. Nagu käesoleva töö teoreetilistest osadest nähtub, on üleminek planaarsetele või ka veelgi keerukamatele võre tüüpidele puhtalt tehniline küsimus ja tähendab reaalselt ühe või mitme mõõtme lisamist matemaatilisse aparatuuri. Sensorvõres toimivate protsesside paremaks kirjeldamiseks kasutatakse ka sondeerivate signaalide üksikuid elemente (*chip*). Adaptiivsed võred on samuti maailmas väga kiirelt arenev teema, kuid kuna see ei kuulu käesoleva töö põhiküsimuste hulka, siis siinkohal neid ei käsitleta.

Töö praktiline pool algab sondeerivate signaalide omaduste (määramatuse funktsioonide) uurimisega. Seda eelkõige seetõttu, et impulssvõimsus ja viiteaja hindamise täpsus on seotud just sondeeriva signaali endaga. Põhirõhk on pööratud määramatuse funktsiooni lõikele $\psi(\tau,0)$. Doplerilise sagedusnihke (ehk objektide liikumiskiiruse) hindamine pole käesoleva töö eesmärgiks, kuna merepõhja kaardistamisel seda ei vajata. Käsitletakse ka signaali energiaga seotud küsimusi. Leitakse, et hajaspektersignaalide kasutamisel on võimalik süsteemi impulssvõimsust oluliselt alandada ning samaaegselt viiteaja hindamise täpsust suurendada. Erilist tähelepanu on pööratud pesakoodide kasutamisele. Pesakoodidel põhinevad koodid võimaldavad oluliselt suurendada sonari või radari tegevusraadiust.

Töö järgmises osas vaadeldakse, kuidas hajaspektersignaalidel põhinevad sondeerivad signaalid sensorvõredes käituvad. Kui sellist tüüpi signaal langeb sensorvõrele tema normaali suunalt, siis sensorvõre käitub adekvaatselt, mis tähendab, et füüsiliselt liigutatava sonari (või radari) [20] korral pole vaja täiendavaid signaalitöötluse meetodeid kasutada. Välja arvatud optimaalse vastuvõtu osa mis peab arvestama sondeeriva signaali struktuuriga. Samas on

pesakoodide optimaalne vastuvõtt väga ressursimahukas. Samuti on teada signaalide kvadratuurkomponentide eraldamise algoritmi keerukus. Töös pakutakse välja uudne lahendus signaalide optimaalseks vastuvõtuks otse vahesagedusel, mis võimaldab keerukast kvadratuurkomponentide eraldamise algoritmist loobuda.

Edasi vaadeldakse hajaspektersignaalide käitumist sensorvõres, kui sondeeriv signaal satub sensorvõrele tema normaali suhtes mingi nurga all. Kõigepealt kasutatakse mudelina klassikalist faasivõret ning selgitatakse, et klassikaline faasivõre pole hajaspektersignaalide korral suunadiagrammi juhtimiseks kasutatav. Käesolevas töös tuuakse ära vastav detailne analüüs. Seejärel on lahendusena toodud kolm erinevat algoritmi MATRIX, Advanced FFT ning käesoleva töö autori poolt välja töötatud Block-phase meetod. Hinnatud on ka nende kvaliteedinäitajaid ning tehnilist realiseeritavust. MATRIX algoritm on tehniliselt lihtne, kuid vajab kõrget diskreetimissagedust, Advanced FFT algoritm annab häid tulemusi, kuid on ressursimahukas. Tasub veel märkida, et nimetatud algoritm kujutab endast alternatiivi suunadiagrammide formeerimise adaptiivsetele meetoditele. Block-phase meetod annab peaagu sama häid tulemusi kui Advanced FFT algoritm kuid seda oluliselt väiksema arvutusmahu juures. Uudne on seejuures dünaamiliselt muutuvate alamvõrede kasutamine, mis võimaldab elektoonselt skaneerida 180 kraadi ulatuses kasutades ökoloogiliselt ohutuid hajaspektersignaale madala võimsuse juures.

Käesolev töö on oma olemuselt teoreetilis-uurimuslik. Samas on siin toodud uudseid põhimõtteid hakatud loodavates sonar- ja radarsüsteemides rakendama.

8.2 SONARSÜSTEEMIDE TÜÜBID

Sonarid kasutavad erinevad suunadiagrammide formeerimise meetodeid sõltuvalt konkreetselt nendele pandud ülesannetest. Sonarid jagunevad kahte suurde klassi milleks on külgvaatlussonarid (*Sidescan sonar*) ja kiirtelehviksonarid (*Multibeam sonar*). Külgvaatlussonar on võimeline kaardistama väga laia sektorit merepõhjast. Tema maksumus on suhteliselt madal ja teda on ökonoomne kasutada, kuid samas jääb ta objektide asukoha määramise täpsuselt kiirtelehviksonaritele alla. Eriti tuleb see välja ebatasaste merepõhjade korral ning on põhjustatud väikesest sensorite arvust. Kiirtelehviksonar omab võrreldes külgvaatlussonariga väiksemat ruumilist eraldusvõimet (tulenevalt sensorvõre suunadiagrammi pealehe laiusest) ning haarab korraga merepõhjast väiksema osa, kuid tema positsioneerimise täpsus on suurem. Kiirtelehviksonareid soovitatakse kasutada just siis, kui merepõhi on väga ebatasane. Tuleb märkida, et kui külgvaatlussonari mõõtetulemused saavad rikutud kui tegemist on üheaegsete mitmekordsete peegeldustega, siis kiirtelehviksonari mõõtetulemuse rikub vaid situatsioon, kui objektid millelt signaalid tagasi peegeldusid asetsevad teineteisele liialt lähedal. Seega on kiirtelehviksonarite juures üheks oluliseks küsimuseks resolutsiooni suurendamine. Maailmas on välja töötatud erinevaid spektraalanalüüsil baseeruvaid meetodeid resolutsiooni

suurendamiseks [5]. Nendeks on näiteks: Minimum Variance, Eigen Vector, MUSIC ja Minimum Norm. Reeglina annavad need meetodid parema tulemuse kui klassikaline, Fourier' teisendusel baseeruv suunadiagrammi formeerimine. Parameetrilistest meetoditest võiks nimetada veel Root-Music ja ESPRIT meetodit.

Paljukanalilised aktiivsonarid, mis kinnitatakse jäigale traaversile on üks lihtsamaid sonarsüsteeme. Siin toimivad kõik kanalid iseseisvalt ja ainult ühel sagedusel. Probleemiks on suunadiagrammide ülekattuvuste tekkimine suurtel sügavustel ning samuti määramatuse piirkondade tekkimine madalate mõõtesügavuste korral. Probleemi lahendusena kasutatakse kas kanalite kommuteerimist või siis ka poolaktiivseid süsteeme, kus sirgjoonelise traaversi asemel kasutatakse ringjoone poolkaart. Sellisel juhul on kõik kanalid ruumiliselt lahutatud sensorite ruumilise selektiivsuse tõttu [6].

8.3   SONARSÜSTEEMIDE PÕHILISED TEHNILISED ANDMED

Sonarsüsteemide projekteerimisel peetakse silmas järgmisi tehnilisi andmeid

1. Kanduri lubatud kiirus, et mõõtetulemus oleks täpne.
2. Mõõtepiirkond ehk tegevusraadius.
3. Kauguse mõõtetäpsus kas üldiselt või piirkonniti.
4. Töösageduste piirkond.
5. Implementeeritud sondeerivad signaalid.
6. Sondeerimise sagedus.
7. Saatja väljundvõimsus.
8. Üheaegselt haaratav vaatlusnurk.
9. Anduri suunadiagrammi pealehe laius.
10. Tarbitav võimsus.
11. Nõuded juhtarvutile.
12. Kasutatavad liidesed.
13. Kanalite arv

8.4   LAHENDAMISELE KUULUVAD ÜLESANDED

8.4.1   Sonarsüsteemide impulssvõimsuse alandamine

Objektide kauguse hindamisel mängib olulist rolli signaali ajalis/ruumiline kestvus. Mida lühem signaal, seda täpsem on tulemus. Samas, kui me soovime sonarile suurt tegevusraadiust, peame kasutama suure energiaga signaale. Arvestama peame ka müraga ümbritsevas keskkonnas. Mida suurem on sondeeriva signaali energia, seda kõrgem on ka objekti avastamise tõenäosus mürade taustal. Signaali võimsuse suurendamine põhjustab teisest küljest jälle negatiivseid nähtuseid. Kõigepealt muutuks suurel impulssvõimsusel töötav sonar keskkonnale ohtlikuks. Kui rääkida

sõjalisest aspektist, siis ka vaenlasele kergelt avastatavaks. Seega on küsimus, milliseid sondeerivaid signaale tuleks kasutada, et sonarsüsteemi impulssvõimsus kahaneks kuid muud taktikalised näitajad jääksid vähemalt samaväärseks. Antud küsimust käsitletakse täpsemalt käesoleva töö peatükis 5.1

8.4.2 Lahutusvõime saavutamine suurte nurkade korral

Klassikaliselt vaadeldakse sensorsüsteemi suunadiagrammi formeerimist kitsaribaliste sondeerivate signaalide korral. On teada, et faasilise kompensatsiooni korral muutub suunadiagrammi pealehe laius seda laiemaks, mida suuremaks muutub sondeeriva signaali võrele langemise nurk sensorvõre normaali suhtes. Teemat on põhjalikumalt käsitletud käesoleva töö peatükis 4.3. Lähtudes aga sonarsüsteemide impulssvõimsuse alandamise nõudest, peame me aga loobuma klassikaliste kitsaribaliste sondeerivate signaalide kasutamisest ja võtma kasutusele hajaspektersignaalid (vt. peatükk 5.1). Seega taandub signaalitöötlus sensorvõres hoopis teistele alustele ja me peame uurima, kuidas hajaspektersignaalid sensorvõres käituvad ning kuidas neid töödelda, et saavutada rahuldavaid või isegi paremaid tulemusi. Eelkõige pakuvad huvi situatsioonid, kus hajaspektersignaalid langevad võrele tema normaali suhtes erinevate nurkade alt. Milliseks muutub süsteemi lahutusvõime? Et ülesannet lahendada, tuleb luua sondeerivate signaalide ning sensorvõre matemaatilised mudelid ning viia nad analüütiliselt kokku. Uurides sensorvõre dünaamikat erinevate sondeerivate signaalide korral, on võimalik välja töötada erinevad algoritmid suunadiagrammide formeerimiseks. Käesolevas töös analüüsitakse kolme erinevat algoritmi ning nende kvaliteedinäitajaid. Antud ülesanne on käesoleva töö peaülesandeks ja on suures osas käsitletud käesoleva töö peatükkides 5.2-5.8.

8.4.3 Optimaalse vastuvõtu meetodite analüüs

Merepõhja kaardistamisel on olulisimaks tegevuseks objektide kauguse ja asukoha hindamine. Objektide kauguse hindamiseks peab süsteem realiseerima määramatuse funktsiooni lõike $\psi(\tau,0)$, mis taandub üldjuhul optimaalsele vastuvõtjale. Optimaalne vastuvõtt on ressursimahukas protseduur. Samuti on tehniliselt küllalt keerukas kvadratuurkomponentide eraldamise algoritm. Siit tuleneb kaks ülesannet: Kas on võimalik efektiivselt integreerida omavahel suunadigrammi formeerimine ja optimaalne vastuvõtt (peatükid 5.4 ja 5.6) ning kas on võimalik, kasutades modifitseeritud optimaalset vastuvõtjat, loobuda kvadratuurkomponentide leidmisest (peatükk 5.6).

8.4.4 Tulemuste hindamine modelleerimise abil

Tänapäeval kasutatakse maailmas laialdaselt kahte tüüpi matemaatikapakette MATLAB ja MathCad. Üheks esmaseks ülesandeks on nendevahelise valiku tegemine. Sellele pole pühendatud eraldi peatükki antud töös kuid esialgsete hinnangute alusel osutus sobivamaks variandiks pakett MathCad (v.13.1). Seda eelkõige seetõttu, et keerukate matemaatiliste avaldiste realiseerimine on MathCad-is mõnevõrra lihtsam. Eelkõige puudutab see unikaalsete matemaatiliste avaldiste sisestamist, sest puudub vajadus skripti kirjutamiseks. Kõik käesolevas töö esitatud tulemused ja graafikud on saadud modelleerimise tulemusena. See kehtib ka töö alguses olevate teoreetiliste osade kohta. MathCad-i tehniliste failide väljatrükid pole käesolevasse töösse lisatud kuid on vajadusel eraldi kättesaadavad.

8.4.5 Realiseerimisvõimaluste analüüs ja hinnang

Kuigi käesolev töö on uurimusliku kallakuga, tuleb anda jäme hinnang ka realiseerimisvõimaluste kohta. Teemat on käsitletud peatükis 6. Eelkõige puudutab see nõutavat arvutusvõimsust ja mälumahtu. Seoses arvutustehnika kiire arenguga on saanud võimalikuks ka selliste algoritmide kasutamine, mida veel paar aastat tagasi poleks olnud võimalik realiseerida. Märgime siinjuures etteruttavalt, et käesolevas töös toodud põhimõtted on rakendamisel Eestis loodavate sonar- ja radarsüsteemide juures.

8.5 MODELLEERIMISE TULEMUSED, SONDEERIVA SIGNAALI JA ALGORITMI VALIK

Sondeerivate signaali analüüs on läbi viidud käesoleva töö peatükis 5.1. Lähtudes impulssvõimsuse alandamise nõudest ning viiteaja hindamise täpsusest on kõige efektiivsem kasutada Barkeri koodidel põhinevaid signaale. M-jadade kasutamine on võimalik kuid sel juhul on vaja Barkeri koodidega võrdväärsete tulemuste saavutamiseks kasutada pikemaid koodijadasid. See raskendab sensorvõrele lähemal asuvate objektide avastamist. Kõige efektiivsemad sondeerivad signaalid saame, kui kasutame Barkeri koodide alusel sünteesitud pesakoode kuna need tagavad erakordselt kitsa ekstremaalpiirkonna ning sama kõrvallehtede nivoo taseme nagu klassikaliste Barkeri koodide korral. Probleemiks võib osutuda jällegi signaalide ruumiline pikkus, mis suurendab süsteemi minimaalset tegevusraadiust. Seetõttu on süsteemide praktilisel realiseerimisel otstarbekas muuta sondeeriva signaali valik lihtsalt konfigureeritavaks.

Mis puudutab sondeerivate signaalide dünaamikat sensorvõres (peatükk 5.2), siis panime tähele, et üldine käitumismudel on neil sama ja seotud ikkagi signaali

lühima elemendi kestvusega. Mõningad erinevused tekkisid väga pikkade pesakoodide kasutamisel (sensorvõre väljundsignaali keskmine amplituud jäi suurte nurkade korral mõnevõrra kõrgemaks kui traditsiooniliste signaalide kasutamisel) kuid dünaamika pool ei ole sondeeriva signaali valikul siiski oluliseks faktoriks. Pigem määravad sondeeriva signaali valiku ikkagi minimaalne ja maksimaalne tegevusraadius ning signaali korrelatsiooni omadused.

Algoritmi valik sõltub konkreetsetest olukordadest, saadaolevast riistvarast jne. Võrreldes teoreetilisi tulemusi (peatükid 5.3, 5.4 ja 5.5) võib tõdeda, et kõik nad on realiseeritavad ning annavad teoreetilises plaanis väga häid tulemusi. Sisuliselt on võimalik taandada kogu nurkade vahemik $\beta_\gamma = \pm 90^0$ lähedaseks situatsioonile $\beta_\gamma = 0$. Kõige korrektsemaks variandiks võib lugeda viidete kompenseerimist sagedusruumis kuid samas on see meetod ka küllalt ressursimahukas. Maatriksalgoritm on oma põhimõttelt kõige lihtsam kuid nõuab piisava täpsuse saavutamiseks küllalt kõrget diskreetimissagedust (vt. peatükk 5.8.1) ning kogu optimaalse vastuvõtu osa tuleb eraldi realiseerida. Märgime siinjuures, et maatriksalgoritmi korral on otstarbekas kasutada koherentse kogumise põhimõttel töötavat optimaalset vastuvõtjat (peatükk 5.6). See annab võimaluse loobuda kvadratuurkomponentide eraldamise algoritmist. Minimaalne diskreetimissagedus peaks olema vähemalt 4 diskreeti perioodi kohta. Ideaalis isegi suurem (peatükk 5.8.2).

Plokk-faas meetod annab küllalt häid tulemusi kui peame kinni reeglist, et signaali ühe elemendi (*chip*) ruumilise pikkuse ja alamvõre pikkuse korral kehtib seos $\beta_\gamma \le \beta_{kr}$. Kaotame küll veidi optimaalse vastuvõtja väljundsignaali pealehe nivoos, kuid see kadu ei ole märkimisväärne. Oluline on see, optimaalse vastuvõtja pealehe laius ja üldine kuju ei muutu. Ka kõrvallehtede tase jääb samaks. Veel tuleb märkida, et plokk-faas meetod ei ole sondeeriva signaali suhtes invariante. Tema konkreetne realisatsioon (moodustuvate alamvõrede arv) sõltub sondeerivast signaalist (täpsemalt tema lühima elemendi kestvusest/ruumilisest pikkusest).

8.6 REALISEERIMISVÕIMALUSTE ANALÜÜS

8.6.1 Üldist

Tänapäeval on süsteemide projekteerimisel võimalik kasutada kõiki digitaalse signaalitöötluse eeliseid ning kõrget integreerituse astet. Hetkel toodetakse juba digitaal-analoog muundureid, mille diskreetimissagedused ulatuvad 500 *MHz*.-ni. Signaaliprotsessorid suudavad sooritada miljardeid operatsioone sekundis ja kasutatavad mälumahud ulatuvad gigabaitidesse. Riistvara maksumus on samal ajal jäänud samaks või isegi vähenenud. Kõrge integreerituse aste võimaldab toota väikesemõõtmelisi ning kergekaalulisi süsteeme. Seega pole riistvara tänapäeval

enam nii suureks probleemiks kui see oli võibolla mõned aastad tagasi. Aina olulisemaks muutuvad tarkvara ja algoritmidega seotud küsimused. Kogu raadiotehnika on muutumas täisdigitaalseks. Areneb SDR (*Software Defined Radio*) tehnoloogia kus seatakse eesmärgiks digitaliseerida signaal nii antenni (sensori) lähedalt kui võimalik.

Reeglina koosneb sonarsüsteem digitaalsest ja analoogsest osast. Analoogosa hõlmab endas saatjaid ja vastuvõtjad ning digitaalosa signaaliprotsessoreid, mäluseadmeid ning analoog-digital ja digital-analoog muundureid. Suunadiagrammi formeerimine teostatakse täisdigitaalselt. Sonarsüsteemi juurde integreeritakse ka PC-l baseeruv arvuti mis täidab eelkõige juhtimise ja presentatsiooni rolli. Andmete ülekanne spetsialiseeritud riistvara ja PC vahel toimub kas USB või ja RS232 vahendusel. Võimalik on kasutada ka uuemaid, video ülekandeks ette nähtud liideseid. Kui spetsialiseeritud riistvara on realiseeritud arvutikaardina, võib ühenduslüliks olla PCI või PCI Express. Süsteemi juhtimise ja tulemuste graafilise esitamisega saab hakkama iga tänapäevane PC, mille protsessori taktsagedus on vähemalt 1,4 *GHz* ning operatiivmälu 512 *MB*. Järgnevalt toome nõutava arvutusvõimsuse jämedad hinnangud konkreetsete näidete baasil eesmärgiga hinnata algoritmide üldist tehnilist realiseeritavust. Konkreetne arvutusvõimsus sõltub ikkagi kasutatavatest signaalidest, nõutud tegevusraadiusest, sensorvõre kanalite arvust ja paljudest muudest faktoritest.

8.6.2 Faasiline kompensatsioon

Klassikaline faasiline kompensatsioon taandub kiire Fourier' teisenduse (FFT) arvutamisele. Siinjuures peame arvestama, et kiire Fourier' teisenduse korral peab teisenduse periood olema esitatav kahe astmetega. Seega $N = 81$ elemendilise võre korral peame võtma Fourier' teisenduse pikkuseks 128. Kasutades klassikalist kahese alusega FFT algoritmi, saame tehete arvuks 896 kompleksarvude summeerimise tehet ja 448 kompleksarvude korrutustehet. Optimaalse vastuvõtja poolt hõivatav ressurss on seotud tugisignaali pikkusega. Kui tugisignaali pikkuseks on näiteks 100 diskreeti, siis vajalik arvutusmaht on 100 summeerimis- ja korrutustehet koos mäluoperatsioonidega.

8.6.3 Maatriksalgoritm

Lähtume peatükis 5.3 toodud juhust, kui kasutusel on 5 elemendilise Barkeri koodi alusel sünteesitud pesakood ühe elemendi kestvusega $\tau_e = 25\,\mu s$. Diskreetimissageduse $fs = 1\,MHz$ juures kujuneb signaali kestvuseks $L = 25 \cdot 25 = 625$ diskreeti. Sensorite arvu $N = 81$ ja sensorite omavahelise

116

kauguse $d = 0.0015$ korral saame maksimaalseks puhvri pikkuseks 705 diskreeti. Seega moodustub meil sensorvõre taha 81×705 maatriks mis sisaldab 57105 kompleksarvu. Kui kompleksarvude säilitamiseks kasutada 4 baiti, saaksime nõutavaks mälumahuks 228420 baiti. Siit tuleneb, et signaalitöötluseks oleks igal juhul otstarbekas kasutada vähemalt 32 bitiseid süsteeme. Kui süsteem on realiseeritud tsirkulaarsete puhvrite baasil, siis see tähendab, et signaaliprotsessor peab suutma $1 \mu s$ jooksul sooritada 228420 baidi mäluoperatsioonid. Reeglina on mäluoperatsioonid signaaliprotsessorites realiseeritud spetsiaalkäsustiku abil, mis realiseerivad andmete nihutamise mälus ühe masintsükli jooksul või ka kiiremini. 32 bitise süsteemi korral teeks see siis $57.1 \times E9$ mäluoperatsiooni sekundis kui kogu maatriksi sisu oleks vajalik iga järgneva diskreedi korral ringi tõsta. Lisaks on vajalik $1 \mu s$ jooksul sooritada $N = 81$ kompleksarvude summeerimistehet, 81 indeksite summeerimistehet ning 81 võrdlustehet. Kui soovitakse kasutada erikujulist amplituudiakent, siis lisandub veel 81 kompleksarvude korrutustehet. Kui valemite 5.3.7 ja 5.3.8 alusel arvutatavad suurused on eelnevalt välja arvutatud ja salvestatud protsessori mällu, siis täiendavaid korrutustehteid ei tule. Tuleb arvestada aga sellega, et kompleksarvude summeerimine nõuab kahte reaalarvuga tehet ning kompleksarvude korrutamine nõuab kahte summeerimise ja nelja reaalarvudega korrutustehet. Võrdlustehete sooritamine on ekvivalentne kahe matemaatilise tehtega (kasutab protsessori kahte masintsüklit). Seega peab ühikulise amplituudiakna korral süsteem sooritama 405 tehet $1 \mu s$ jooksul (ehk 405 miljonit summeerimistehet tehet sekundis). Muude amplituudiakende kasutamise korral lisandub veel 162 summeerimistehet ning 324 korrutustehet $1 \mu s$ jooksul. Arvestades, et tänapäevastes signaaliprotsessorites pole vahet summeerimis- ja korrutustehete ajalises kestvuses, siis saame lõppkokkuvõttes 891 tehet $1 \mu s$ jooksul. (891 miljonit tehet sekundis). Kui tegu on 625-st diskreedist koosneva signaaliga, siis tema optimaalsele vastuvõtule (kui optimaalne vastuvõtja on realiseeritud klassikalisi printsiipe silmas pidades) veel vähemalt 1250 operatsiooni $1 \mu s$ jooksul. (1250 miljonit tehet sekundis) Kogu süsteemi arvutusvõimsuse jämedaks hinnanguks kujuneb 2141 miljonit tehet sekundis. Sellise jõudluse tagab näiteks üldotstarbeline TigerSHARC protsessor ADSP-TS101S. Süsteem on võimalik realiseerida ka selliselt, et kogu tagasipeegeldunud signaal salvestatakse suuremahulistesse mälumassiividesse. Kui salvestus on lõppenud toimub järeltöötlus juba mitte reaalajas. Kasutusel võivad olla ka paralleelsed protsessorsüsteemid, mida omavahel kommuteeritakse. Hinnang järeltöötluse realiseerimiseks vajalikule mälumahule on toodud järgmises peatükis.

8.6.4 Viidete kompenseerimine sagedusruumis

Lähtume peatükist 5.4 kui kasutusel on 5 elemendilise Barkeri koodi alusel sünteesitud pesakood ühe elemendi kestvusega $\tau_e = 25 \mu s$. Kui

kvadratuurkomponendid on eraldatud, saame kasutada vähendatud diskreetimissagedust $fs = 0.5\,MHz$. Signaali kestvuseks kujuneb $L = 313$ diskreeti. Sensorite arvu $N = 81$ ja sensorite omavahelise kauguse $d = 0.0015$ korral saame maksimaalseks puhvri pikkuseks 353 diskreeti kui kasutada tsirkuleerivatel puhvritel põhinevat süsteemi. Seega moodustub meil sensorvõre taha 81×353 maatriks mis sisaldab 28593 kompleksarvu. 32 bitise süsteemi korral teeks see siis $28.6 \times E9$ mäluoperatsiooni sekundis kui kogu maatriksi sisu oleks vajalik iga järgneva diskreedi korral ringi tõsta.

Antud meetodi korral on vajalik igas kanalis leida kiire Fourier teisendus. Kuna lähim kahe aste 353-le on 512, tuleb kasutada 512-nse perioodiga kiire Fourier teisendust. Vajaminev kompleksarvude summeerimistehete arv ühes kanalis on 4608 ja korrutustehete arv 2304. Lisaks tuleb sooritada veel 512 komplekse kaalukoeffitsiendi korrutamine kui avaldise 5.4.4 väärtused on kõikide võrekanalite ja diskreetsete sageduste jaoks eelnevalt välja arvutatud. Kuna sensorite arv on 81, siis tuleb toodud arvud korrutada 81-ga. Optimaalse vastuvõtu tarbeks tuleb kõik spektriväärtused summeerida, mis lisab tehete arvule veel $81 * 512 = 41472$ summeerimistehet. Tehete arvuks enne optimaalset vastuvõttu kujuneb $81 * (4608 + 2301 + 512 + 512) = 642573$ komplekstehet. Kui tugisignaali kaakompleks- spekter on eelnevalt mällu salvestatud, siis optimaalne vastuvõtt lisab $4608 + 2301 + 512 = 7421$ tehet ning summaarseks tehete arvuks kujuneb 649994 komplekstehet $2\,\mu s$ jooksul ehk 324 miljardit tehet sekundis. On selge, et sellise meetodi kasutamisel on otstarbekas mitte rakendada tsirkuleerivatel puhvritel põhinevat töötlust, vaid koguda objektilt tagasipeegeldunud signaal suurtesse mälumassiividesse ning sooritada hilisem järeltöötlus. Arvestades, et laine levimiskiirus vees on $c = 1500\,m/s$ ning diskreetimissagedus $fs = 0.5\,MHz$, siis 200 meetrise tegevusraadiuse saavutamiseks peaks massiivi suurus olema 81×133333 diskreeti. Kui iga diskreet oleks esitatud 32 bitise arvuga, siis vajalik mälumaht on 44 MB. Arvestades seda, et säilitada tuleb ka koeffitsientide massiive, siis orienteeruvaks mälumahuks kujuneb 128 MB mis tänapäeval pole probleem. Muidugi suureneb sellisel juhul Fourier' otse- ja pöördteisenduste maht, kuid kuna seda pole vaja sooritada kahe üksteisele järgneva diskreedi vahelisel ajal, siis üldine nõudlus arvutusvõimsusele väheneb. Vajadusel on võimalik rakendada kommuteeritavaid töötlussüsteeme, mis suurendab sondeerimise kiirust.

8.6.5 Plokkmeetod

Nagu mainitud, sisaldab plokkmeetod faasilise kompensatsiooni ja maatriksalgoritmi. Signaalipuhvrite koostamisel võib lähtuda punktis 6.2.2 toodud põhimõtetest. Nõutava arvutusvõimsuse hindamisel lähtume avaldisest 5.5.10. Sisemine summa on taandatav kiirele Fourier' teisendusele. Kuna sensorvõre jagamisel alamvõredeks lühenevad Fourier' teisenduste pikkused, siis kogu võre

töötlus toimub kiiremini võrreldes sellega, kui Fourier' teisendus arvutataks korraga üle kõikide võre elementide. Näiteks 81 elemendilise sensorvõre korral peaksime kasutama 128 punktilist Fourier' teisendust, mis eeldab 896 kompleksarvu summeerimist ja 448-t kompleksarvu korrutustehet. Jagades võre 9-ks alamvõreks pikkusega 9 elementi, saame kasutada 16 punktilist Fourier' teisendust mis on sooritatav 64 summeerimis- ja 32 korrutustehtega. Arvestades, et alamvõrede arv on 9, saame summaarseks tehete arvuks 576 kompleksarvu summeerimist ja 288 korrutamist. Lisaks on vaja sooritada veel 9 kompleksarvu summeerimist, 54 indekseerimistehet ning 18 võrdlustehet igal ajahetkel. Arvestades komplekstehete sooritamiseks vajaminevate tehete arvu, saame reaaltehete arvuks 1836 summeerimist (võrdlustehe on võrdsustatud kahe tehtega) ning 1152 korrutamist mis teeb kokku 2988 tehet $2\,\mu s$ jooksul kui $fs = 0.5\,MHz$ (1494 miljonit tehet sekundis). 313 diskreedist koosneva signaali korral lisandub veel optimaalse vastuvõtu tarbeks 626 tehet $2\,\mu s$ jooksul (313 miljonit tehet sekundis). Kogu süsteemi arvutusvõimsuse jämedaks hinnanguks kujuneb 1807 miljonit tehet sekundis. Sellise jõudluse tagab näiteks üldotstarbeline TigerSHARC protsessor ADSP-TS101S.

8.7 JÄRELDUSED

Käesolevas doktoritöös sai põhiküsimusena käsitletud sensorvõre suunadiagrammi juhtimisega seotud küsimusi hajaspektersignaalide korral. Lisaks on vaadeldud ka sondeerivate signaalide omadusi ning signaalide optimaalse vastuvõtuga seonduvat.

Peatükis 4 on vaadeldud käesoleva töö teoreetilisi aluseid, akustiliste lainete levimist keskkonnas, kompleksapertuuri teooriat, võre teooriat ning signaalitöötluse klassikalisi meetodeid võredes. Need peatükid olid referatiivse iseloomuga ja mõeldud eelkõige lugeja kurssiviimiseks käesoleva töö põhialustega. Samas on paljud sealtoodud põhimõtted käesoleva töö autori poolt modelleeritud ja tulemused graafiliselt esitatud. Ühest küljest oli muidugi võimalik veenduda teoreetiliste tulemuste paikapidavuses kuid põhivajaduse modelleerimise järele juba selles etapis tingis soov luua korralik modelleerimiskeskkond põhiküsimuste käsitlemiseks. Modelleerimiskeskkonnaks sai valitud matemaatikapakett MathCad versioon 13.1. Valik MathCad-i kasuks sai langetatud seetõttu, et keeruliste (mittestandardsete) matemaatiliste avaldiste sisestamine on seal hõlpsam võrreldes näiteks MATLAB-ga. Samas toimuvad arvutused MathCad-i keskkonnas küllalt aeglaselt mis lõppkokkuvõttes tingis vajaduse kaasaegsema arvutustehnika järele.

Peatükk 5.1 käsitles sondeerivaid signaale ja nende määramatuse funktsioone. Põhihuvi pakkusid siinjuures Barkeri koodide alusel faasmanipuleeritud sondeerivad signaalid. Sellist tüüpi signaalid on head just viivituskestvuse mõõtmise seisukohalt. Samas sai tõdetud, et kui M-jadade alusel

faasmanipuleeritud signaalid on omal kohal sidesüsteemides, siis lokatsiooni koha pealt jäävad nad Barkeri koodidele alla (eelkõige korrelatsioonifunktsioonide kõrvallehtede kõrgema nivoo tõttu). Barkeri koodid aga eksisteerivad teatavasti pikkuseni 13 elementi mis ühest küljest ei lase korrelatsioonifunktsiooni ekstremaalpiirkonna laiust väga kitsaks suruda. Probleemist aitab üle Barkeri koodide alusel sünteesitud pesakoodide kasutamine. Modelleerimise tulemus näitas, et Barkeri koode selliselt pesastades on võimalik saada kitsamaid ekstremaalpiirkondi ning alandada ka signaali võimsust. Samas kõrvallehtede nivoo (minimaksne jääk) jääb samale tasemele kui pesastamata Barkeri koodide korral. Pesakoode on võimalik sünteesida ka M-jadade alusel kuid kuna nende minimaksne jääk on suurem, siis pole nende kasutamine jällegi otstarbekas. Pesakoodide kasutamist võib piirata süsteemi tegevusraadius. Väga pikkade koodide kasutamisel muutub problemaatiliseks lähedal asuvate objektide avastamine.

Samuti sai käsitletud sondeeriva signaali võimsuse alandamisega seotud küsimusi. Jõuti järelduseni, et samade mitteenergeetiliste näitajate juures on võimalik alandada signaali võimsust B^2 võrra (suurus B tähistab signaali baasi). Praktilistes lahendustes võimalda see alandada sonarsüsteemi võimsust mõne vatini.

Peatükk 5.2 käsitles praktilisi lahendusi hajaspektersignaalide kasutamise kohta sondeerivate signaalidena sensorvõredes. On teada, et pika kestvusega kitsaribaliste sondeerivate signaalide kasutamisel muutub sensorvõre suunadiagramm võrele langemise nurga suurenemisel (sensorvõre normaali suhtes) teatud määral laiemaks. Töö üheks eesmärgiks oli uurida laiaribaliste ning lühikese ekvivalentse kestvusega hajaspektersignaalide dünaamikat sensorvõredes. Et probleem olemus tuleks paremini välja, sai alustatud üksiku lühikese kestvusega impulsi (st. impulsi ruumiline pikkus oli oluliselt väiksem võrreldes sensorvõre ruumilise pikkusega) käitumise uurimisega. Nagu selgus, hakkas sensorvõre suunadiagramm ajas muutuma ning lisaks sellele suurenes ka suunadiagrammi laius. Seda eelkõige seetõttu, et lühikese ruumilise kestvusega impulss suudab üheaegselt aktiviseerida vaid teatud osa sensorvõrest. Oluliseks parameetriks osutus seejuures nn. kriitiline nurk β_{kr} ,mille puhul eksisteerib vähemalt üks ajahetk, mille korral on aktiviseeritud kõik sensorvõre sensorid. See kriitiline nurk oli aluseks plokk-faas meetodi väljatöötamisel kuna sellise nurga korral on optimaalse vastuvõtja väljundsignaali maksimumväärtus veel aktsepteeritav. Järgnevalt sai uuritud Barkeri koodide alusel faasmanipuleeritud signaalide dünaamikat sensorvõredes. Selgus, et nende käitumismudel on üldjoontes sarnane ning seotud ikkagi sondeeriva signaali lühima elemendi (*chip*) kestvusega. Modelleerimise tulemused näitasid, et kriitilise nurga β_{kr} korral optimaalse vastuvõtja väljundsignaali pealehe laius ei muutu ning mõju on vaid amplituudis. Signaal võrele langemise nurga suurenemisel üle kriitilise nurga hakkas aga optimaalse vastuvõtja väljundsignaali pealehe laius suurenema mis avaldab otseselt negatiivset mõju viiteaja hindamise täpsusele. Pesakoodide korral paistis silma, et signaali võrele langemise nurga

suurenemisel suurenes küll võre väljundsignaali moonutus, kuid tema maksimumväärtus ei kahanenud. Nähtus on põhjustatud sellest, et pesakood on iseenesest juba küllalt pikk. Huvitav oli ka tõik, et signaali võrele saabumise nurga suurenemisel üle β_{kr} väärtuse ei muutnud enam oluliselt optimaalse vastuvõtja väljundsignaali kuju. Samas on jälle optimaalse vastuvõtja väljundsignaali pealehe laius suurenenud nii, et viiteaja hindamise täpsus kannatab sel juhul ikkagi. Tekkis veel mõte rakendada iga nurga jaoks omaette tugisignaali, ehk kasutada tugisignaalina teadaolevalt moonutatud võre väljundsignaali, kuid modelleerimine näitas, et mingit efekti sellega ei saavuta.

Peatükis 5.3 käsitlesime põhimõtteliselt lihtsaimat meetodit hajaspektersignaalide töötlemiseks sensorvõredes, milleks on viidete kompenseerimise maatriksalgoritm. Süsteemi eeliseks on põhimõtteline lihtsus, kuid samas on ta tundlik diskreetimissageduse suhtes. Uuringud näitasid, et meetod töötab normaalselt diskreetimissagedusel, mis tagab 4 diskreeti ühe signaaliperioodi kohta. Kui süsteem töötab korrektselt, tagab ta signaali suvalise võrele langemise nurga $\beta_{\gamma} = \pm 90^0$ korral ekvivalentse olukorra situatsiooniga $\beta_{\gamma} = 0^0$ (sensorvõre normaali suhtes). Mõju avaldab ka laine levikukiiruse muutus, mis võib tuleneda kas keskkonna temperatuuri või muude faktorite muutustest. Analüüs näitas, et algoritm töötab adekvaatselt vahemikus $\Delta c = \pm 20 \, m/s$. Vajaliku arvutusvõimsuse poolest võib algoritm olla realiseeritud ka tsirkuleerivate puhvrite baasil, mis võimaldab oluliselt suurendada süsteemi tegevusraadiust ilma, et peaksime suurendama tarvilikku mälumahtu.

Peatükis 5.4 on vaadeldud viidete kompenseerimist ning suunadiagrammi formeerimist sagedusruumis. Kõigepealt sai üle mindud sondeerivate signaalide kompleksamplituudidele ja selle tarbeks loodud täpne matemaatiline mudel viivitunud sondeerivate signaalide kohta sensorvõre erinevates kanalites. Mudeli paikapidavust on käesolevas töös kontrollitud nii reaalsignaali taastamisel tema kompleksamplituudidest kui ka rakendades võrele klassikalist faasilist kompensatsiooni (väljundsignaali kuju oli varasemast teada). Modelleerimisel selgus, et kompleksamplituudide korral on oluline kompenseerida nii signaalide ajalised viited kõikidel sagedustel kui ka faas. Seega valitakse vaadeldud algoritmi korral kompleksskaalud igale sagedusele individuaalsed mis tähendab, et meil on võimalik konstrueerida sagedusest sõltumatu suunadiagramm. Oluline on ka see, et suunadiagrammi kuju ja kõrvallehtede tase on määratud vaid amplituudikaaludega ning me saame konstrueerida sagedusest sõltumatuid suvalise kujuga suunadiagramme. Põhimõtteliselt on meetod alternatiiviks suunadiagrammide formeerimise adaptiivsetele meetoditele. Meetod pole ka väga tundlik diskreetimissageduse suhtes. Modelleerimine näitas veel, et kui süsteem töötab korrektselt, tagab ta signaali suvalise võrele langemise nurga $\beta_{\gamma} = \pm 90^0$ korral lähedase olukorra situatsiooniga $\beta_{\gamma} = 0^0$ nii nagu maatriksalgoritmigi korral.

Meetodi eeliseks on veel võimalus realiseerida koheselt optimaalne vastuvõtt sagedusruumis. Meetodi puuduseks on väga suur arvutuste maht kui realiseerida ta tsirkulaarsete puhvrite baasil. Siin on otstarbekas salvestada kogu tagasipeegeldunud signaal protsessori mällu ning realiseerida süsteem järeltöötluse põhimõttel.

Peatükis 5.5 sai vaadeldud plokk-faas meetodit mis integreerib faasilise kompensatsiooni ja maatriksalgoritmi. Meetod annab küllalt häid tulemusi kui peame kinni reeglist, et signaali ühe lühima elemendi (*chip*) ruumilise pikkuse ja konkreetse alamvõre pikkuse korral kehtib seos $\beta_\gamma \leq \beta_{kr}$. Optimaalse vastuvõtja väljundsignaali pealehe nivoo küll väheneb, kuid see kadu ei ole märkimisväärne. Optimaalse vastuvõtja väljundsignaali pealehe laius ja üldine kuju ei muutu ja kõrvallehtede tase jääb samaks. Samas ei ole plokk-faas meetod sondeeriva signaali suhtes invariante. Tema konkreetne realisatsioon (moodustuvate alamvõrede arv) sõltub konkreetsest sondeerivast signaalist (täpsemalt tema lühima elemendi kestvusest/ruumilisest pikkusest). Analüüs näitas ka seda, et optimaalses vastuvõtjas pole iga partsiaalsuuna jaoks eraldi tugisignaalide salvestamine mõttekas. Matemaatiliste tehete arvu ja seega nõutavat arvutusvõimsust on võimalik vähendada kui salvestada viidete väärtused ja muud parameetrid kõikide partsiaalsuundade jaoks eelnevalt mällu. Suunadiagrammi leidmiseks on leitud sensorvõre väljundsignaalid kõikide diskreetsete nurkade korral. Modelleerimise tulemused näitasid, erinevalt klassikalisest faasilisest kompensatsioonist ei suurene suunadiagrammi pealehe laius suurte nurkade korral. See kehtib ka maatriks- ja FFT algoritmi korral. Plokk-faas meetodi eelisteks võiks lugeda mõistlikku matemaatiliste tehete arvu, mis võimaldab süsteemi realiseerida ka tsirkulaarsete puhvrite baasil. Kui sondeeriv signaal langeb võrele tema normaali suunalt, toimub süsteemis vaid signaalielementide summeerimine. Kui signaal langeb võrele tema normaali suhtes mingi nurga all, toimub sensorvõre jagamine alam (faasi) võredeks. Seejuures nõutav arvutusmaht isegi väheneb võrreldes klassikalise faasivõrega, kuna Fourier' teisenduse arvutamine toimub väiksemate plokkide kaupa.

Peatükis 5.6 sai põhjalikult käsitletud optimaalse filtreerimisega seonduvaid küsimusi. Modelleeritud on optimaalne filter viie elemendilise Barkeri koodi tarbeks. Kui sondeerivaks signaaliks on binaarse faasmanipulatsiooniga impulsssignaalid, siis signaali algfaas ei paku meile huvi ning oluline on elimineerida algfaasi mõju vastuvõetud signaali amplituudile. Peatükis leitakse, et algfaasi suhtes invariantsuse tagamiseks pole kvadratuurkomponentide eraldamine vajalik ning see võimaldab meil loobuda küllalt keerukast kvadratuurkorrelaatoriga vastuvõtjast. Toodud on uudne koherentse kogumisega optimaalse vastuvõtja struktuurskeem ning modelleerimise tulemused. Selline optimaalne vastuvõtja annab samad tulemused mis kvadratuuralgoritm, kuid on viimasest tunduvalt lihtsam ning võimaldab optimaalset vastuvõttu otse vahesagedusel. Vastuvõtjat on

otstarbekas kasutada koos viidete kompenseerimise maatriksalgoritmiga. Mõlemad vajavad normaalseks tööks diskreetimissagedust 4 diskreeti perioodi kohta.

Kokkuvõtteks võib öelda, et Barkeri koodide alusel moodustatud sondeerivate signaalide kasutamine võimaldab vähendada sonarsüsteemide impulssvõimsust ning samas suurendada viiteaja hindamise täpsust. Kasutades töös toodud signaalitöötluse algoritme, on võimalik saavutada lähedane lahutusvõime situatsiooniga $\beta_\gamma = 0^0$ kõikide signaali võrele langemise nurkade korral. Sondeeriva signaali valik tuleks teha operatiivselt konfigureeritavaks. Kõik toodud algoritmid on tänapäevase mikroprotsessortehnika taseme juures teostatavad. Süsteemi digitaalosa realiseerimiseks võib kasutada TigerSHARC protsessorit ADSP-TS101S. Prognoositav mälumaht oleks 128-256MB.

Väited, mis esitatakse avalikule kaitsmisele

1. Hajaspektersignaalide kasutamine sonar- või radarsüsteemides võimaldab sõltuvalt signaalist vähendada süsteemi poolt väljakiiratavat võimsust 3-169 korda ning suurendada samal ajal mõõtetäpsust faktori $KV \cdot KH$ (3-169) võrra võrreldes sama kestvusega kuid impulsisisese modulatsioonita signaaliga. Kasutades uudseid pesastatud koode, on võimalik sonari või radari tegevusraadiust märgatavalt suurendada.
2. Klassikaline faasivõre ei sobi sonari suunadiagrammi elektriliseks juhtimiseks hajaspektersignaalide korral kuna hajaspektersignaali element aktiviseerib vaid osa sensorvõrest kui ta saabub sensorvõrele nurga alt.
3. Probleemi lahendamiseks võib kasutada kolme algoritmi milledeks on:

    a. maatriksalgoritm (*MATRIX*),
    b. viidete kompenseerimine sagedusruumis (*Advanced FFT*),
    c. plokkmeetod (*Block-phase*). Plokkmeetod kasutabantud kontekstis uudse lahendusena dünaamiliselt muutuvaid alamvõresid.

4. Kasutades käesoleva töö autori poolt välja töötatud plokkmeetodit, on võimalik suurendada kauguse mõõtetäpsust vastavalt punktis 1 toodule ja radiaalset resolutsiooni 2-3 korda suurte nurkade korral koos samaaegse süsteemi impulssvõimsuse ja arvutusvõimsuse vähendamisega.

REFERENCES

1.   Richard O. Nielsen. Sonar Signal Processing. Artech House Inc, Boston, London, 1991, 365p.

2.   Lawrence J. Ziomek. Fundamentals of Acoustic Field Theory and Space-Time Signal Processing. CRC Press Inc, Boca Raton, Ann Arbor, London, Tokyo, 1995, 692p.

3.   Peter M. Clarkson. Optimal and Adaptive Signal Processing. CRC Press Inc., 2000 Corporate Blvd., N.W., Boca Raton, Florida 33431, 1993, 529 pp.

4.   Technology assessment for NOAA Near shore mapping and charting survey system. Naval Command, Control and Ocean Surveillance Center, RDT&E Division Detachment, Warminister, PA. October 1994.

5.   Are Rønhovde. High Resolution Beamforming of SIMRAD EM3000 Bathymetric Multibeam Sonar Data. Cand Scient thesis. University Of Oslo, Department of Informatics. October 1999.

6.   Ilmar Arro. Sonartehnika. Tallinna tehnikaülikooli kirjastus, Tallinn, 1998, 136 lk.

7.   Ilmar Arro. Signaalide digitaaltöötlus. Tallinna tehnikaülikooli kirjastus, Tallinn 1996.

8.   Ilmar Arro, Alina Gavrijaševa. Pidevsignaalide töötlemine. Tallinna tehnikaülikooli kirjastus 2004. 235 lk.

9.   Toomas Ruuben. Advanced FFT and Block-Phase Beamforming for sensor Arrays. UDT Europe 2005, Conference Proceedings, 21-23 june 2005, RAI International Exhibition & Congress Center, Amsterdam, The Netherlands, CD-rom.

10.   Toomas Ruuben. The influence of the changes of wave propagation speed on sensor arrays. UDT Europe 2003, Conference Proceedings, 24-26 June 2003, Malmö Mässan Exhibition and Conference Centre, Malmö, Sweden CD-rom.

11.   Toomas Ruuben. The dynamics of signals with spread spectrum in sensor arrays. UDT Europe 2002, Conference Proceedings, 18-20 June 2002, Palasport, La Spezia, Italy, CD-rom.

12.   Ilmar Arro, Toomas Ruuben, Valeri Kozevnikov. Multi-Beam Sonar with Spread Spectrum Signals. UDT Europe 2001, Conference Proceedings, 25-28 June 2001, Hamburg Congress Centre, Hamburg, Germany, CD-rom.

13.   Ilmar Arro, Raivo Portsmuth, Toomas Ruuben. High Resolution Multi-Beam Sonar. UDT Europe 2000, Conference Proceedings, 26-29 June 2000, Wembley Conference Centre, London, UK, CD-rom.

14.   Edited by James D. Taylor. Introduction to ultra-wideband radar systems. Retried, U.S. Air Force. CRC Press 1995. London, Tokyo. 670p.

15. Ivo Müürsepp. Faasmanipuleeritud sondeerivate signaalide vastuvõtja optimeerimine. Tallinna Tallinna Tehnikaülikool, Eesti Elektroonikaühing, XII rahvusvahelise telekommunikatsioonipäeva materjalid. Raadiotehnika 2005. Tehnikaülikooli kirjastus 2005.

16. Ivo Müürsepp. Juhusliku algfaasiga impulss-signaali optimaalne vastuvõtt ja häirekindlus. Tallinna Tallinna Tehnikaülikool, Eesti Elektroonikaühing, X rahvusvahelise telekommunikatsioonipäeva materjalid. Ringhääling 2003. Tehnikaülikooli kirjastus 2003.

17. Alina Duhnik. Külgvaatlussonari sondeeriva signaali modelleerimine. Tallinna Tallinna Tehnikaülikool, Eesti Elektroonikaühing, X rahvusvahelise telekommunikatsioonipäeva materjalid. Ringhääling 2003. Tehnikaülikooli kirjastus 2003.

18. Valery P. Ipatov. Spread Spectrum and CDMA. John Wiley & Sons Ltd, The Atrium, Southern Gate, Chichester, West Sussex, England 2005.

19. Merrill I. Skolnik. Introduction To Radar Systems. McGraw-Hill 2001 USA 2001.

20. Merrill I. Skolnik. Radar Handbook . McGraw-Hill 2001 USA 1990.

21. Emmanuel C. Ifeachor, Barrie W. Jervis. Digital Signal Processing. A Practical Approach. Second edition. Prentice Hall, England 2002.

22. Edward W. Kamen, Bonnie S. Heck. Fundamentals of signals and systems using MATLAB. Prentice Hall, C1997.

23. Edward W. Kamen, Bonnie S. Heck. Fundamentals of signals and systems using the web and MATLAB. Prentice Hall, C2004.

24. MathSoft, Inc. MathCad User's Guide (http://www.mathsoft.com)

25. MathSoft, Inc. Reference Manual (http://www.mathsoft.com)

26. Vinay K. Ingle, Johnn G. Proakis. Digital Signal Processing using MATLAB, Second Edition. Northeastern University 2007.

27. John G. Proakis, Dimitris G. Manolakis. Digital signal Processing. Fourth Edition. Pearson Prentice Hall, 2007.

28. Dennis W. Ricker. Echo Signal Processing. Kluwer academic publishers 2003.

29. Mark A. Richards. Fundamentals of Radar Signal Processing. The McGraw-Hill Companies, USA 2005.

30. Harry L. Van Trees. Detection, Estimation, and Modulation theory. Part 3. Radar-Sonar Signal Processing and Gaussian Signals in Noise. Wiley 2001.

31. Ilmar Arro, Julia Derkats. Digisignaalide töötlemine. Tallinna tehnikaülikooli kirjastus, Tallinn, 2005.

32. P. M. Woodward, B.A. Probability and Information Theory, with Applications To Radar. Artech House Books, Dedham, Massachusetts 1980.

33. Richard G. Wiley. The Analysis of Radar Signals. Second Edition. Electronic Intelligence. Artech House. Boston, London 1993.

34. Yakov D. Shirman. Computer Simulation of aerial Target Radar Scattering, Recognition, Detection, and Tracking. Artech House. Boston, London 2002.

35. Simon Haykin. Adaptive Radar Signal Processing. WILEY-INTERSCIENCE. A John Wiley & Sons, Inc., Publication 2007.

36. Henri Maître. Processing of Synthetic Aperture Radar Images. WILEY Digital Signal And Image Processing Series. ISTE Ltd, John Wiley & Sons, Inc.2008

37. Glyn James. Advanced Modern Engineering Mathematics. Third Edition. Pearson Education Limited 1993, 2004.

38. R J Mailloux. Subarray Technnology for Large Scanning Arrays, Proceedings of The Second European Conference on Antennas and Propagation 11-16 November 2007 EICC, Edinburgh, UK.

39. G Caille, Y Cailloce, C Guiraud, D Auroux, T Touya, M Masmousdi, Paul Sabatier. Large Multibeam Array Antennas with Reduced Number of Active Chains. Proceedings of The Second European Conference on Antennas and Propagation 11-16 November 2007 EICC, Edinburgh, UK.

40. C Fischer, C Schaefer, C Heer. Digital Beamforming Antenna for Synthetic Aperture Radar. Proceedings of The Second European Conference on Antennas and Propagation 11-16 November 2007 EICC, Edinburgh, UK.

41. P Cerny, M Mazanek, M Mudroch. Measurement Methods of Impulse Radiation Characteristics for Ultra Wideband Antennas. Proceedings of The Second European Conference on Antennas and Propagation 11-16 November 2007 EICC, Edinburgh, UK.

42. F Merli, J F Zurcher, A K Skrivervik, A Freni. Design of a Directive Ultra-Wideband Antenna. Proceedings of The Second European Conference on Antennas and Propagation 11-16 November 2007 EICC, Edinburgh, UK.

43. Heinz-Peter Feldle. State of Active Phased Array Technology. Proceedings of The International ITG-Conference on Antennas INICA 2007.March 28-30, 2007. Arabella Sheraton, München.

44. Kathrein-Werke. Arrays and Multiple Antennas. Proceedings of The International ITG-Conference on Antennas INICA 2007.March 28-30, 2007. Arabella Sheraton, München.

45. Christian Sturm, Malgorzata Porebska, Grzegorz Adamiuk, Werner Wiesbeck. Simulation and Measurement Based Correlation Estimation for Ultra Wideband Antenna Arrays. Proceedings of The International ITG-Conference on Antennas INICA 2007.March 28-30, 2007. Arabella Sheraton, München.

46. Grisha Valentinov Spasov, Boris Yosifov Ribov. Spread spectrum for wireless systems using PIC based micro-controllers as a spreader. Technical University-branch Plovdiv.

CURRICULUM VITAE

1. **Personal Data**

Name	Toomas Ruuben
Date and place of birth	18.07.1968, Tartu, Estonia
Citizenship	Estonian
Marital status	Married
Children	Risto Ruuben (birth 15/05/94)
	Ardo Ruuben (birth 05/10/95)

2. **Contact Data**

Address	Ehituse 18-18, Jüri village, Rae township, Harjumaa, 75301.
Phone	+3725178684
E-mail	truuben@lr.ttu.ee

3. **Education**

Educational Institution	Graduation Time	Speciality/grade
Tallinn University of technology		PhD student in TUT.
Tallinn University of technology	12/1998	M. Sc. E.E. scientific degree from department of Computer Science and Automation.
Tallinn University of technology	06/1993	Engineer's Diploma from department of Radio and Communication Engineering.
A. Kesler's. Kohtla-Järve Secondary School.	06/1986	Subprofessional. Math and physics-biased class.
Jõhvi musical school	06/1986	Harp, trombone.

4. **Language Skills**

Language	Level
Estonian	Mother Tongue
Russian	Intermediate
Inglise	Intermediate

5. Special Courses

Course Date and time	Educational institution or organization
08/1994 (Finland)	Teleste OY Finland
14/2000 (Estonia)	Ericsson AB
11/2001 (France)	Gemplus France
12/2007 (Sweden)	MathWorks
10/2008 (Sweden)	MathWorks
08-11/2008 (Estonia)	University of Tartu

6. Professional employment

Period	Institution	Position
09/2006 -	Tallinn University of technology. Department of Radio and Communication Engineering. Chair of signal processing.	Assistant
09/2005-08/2006	Tallinn University of technology. Department of Radio and Communication Engineering. Chair of signal processing.	Extraordinary assistant
09/1998-08/2001	Tallinn University of technology. Department of Radio and Communication Engineering. Chair of signal processing.	Assistant
09/1995-01/1997	Tallinn University of technology. Department of Radio and Communication Engineering. Chair of signal processing.	Assistant.
09/2004 -	Voicecom OÜ.	Project manager.
08/1994-09/1994	Telag AS.	Project engineer.
01/1994-07/1994	Voicecom AS.	Radio engineer.
08/1991-12/1993	Univoice AS.	Engineer.
06/1991-07/1991	Laboratory of Phonetics and Speech Technology.	Engineer-student (improver).

	Institute of Cybernetics at Estonian Academy of Sciences (1991)	
08/1989-08/1989	Kohtla-Järve milk factory	Locksmith of the measurement systems.

7. Scientific Work

Project: Research in Telecommunications Technology
Organization: Faculty of Infotecnology, Department of Radio and Communication Engineering, Chair of Telecommunication.
Participation: Researcher
Duration: 01.01.03-31.12.07
Abstract:

Design of wideband equipment for telecommunications systems, applications of complex signals to the estimation of distance, angle and velocity of an object by means of radar and sounding equipment. Development of ecologically safe sonars.

Project: Employment of visiting professor at the Department of Radio and Communications Engineering to improve the level of graduate couses.
Organization: Faculty of Infotecnology, Department of Radio and Communication Engineering, Chair of Radioengineering.
Participation: Researcher
Duration: 01.02.06-30.06.08
Abstract:

Objective of the project is to employ quest instructor by the Department of Radio and Communications Engineering to improve the existing Master programme courses, to develop new courses, and to conduct instruction at the Department.

Project: Monitoring, jamming, and neutralizing of radio-controlled systems.
Organization: Faculty of Infotecnology, Department of Radio and Communication Engineering.
Participation: Researcher
Duration: 01.01.07-31.12.10

Abstract:

Objective of the project is to develop monitoring and jamming devices for Estonian ministry of defence.

List of publications

1. Toomas Ruuben, Julia Derkats. Some Methods of Signal Processing and Beamforming in Hydrographic Applications. Elektronika ir Elektrotechnika 2008 vol. 6. Pages 27-32. ISSN 1392-1215.
2. Ants Meister, Toomas Ruuben. Some Signal Processing Aspects in Software Defined Radios. Elektronika ir Elektrotechnika 2008 vol. 4. Pages 97-100. ISSN 1392-1215.
3. Toomas Ruuben. The Dynamics of Signals with Spread Spectrum in Sensor Arrays, Some Aspects of Digital Beamforming. The Second European Conference on Antennas and Propagation (EuCAP 2007). The Edinburgh International Conference Centre, UK 11-16 November 2007.
4. Toomas Ruuben. Advanced FFT and Block-Phase Beamforming for sensor Arrays. UDT Europe 2005, Conference Proceedings, 21-23 june 2005, RAI International Exhibition & Congress Center, Amsterdam, The Netherlands, CD-rom.
5. Toomas Ruuben. Mobiilsed sisuteenused ja GSM-tehnoloogiad A&A (2004) 1, lk. 21-27.
6. Toomas Ruuben. Mobiilsed sisuteenused ja USSD-tehnoloogia A&A (2004) 3, lk 34-44.
7. Toomas Ruuben. The influence of the changes of wave propagation speed on sensor arrays. UDT Europe 2003, Conference Proceedings, 24-26 June 2003, Malmö Mässan Exhibition and Conference Centre, Malmö, Sweden CD-rom.
8. Toomas Ruuben. The dynamics of signals with spread spectrum in sensor arrays. UDT Europe 2002, Conference Proceedings, 18-20 June 2002, Palasport, La Spezia, Italy, CD-rom.
9. Ilmar Arro, Toomas Ruuben, Valeri Kozevnikov. Multi-Beam Sonar with Spread Spectrum Signals. UDT Europe 2001, Conference Proceedings, 25-28 June 2001, Hamburg Congress Centre, Hamburg, Germany, CD-rom.
10. Ilmar Arro, Raivo Portsmuth, Toomas Ruuben. High Resolution Multi-Beam Sonar. UDT Europe 2000, Conference Proceedings, 26-29 June 2000, Wembley Conference Centre, London, UK, CD-rom.

8. Theses Accomplished and Defended

1. Toomas Ruuben. Pulse-to-tone conversion technology in interactive voice response systems. M. Sc Thesis.Tallinn 1998.
2. Toomas Ruuben. The discovery of the request in uniterm. Graduate Engineer Thesis. Tallinn 1993.

9. Research Interest

1. Signals with spread spectrum in sensor arrays.
2. Spectral analysis and topics related with this.
3. Info systems, programming (C++).
4. SDR (Software Defined Radio).

10. Other Research Projects

1. Programming of microcontrollers and signal processors (ATMEL, TMS, PIC).
2. EMT mobile parking system (executor, programmer).
3. Mobile services. EMT data system 1711, EMT Mobile games platform (executor, programmer).
4. Estonian rescue service. Control software for the communications trancievers. Realization and implementation. Project manager.
5. Developing of SMS Gateways, Realization and implementation. Project manager. (Hansapank).
6. "SAXESS to TRAXESS" gateway for the Tallinn stock exchange (HEX). Transmit securities information from Sweden to the Baltic states (Estonia, Latvia, Lithuania).
7. Interactive voice responce systems (IVR). Programmer and developer.

ELULOOKIRJELDUS

1. **Isikuandmed**
   Ees- ja perekonnanimi   Toomas Ruuben
   Sünniaeg ja –koht   18.07.1968, Tartu linn, Eesti
   Kodakonsus   Eesti
   Perekonnaseis   Abielus
   Lapsed   Kaks kooliealist last: Risto Ruuben (sünd
                                15/05/94), Ardo Ruuben (sünd 05/10/95).

2. **Kontaktandmed**
   Aadress   Ehituse 18-18, Jüri alevik, Rae vald,
   Harjumaa, 75301.
   Telefon   +3725178684
   E-posti aadress   truuben@lr.ttu.ee

3. **Hariduskäik**

Õppeasutus (nimetus lõpetamise ajal)	Lõpetamise aeg	Haridus (eriala/kraad)
Tallinna Tehnikaülikool		Doktorant
Tallinna Tehnikaülikool	12/1998	Tehnikateaduste magister. Arvuti- ja süsteemitehnika eriala.
Tallinna Tehnikaülikool	06/1993	Raadioinsener. Raadiotehnika eriala
A. Kesleri nim. Kohtla-Järve keskkool	06/1986	Keskharidus. Matemaatika ja füüsika süvendatud õpe.
Jõhvi Lastemuusikakool	06/1986	Rahvakannel, tromboon

4. **Keelteoskus**

Keel	Tase
Eesti	Kõrgtase
Vene	Kesktase-
Inglise	Kesktase-

5. **Täiendõpe**

Toimumise aeg	Korraldaja
08/1994 (Soome)	Teleste OY Finland

14/2000 (Eesti)	Ericsson AB
11/2001 (Prantsusmaa)	Gemplus France
12/2007 (Rootsi)	MathWorks
10/2008 (Rootsi)	MathWorks
08-11/2008 (Eesti)	Tartu Ülikool

6. Teenistuskäik

Töötamise aeg	Ülikooli, teadusasutuse või muu organisatsiooni nimetus	Ametikoht
09/2006 -	Tallinna Tehnikaülikool. Raadio- ja sidetehnika instituut. Signaalitöötluse õppetool.	Assistent.
09/2005-08/2006	Tallinna Tehnikaülikool. Raadio- ja sidetehnika instituut. Signaalitöötluse õppetool.	Erakorraline assistant.
09/1998-08/2001	Tallinna Tehnikaülikool. Raadio- ja sidetehnika instituut. Signaalitöötluse õppetool.	Assistent
09/1995-01/1997	Tallinna Tehnikaülikool. Raadio- ja sidetehnika instituut. Signaalitöötluse õppetool.	Assistent.
09/2004 -	Voicecom OÜ.	Projektijuht.
08/1994-09/1994	Telag AS.	Projektiinsener.
01/1994-07/1994	Voicecom AS.	Raadioinsener.
08/1991-12/1993	Univoice AS.	Elektroonik.
06/1991-07/1991	Eesti TA Küberneetika Instituut, foneetika ja kõnetehnoloogia sektor	Insener-õpilane (praktika).
08/1989-08/1989	Kohtla-Järve piimatoodete kombinaat	Kontrollmõõteriistade remondi lukksepp.

7. Teadustegevus

Teema: Telekommunikatsioonitehnika-alased uuringud

Organisatsioon	TTÜ Infotehnoloogia teaduskond, RSTI, Telekommunikatsiooni õppetool.
Osalus	Täitja
Ajavahemik	01.01.03-31.12.07
Annotatsioon:	

Keeruliste signaalide kasutamine objektide kauguse, nurga ja kiiruse hindamiseks radar- ja sonarseadmete abil; ökoloogiliselt ohutute sonarite/radarite väljatöötlus

Teema:	Välisõppejõu kutsumine TTÜ raadio- ja sidetehnika instituuti eesmärgiga arendada telekommunikatsiooni eriala magistriõppes.
Organisatsioon	TTÜ Infotehnoloogia teaduskond, RSTI.
Osalus	Täitja
Ajavahemik	01.02.06-30.06.08
Annotatsioon:	

Projekti eesmärgiks on kutsuda välisõppejõud Raadio- ja sidetehnika instituuti et täiendada olemasolevaid magistriõppe kursusi ning luau uusi kursusi. Samuti luua uusi välissuhteid.

Teema:	Raadiojuhtimisega süsteemide talitluse monitooring, häirimine ja neutraliseerimine
Organisatsioon	TTÜ Infotehnoloogia teaduskond, RSTI.
Osalus	Täitja
Ajavahemik	01.01.07-31.12.10
Annotatsioon:	

Projekti eesmärgiks on monitooringu ja häireseadmete väljatöötlus Eesti kaitseministeeriumle.

Publikatsioonid

1. Toomas Ruuben, Julia Derkats. Some Methods of Signal Processing and Beamforming in Hydrographic Applications. Elektronika ir Elektrotechnika 2008 vol. 6. Pages 27-32. ISSN 1392-1215.
2. Ants Meister, Toomas Ruuben. Some Signal Processing Aspects in Software Defined Radios. Elektronika ir Elektrotechnika 2008 vol. 4. Pages 97-100. ISSN 1392-1215.
3. Toomas Ruuben. The Dynamics of Signals with Spread Spectrum in Sensor Arrays, Some Aspects of Digital Beamforming. The Second European Conference on Antennas and Propagation (EuCAP 2007). The Edinburgh International Conference Centre, UK 11-16 November 2007.

4. Toomas Ruuben. Advanced FFT and Block-Phase Beamforming for sensor Arrays. UDT Europe 2005, Conference Proceedings, 21-23 june 2005, RAI International Exhibition & Congress Center, Amsterdam, The Netherlands, CD-rom.
5. Toomas Ruuben. Mobiilsed sisuteenused ja GSM-tehnoloogiad A&A (2004) 1, lk. 21-27.
6. Toomas Ruuben. Mobiilsed sisuteenused ja USSD-tehnoloogia A&A (2004) 3, lk 34-44.
7. Toomas Ruuben. The influence of the changes of wave propagation speed on sensor arrays. UDT Europe 2003, Conference Proceedings, 24-26 June 2003, Malmö Mässan Exhibition and Conference Centre, Malmö, Sweden CD-rom.
8. Toomas Ruuben. The dynamics of signals with spread spectrum in sensor arrays. UDT Europe 2002, Conference Proceedings, 18-20 June 2002, Palasport, La Spezia, Italy, CD-rom.
9. Ilmar Arro, Toomas Ruuben, Valeri Kozevnikov. Multi-Beam Sonar with Spread Spectrum Signals. UDT Europe 2001, Conference Proceedings, 25-28 June 2001, Hamburg Congress Centre, Hamburg, Germany, CD-rom.
10. Ilmar Arro, Raivo Portsmuth, Toomas Ruuben. High Resolution Multi-Beam Sonar. UDT Europe 2000, Conference Proceedings, 26-29 June 2000, Wembley Conference Centre, London, UK, CD-rom.

8. Kaitstud lõputööd

1. Toomas Ruuben. Pulss-toon konverteerimise tehnoloogia interaktiivsetes telefoniteenussüsteemides. Magistritöö.Tallinn 1998.
2. Toomas Ruuben. Päringute tuvastamine teabeterminaalis. Diplomitöö. Tallinn 1993.

9. Teadustöö põhisuunad

1. Hajaspektersignaalid sensorvõredes.
2. Spektraalanalüüs ja sellega seonduv.
3. Infosüsteemid, programmeerimine.
4. SDR (Tarkvaraliselt määratud raadio).

10. Teised projektid

1. Mikrokontrollerite programmeerimine (ATMEL, TMS, PIC).
2. EMT mobiilne parkimine.
3. Mobiilsed sisuteenused. EMT infosõnum 1711, EMT M-mängude platvorm.
4. Eesti päästeameti raadiojaamade juhtimise tarkvara väljatöötlus, realiseerimine ja juurutamine

5. SMS lüüside väljatöötamine, realiseerimine ja juurutamine (Hansapank, Pankade kaardikeskus).
6. "SAXESS to TRAXESS" lüüsi realiseerimine väärpaberibörsi HEX tarbeks. Vahendab väärtpaberiinfot Rootsist Balti riikidele.
7. Interaktiivsete telefoniteenussüsteemide projekteerimine.